2017

NANOTEXTURED TITANIUM SURFACES FOR IMPLANTS: MANUFACTURING AND PACKAGING ASPECTS

Sachin Bhosle
Michigan Technological University, smbhosle@mtu.edu

NANOTEXTURED TITANIUM SURFACES FOR IMPLANTS: MANUFACTURING AND PACKAGING ASPECTS

By

Sachin M. Bhosle

A DISSERTATION

Submitted in partial fulfillment of the requirements for the degree of

DOCTOR OF PHILOSOPHY

In Mechanical Engineering-Engineering Mechanics

MICHIGAN TECHNOLOGICAL UNIVERSITY

2017

This dissertation has been approved in partial fulfillment of the requirements for the Degree of DOCTOR OF PHILOSOPHY in Mechanical Engineering-Engineering Mechanics.

Department of Mechanical Engineering-Engineering Mechanics

Dissertation Advisor: *Dr. Craig R. Friedrich*

Committee Member: *Dr. Chang Kyoung Choi*

Committee Member: *Dr. Yoke Khin Yap*

Committee Member: *Dr. Tolou Shokuhfar*

Department Chair: *Dr. William W. Predebon*

To my parents –

Table of Contents

Preface

The material included in this dissertation is prepared independently by Sachin Bhosle and collaboratively with other researchers. All research experimentation planning and data analysis was guided by advisor Dr. Craig R. Friedrich. All materials presented in chapters 2-7 are obtained under guidance of and using the facilities and equipments provided by Prof. Craig R. Friedrich. Sachin Bhosle performed the experiment, collected and analyzed the data. Manuscripts written by the first author and co-authors have provided critical review and comments to improve the final version.

Dr. Radheshyam Tewari has performed part of experiments presented in chapter 3 and analyzed the obtained data. Prof. Jeffrey Allen has provided the lab space to perform part of the experiments in chapter 4. Dr. Edward Latila provided guidance and helped analyze the data presented in chapter 5. Wentao Yao performed TEM analysis presented in chapter 5.

A substantial portion of this dissertation is planned for journal submission.

Acknowledgements

I express my deep gratitude and appreciation to my advisor professor Craig R. Friedrich. His motivational advices and invaluable guidance paved the way for me to grow as a researcher and develop my career. This dissertation is simply impossible without him.

I thank Dr. Edward Laitila, Dr. Radheshyam Tewari and Mr. Owen Mills for their guidance and helpful discussions. I am thankful for all their assistance. I would also like to convey thanks to the Ministry and Faculty of Mechanical Engineering, MuSTI, ACMAL of MichiganTech for providing the financial means and laboratory facilities.

I would like to acknowledge my committee members, professor Yoke Khin Yap, professor Chang Kyoung Choi, professor Tolou Shokuhfar. I would like to thank Dr. Suryaji. R. Bhonsle who has always been one of my best counselors and authorities at Vidya Pratishthan education foundation, Baramati, MH, India for their encouragement and support.

Lastly, yet importantly, my deepest gratitude goes to my family for unflagging love and support. My father Adv. Madhavrao E. Bhosle, who spare no effort to provide the best possible environment for me to grow up and have the highest level of education. He had been a role model for me. My wife Mrs. Rani Bhosle for her constant support and endless love. I cannot ask for more from my child, Harshwardhan Bhosle as he is simply perfect. My in-laws, Digambarrao Thombre family, who were always available to support me, I thank them for their understanding through the duration of my studies.

Abstract

It has been shown that nanotexturing the surface of otherwise smooth titanium orthopedic materials increases osteoblast proliferation *in vitro*, and the bone-implant contact area and pullout force *in vivo*. However, this prior work has not focused on the requirements for scale-up to industrial processes. This dissertation reports on titanium surface modifications by electrochemical anodization using a benign NH_4F electrolyte, and a hybrid electrolyte also containing AgF, rather than hazardous hydrofluoric acid used elsewhere. Nanotube fabrication of Ti6Al4V foils, rods, thermal plasma sprayed commercial implants, and laser and e-beam melted powder materials was demonstrated.

It was found that the nanotextured morphology depends on electrolyte composition, and dimensional variation depends on anodization conditions using different NH_4F and ethylene glycol electrolytes. The fluorine concentration was found to be the most influential factor affecting formation of porous nanostructures.

Recognizing the importance of packaged implant storage, the wetting behavior of nanotube surfaces was investigated. It was found that increased surface hydrophobicity due to aging in air can be restored by annealing, and the release of residual fluorine from the surface was measured. The kinetics of the amorphous to crystalline anatase transformation of nanotubes was quantified with isochronal and isothermal experiments by X-ray diffraction and transmission electron microscopy. The anatase phase transformation of TiO_2 nanotubes was achieved in as little as 5 minutes at 350C, in contrast to reports of higher temperature and for hours.

The fluorine consumed by the formation of the nanotubes during anodization was analyzed and sources of fluorine consumption were identified. Fluorine from the electrolyte is removed and retained in the nanotubes and by the metal removed to form the nanotubes. A metric describing the fluorine removed from the electrolyte per anodized area was developed to help quality control in manufacturing scale-up.

A single-step anodization with controlled nanosilver deposition within and among the nanotubes, using a new hybrid electrolyte of NH_4F and AgF was demonstrated.

Successful fabrication of potentially antibacterial nanotubes on foils, rods and thermal plasma sprayed surfaces was demonstrated and nanosilver concentration was quantified. These new understandings led to improved manufacturing and storage technologies needed for regulatory approvals of nanotextured titanium surfaces for better orthopedic implants.

Chapter 1

Introduction

With ever growing interest and rapid developments, biomaterials are used to replace biological structures due to their potential to improve longevity and quality of human life. Human bone is a highly porous composite material filled with different osteogenic cells, fluids and fibers. This visco-elastic, multi-scale structure sometimes needs to be replaced by orthopedic implants upon weakening due to age, damage or disease. Orthopedic implants made of bioinert metals, being able to bear loads for several decades, are preferred endoprostheses. Pure titanium and Ti6Al4V alloy are the preferred materials for orthopedic implants due to their biocompatibility and toughness, and are being continuously researched to attain improved function of an implant in the human body [1]. Osseointegration of the implant with surrounding bone is not always obvious and may cause implant failure due to improper bone-implant fixation leading to chronic inflammations or infections [2]. One of the challenges in the biomedical field is to improve bone bonding ability due to lack of porosity and ingrowth of apatite deposits in the pores at the bone-implant interface [3]. This results in eventual loosening of the implant due to the lack of osseointegration (osteolysis) which calls for modifications in implant surfaces. In 2015, total hip arthroplasty (THA) and total knee arthroplasty (TKA) were reported to be the fastest growing orthopedic implant segment in the U.S. with an increase in revision surgeries of 2.9% (hip) and 5.8% (knee) respectively [4]. The market share for hip and knee implants in 2015 was $7.5 billion ($3.1 billion-hip and $4.4 billion-knee) [4]. Kurtz

et al. reported the estimated hospital costs for treating periprosthetic total joint (hip and knee) infections was $320 million in 2001, $566 million in 2009, and is anticipated to rise to $1.62 billion in 2020 [5]. A recent Medicare database review of nearly 1.5 million total knee arthroplasty procedures indicated a primary infection incidence of 1.1%. The data also identified a 19% rate of recurrence of infection following multi-stage treatment, compared to 24.6% rate of recurrence for patients that underwent a single-stage treatment [6]. Engineering nanostructures on the implant surface, giving enhanced osteogenic cell interactions and capable of providing antibacterial properties, is an area of interest. Enhanced osseointegration is more important for specific types of implants, such as TKA tibial tray, THA acetabular cups, interbody spinal cages, pedicle spinal screws, bone fusion screws, and other implants subject to bone-to-implant loosening with current porous fixation technologies. Over the last 15 years, the coated (non-cemented) hip implant market ($3.1B) has increased from 40% to 95%, and the knee market ($4.4B) has been converting about 10 years later. Periprosthetic infection remains a serious health issue with costs approaching $1.6 Billion annually. Especially significant efforts have been undertaken on the design and development of enhanced titanium implant surfaces being a subject of much interest. The enhanced effective surface area of the implant upon nanotexturing of the bulk metal surface has shown to improve bone-implant contact. Among the various surface treatments available to date, nanocrystalline hydroxyapatite coated, macro-micro-nano acid etched, phosphorus coated, TiO_2 with hydroxyapatite coated and TiO_2 nanotube surfaces are preferred competing technologies for implant surface modifications. TiO_2 nanotube surfaces on dental, spinal and orthopedic implants can be advantageous over

current competing technologies with respect to antibacterial abilities, no need to add hydroxyapatite and no impact fatigue. TiO_2 nanotubes on implants provide numerous anchoring sites for cells and a mechanical stiffness environment nearer to native bone than smooth titanium. Nanotubular structures on implant surfaces mimic the natural micro-nano hierarchical system in the body and triggers bio-activity, and their particular ordered structure can be utilized for anti-bacterial functionality [7]. Moreover, nanotubes can be doped with antibacterial agents or anti-inflammatory drugs to further reduce the risks of post-surgery infections [8]. The overall average cost of a titanium hip stem or knee implant system ranges from $2000-$6000. Based on the overall average cost of the components of an orthopedic implant reported from eight companies in 2015, the manufacturing expenses component was 31.5% or $1890 [4]. Thus, launching FDA-510(k) products that reduce infection is a promising industrial approach. Titanium nanotube surfaces allow for a cost-effective combination of infection reduction and osseointegration in one surface treatment. The motivation for creating a nanotextured surface on implants continues to be supported. Researchers at Michigan Technological University have developed a safe technology for the electrochemical anodization of titanium implant surfaces using NH_4F based electrolyte instead of HF (U. S. Patent 9376759) [9, 10]. This work has also resulted in the ability to integrate anti-bacterial nanosilver inside and among the nanotubes in the same process, using a hybrid NH_4F and AgF electrolyte. Thus, looking at short-term complications, such as infection, more greatly affects the cost-effectiveness of THA than the implant term of service and orthopedic industry wants technology that reduces infection while increasing osseointegration. It is important to make this technology more economical and sustainable

from an industrial manufacturing and packaging perspective. Understanding the effect of various processing factors on surface properties of the nanotube layer is also important. Therefore, this dissertation will mainly focus on analysis of processes for surface improvement by synthesis and characterization of nanotextured titanium orthopedic implant surfaces (Fig.1.1).

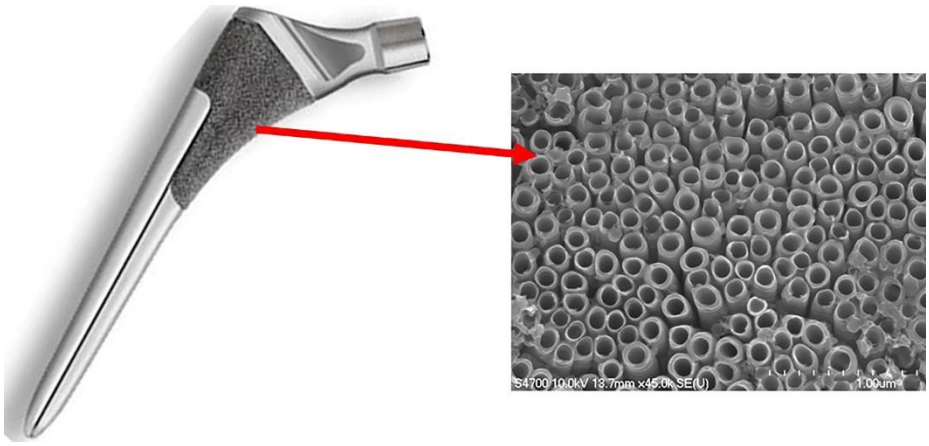

Figure 1.1 Representation of a typical nanotextured titanium implant

Chapter 2 focuses on engineering the nontextured titanium implant surfaces to have various diameters and lengths of nanotubes. In this chapter, the effect of electrolyte composition and anodization parameters on the surface modification of test materials and commercial implants of Ti6Al4V were investigated. To investigate the effect of electrolyte composition on nanotube morphology, two different types of electrolytes, containing different amounts of DI water and NH_4F concentration in ethylene glycol, were used. To analyze the effect of anodization parameters on nanotube dimensions, the anodization voltage and time were varied. Suitable recipes for the successful fabrication of a nanotube layer over a wide range of Ti6Al4V alloy substrates; rolled rods, Kirschner wires, thermal

plasma sprayed surfaces and powder metallurgically manufactured (laser-sintered and electron-beam sintered) porous surfaces were studied. A set of fabrication guidelines to design a process for a specified implant surface morphology and chemical nature are provided.

The fluorine concentration in the electrolyte was found to be the most influential factor affecting the formation of porous nanostructures in the study summarized in Chapter 2. The literature reports a number of studies addressing the growth mechanism and morphologies of TiO_2 nanotubular structures. However, less attention has been paid to the morphological changes upon extensive reuse of the electrolyte, which is critical in an industrial manufacturing scenario, and will require reuse of the same electrolyte over numbers of parts.

Knowing that the chemistry of the process changes with repeated use of the electrolyte, a better understanding of the manufacturing process calls for process investigations involving analysis of the electrolyte condition over a number of electrochemical anodization cycles. Therefore, Chapter 3 describes the dependence of nanotextured surfaces upon reuse of the electrolyte. Previous work undertaken at Michigan Tech demonstrated continuous depletion of fluorine ion concentration in the electrolyte and the present work showed contamination of the electrolyte by the etched-away nanotube surface upon reuse, and the resulting changes in the nanostructure are discussed. This study suggests that, by knowing the area of each duplicate or different implant in a manufacturing process, the fluorine content in the electrolyte needs to be controlled for repeatable results.

After implantation, the immediate biological interaction between the nanotube surface and protein adsorption decides the fate of osteoblast cells. The bio-performance of an implant is influenced by its surface properties. During the past few years, researchers have investigated optical, electrical, wetting, morphological and chemical properties of titanium nanotube surfaces, while very few report on the controlled wettability and chemical composition. The wettability changes upon aging can help predict the wetting condition of a nanotube surface during shelf-life which can lead to improved storage technologies. It is believed that superhydrophilic surfaces help protein adsorption which further can facilitate cell adhesion and reduce bacterial adhesion. This motivated the investigation of ways to alter wettability and chemical composition of nanotube surfaces. Chapter 4, discusses the possibility of restoring hydrophilicity and controlling the residual fluorine in new and aged titanium nanotube surfaces. It was observed that the wettability of a nanotube surface is dominated by the aging effect of environmental adsorbants and the wetting transition from hydrophilic to hydrophobic is irreversible for amorphous nanotubes using UV irradiation. However, the release of residual fluorine from nanotube surfaces was observed as a function of annealing time. Chapter 4, further discusses suitable recipes to fabricate a super-hydrophilic nanotube layer on thermal plasma sprayed pure titanium. These findings will help to understand quality manufacturing and packaging aspects of nanotextured titanium surfaces for better orthopedic implants and to answer possible regulatory concerns.

It was observed that post-anodization heat treatment (annealing) restored hydrophilicity. This type of hydrophilic implant surface allows cells to spread more easily

and evenly. Additionally, annealing can control the residual fluorine in the surface and convert the nanotubes from amorphous to crystalline anatase with slightly better mechanical strength. The annealing temperature and time of 450-550C and 3-4 hours has been widely reported in the literature. Higher temperatures and longer processing time limits the production efficiency in a manufacturing environment. Thus, a quick and low temperature protocol for anatase conversion can be promising. Chapter 5, demonstrates a rapid heat treatment for crystalline conversion of nanotube surfaces. The transformation kinetics of amorphous to anatase titania nanotubes was studied using isothermal and isochronal experiments. The transformation rate coefficient and activation energy for crystalline anatase coalescence is discussed in this chapter. A quick, simple and economical technique is described which can be promising in industrial-scale manufacturing for synthesis of anatase TiO_2 nanotube orthopedic implant surfaces favorable for improved bio-functional properties.

From a manufacturing control perspective, an appropriate amount of fluorine concentration is required in the electrolyte for the formation of nanotubes, which decreases upon reuse of the electrolyte. Thus, accounting for the fluorine depletion during anodization is needed for better process understanding. Chapter 6 focuses on analyzing the amount of fluorine consumed by the formation of titanium nanotube layer and the dissolved metals during anodization of Ti6Al4V alloy foils. Fluorine, being electronegative and relatively small, has the potential to influence protein interactions with implant surfaces in the biological implantation. Incorporation of a controlled amount of fluorine on implant surfaces can improve osseointegration. The literature reports positive effects of fluoride-

modified implant surfaces on osseointegration, but most of it used hazardous chemicals (HF) to modify the fluorine content in the implant surfaces. Titanium nanotube surfaces formed in fluorine containing electrolyte (suggested by our safe technology), contain some amount of residual fluorine which can be tailored to target amounts to help enhance osseointegration. This study showed that the dissolved metals are also a source of fluorine consumption from the bulk electrolyte during anodization.

After investigating more efficient ways to synthesize hydrophilic and crystalline nanotube surfaces, to address the problem of osseointegration, periprosthetic infection in orthopedic surgery calls for surfaces capable of providing long-term antibacterial activity. Once the surface biofilm is formed by bacterial adhesion, it develops a resistance to antibiotic treatment. After understanding the mechanism of bacterial colonization and the biological reasons for survivability, a preventive strategy on and below the implant surface level, to increase local immune response, was identified as a potential winning strategy to promote bacterial inhibition. The needed long-term antibacterial ability can be served with vertically-aligned open-volume nanotube surfaces with integrated nanosilver. Thus, Chapter 7 presents a simple single-step electrochemical anodization process for manufacturing implant surfaces integrated with silver nanoparticles on Ti6Al4V foils, rods and thermal plasma sprayed surfaces using a newly developed hybrid electrolyte. This chapter discusses the processes that control the silver content in the surface to avoid unintended cytotoxicity while ensuring desired nanotube morphology.

Based on the work outlined above, and new understanding of the manufacturing process for developing a nanotube surface on orthopedic implants, several future directions

for the continued analysis and evaluation of surface modifications are suggested in Chapter 8. The first concept focuses on the need to develop a fluorine replenishment strategy for the electrolyte. Second, a comparative analysis of stirred-cell filtration and series filtration of reused electrolyte to remove the dissolved metals during anodization is presented. This will help in the more efficient utilization of reused electrolyte and can greatly reduce the costs in industrial manufacturing. Following the technology described for the synthesis of nano silver integrated antibacterial nanotube surfaces, the clinical applications of this technology will require *in vitro* and *in vivo* analysis of biofilm inhibition and evaluation of antibacterial ability of these surfaces. Additionally, investigation of the most influential factors affecting morphology, while using the newly developed hybrid electrolyte (made with $AgF+NH_4F$) for anodization, will be required.

In total, the work described in this document will contribute towards the development of new implant technology that will help reduce manufacturing costs, prolong the life of the implant, and help improve the quality of life of the patient with reduced personal and financial burden of post-operative infection.

References

[1] Geetha M, Singh AK, Asokamani R, Gogia AK. Ti based biomaterials, the ultimate choice for orthopaedic implants – A review. Progress in Materials Science. 2009;54:397-425.

[2] Aro HT, Alm JJ, Moritz N, Makinen TJ, Lankinen P. Low BMD affects initial stability and delays stem osseointegration in cementless total hip arthroplasty in women: a 2-year RSA study of 39 patients. Acta Orthop. 2012;83:107-14.

[3] Liang B, Fujibayashi S, Neo M, Tamura J, Kim H-M, Uchida M, et al. Histological and mechanical investigation of the bone-bonding ability of anodically oxidized titanium in rabbits. Biomaterials. 2003;24:4959-66.

[4] Hip and knee implant review. Orhopedic Network News. 2016;27.

[5] Kurtz SM, Lau E, Watson H, Schmier JK, Parvizi J. Economic burden of periprosthetic joint infection in the United States. J Arthroplasty. 2012;27:61-5 e1.

[6] Cochran AR, Ong KL, Lau E, Mont MA, Malkani AL. Risk of reinfection after treatment of infected total knee arthroplasty. J Arthroplasty. 2016;31:156-61.

[7] Ganguly; D, Reza. Shahbazian-Yassar, Shokuhfar T. Recent advances in nanotubes for orthopedic implants. Journal of Nanotechnology and Smart Materials. 2014;1:201-10.

[8] Zhao L, Wang H, Huo K, Cui L, Zhang W, Ni H, et al. Antibacterial nano-structured titania coating incorporated with silver nanoparticles. Biomaterials. 2011;32:5706-16.

[9] Friedrich CR, Shokuhfar T. Compositions methods and devices for generating nanotubes on a surface. United States Patent US 9,376,759. 2016.

[10] Shokuhfar T. Structural and Surface Property Characterization of titanium dioxide nanotubes for orthopaedic implants. PhD Dissertation; Michigan Technological University. 2010.

Chapter 2

Engineering nanotextured titanium surfaces*

Abstract

Nanotextured titanium oxide surfaces were obtained by electrochemical anodization of Ti6Al4V alloy. Two different types of electrolytes containing different amounts of water and NH_4F concentration in ethylene glycol were used. This work focused on structural modifications by varying the F^- ion concentration in the electrolyte, anodization voltage and time. The effect of these anodization parameters on nanotextured morphology and dimensions was studied. The titania nanotube diameters ranging from 50 to 135 nm, and the lengths ranging from 0.5 to 5 μm, were obtained. The morphology showed strong dependence on electrolyte composition whereas, the nanotube dimensions showed dependence on anodization voltage and time. To extend the possibility of fabricating nanotubes on a wide range of Ti6Al4V implant surfaces such as rolled surfaces, thermal plasma sprayed surfaces, and next generation orthopedic implant surfaces made by powder metallurgy, were also targeted in this study.

* *The material contained in this chapter is in preparation for submission to a journal or conference proceeding. As the first author of this publication, I have done the fabrication of nanotube surfaces, SEM and EDS characterization, literature review, results analysis and writing the manuscript.*

2.1 Introduction

The corrosion resistance, superior mechanical properties and good biocompatibility makes titanium and its alloys favorable candidate for implant materials [1]. The nanophase materials on orthopedic implants have been suggested to improve bonding between an implant and surrounding bone with aid in bone cell functions [2]. The oxide layer formed by electrochemical anodization has shown improved biocompatibility of titanium implants [3]. In biomedical applications, the control of morphology, dimensions and phase composition plays a vital role in determining the effectiveness of the modified implant surface. A TiO_2 nanotube (TiNT) layer fabricated on implant surfaces by electrochemical anodization enhances osseointegration and stability [4,5]. Zwilling and co-workers reported self-organized anodic nanotube layer of titanium oxide for the first time in 1999, recognizing that the fluorine ions in the electrolyte are responsible for tube formation and the tubular structure formed was amorphous [6]. Gong et al. reported fabrication of TiNTs by electrochemical anodization using hydrofluoric acid based electrolyte with diameters of nanotubes ranging from 25 – 65nm [7]. Electrochemical anodization produces a layer of nanotubes open at the top and closed at the bottom whose diameter and length can be controlled by using appropriate electrolyte concentration, anodization voltage and time. Over the years several research groups have focused on nanotube synthesis using electrochemical anodization with different nanotube diameters ranging from 65 nm to 150 nm and lengths ranging from 250 nm to 134 μm [7-12]. The nanoscale dimensions can change the ionic, electronic and bio-interface properties considerably, which may help to improve reaction/interaction between an implant and the surrounding tissue [13].

Anodization parameters influence nanotube formation causing morphological variations in their length, diameter, wall thickness and inter-tubular spacing. This calls for better understanding of the influential factors governing the self-organization and dimensions of titania nanotubes during the anodization process, focusing on the specific type of electrolyte and anodization conditions from a wide range. Our implant surface modification technology is based on safe, low-cost electrochemical fabrication of nanotextured surfaces on implants. This process uses relatively nonhazardous materials (NH_4F instead of hydrofluoric acid), is environmentally safe and requires minimal maintenance. The objective of the present study was to quantify the effect of electrolyte composition on nanotube morphology and the effect of anodization voltage and time on nanotube dimensions on test materials and commercial implants. To investigate the effect of electrolyte composition on nanotube morphology, two different electrolyte compositions, with different fluorine concentration and deionized water in ethylene glycol were used. To extend the fabrication of nanotubular surfaces over a wide range of Ti6Al4V alloy substrates, rolled rods, Kirschner wires (K-wires), thermal plasma sprayed surfaces (TPS) and powder metallurgically (PM) manufactured (laser-sintered and electron-beam sintered) porous cylinders, were studied in this work. Suitable electrochemical anodization recipes to successfully fabricate a nanotube layer on these surfaces was determined and the morphological and chemical nature of the resulting surfaces was studied. The purpose of this work was to provide a set of fabrication guidelines to design a process for a specified implant surface morphology.

2.2 Materials and Methods

2.2.1 Substrate preparation

Foils (12mm x 12mm x 0.5mm thick) ASTM B 265-11 grade 5 (TIMET, USA), rods (3mm diameter), K-wires (1mm diameter), thermal plasma sprayed (24mm diameter and 12mm long) commercial implant sections of Ti6Al4V alpha/beta titanium alloy were cleaned in deionized (DI) water followed by acetone and dried in air at room temperature. Additionally, two types of powder metallurgically (PM) manufactured porous cylinder implants (8mm diameter x 20mm long) of Ti6Al4V, electron beam sintered (ArCam, USA) and laser-sintered (DMLS, USA) were cleaned ultrasonically in DI water only and dried in air at room temperature.

2.2.2 Fabricating nanotubes

The nanotextured porous surfaces were fabricated by electrochemical anodization using a DC power source (Protek 3006B), with direct current (DC) output 0-60V, 1.5A as shown in Fig.2.1. The surfaces were anodized at room temperature with a graphite rod as the cathode and the titanium alloy as the anode. Two electrolyte recipes used to anodize the nanotubes with specific compositions, as listed in Table 2.1, are hereafter abbreviated LWHF (low-water, high-fluorine) and HWLF (high-water, low-fluorine).

Table 2.1 Anodization conditions used for fabrication of TiNT surfaces

Receipe	Electrolyte solution	Potential (V)	Anodization time
LWHF	98% EG + 2% DI water + 0.6 wt% NH_4F	30 - 60	25 to 40 minutes
HWLF	60% EG + 40% DI water + 0.2 wt% NH_4F	30	1 to 4 h

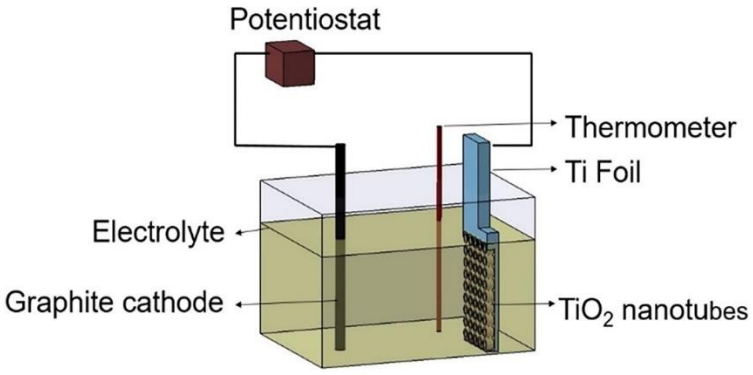

Figure 2.1 Electrochemical anodization setup for fabrication of TiO_2 nanotube surface. The nanotube can be etched on variety of substrates shown in setup as Ti foil.

2.2.3 Surface characterization

Characterization of the anodized surfaces was performed by field emission scanning electron microscopy (FE-SEM, Hitachi S-4700). The wt% chemical compositional analysis of surfaces was by energy dispersive spectroscopy (EDS) with standardless quantitative analysis on the FESEM at 10kV.

2.3 Results and Discussion

2.3.1 Effect of electrolyte recipe on morphology

Electrochemical anodization using two different electrolytes resulted in formation of two different TiNT morphologies (Fig.2.2). Each type of TiNT structure showed a strong dependence on electrolyte composition. The nanotubes formed in the LWHF electrolyte at 60V for 40 minutes produced a honeycomb-like, tightly bound, vertically aligned structure with smooth nanotube walls (Fig.2.2b). These tubes present an ordered and well packed structure (Fig.2.2a). In contrast, the nanotubes formed in the HWLF electrolyte at 30V for 4h produced well-spaced, individual-vertically aligned structures (Fig.2.2c). These nanotubes showed ripples in their side walls (Fig.2.2d).

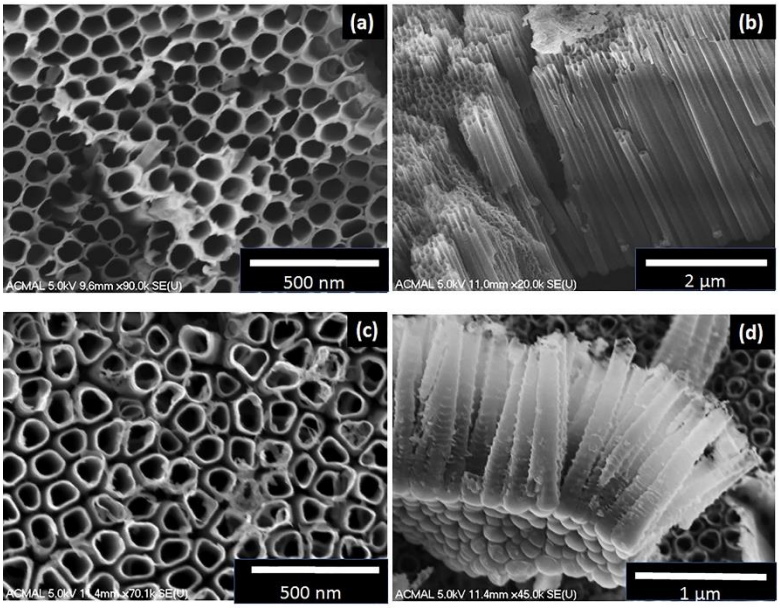

Figure 2.2 Nanotube morphologies obtained with (a-b) LWHF and (c-d) HWLF electrolytes.

2.3.2 Rib formation on tube walls

The major difference observed between the two types of morphologies was the presence of ribs on the external walls of the nanotubes obtained with HWLF electrolyte. The electrochemical oxidation of titanium and subsequent dissolution of oxide by fluoride ions leads to the formation of TiF_6 complexes per the reactions: [14].

$$Ti + 2H_2O \rightarrow TiO_2 + 4H^+ + 4e^-$$

$$TiO_2 + 4H^+ + 6F^- \rightarrow [TiF_6]^{2-} + 2H_2O$$

The rib formation on the tube walls occurs as a result of partial dissolution of $[TiF_6]^{2-}$ complexes between cell boundaries while simultaneous oxide dissolution continues leading to deepening of the main tubes during anodization. The barrier layer formed between adjacent tubes due to partially dissolved complexes, facilitates migration of cations (F^-, O^{2-}) and anions (Ti^{4+}). This leads to film formation (comprised of oxide and fluorine rich complexes) at the nanotube boundaries. Upon dissolution of the fluorine rich metal complexes, the oxide-rich portion results in the formation of ribs on nanotube walls [15].

2.3.3 Effect of voltage with LWHF electrolyte

To study the effect of anodization voltage on nanotube size, the titania nanotube layers were obtained over a range of anodization voltage. The anodization process was carried out for 40 minutes at 30, 40, 50 and 60V in LWHF electrolyte. Fig.2.3. shows the FESEM micrographs of nanotube diameters and lengths. The relationship between anodization voltage (V) and outer nanotube diameter (D) is summarized in Fig.2.4a. The outer diameter of nanotubes ranged from 50±2.5 nm to 100±3nm for anodization voltages from 30 to 60V. Fig.2.4b summarizes the relationship between anodization voltage and nanotube length (L). For 30, 40, 50 and 60V an average length of 1.5, 2.8, 3.9 and 4.7 microns was observed. The bars show the standard deviations of repeated measurements. It was evident that the outer diameter and length increases with anodization voltage and the relationship can be linearized per Eq. (1) for diameter, and Eq. (2) for length, over the specified range of voltage between 30 to 60V.

$$D = 1.4V+12 \qquad (1)$$

$$L = 0.1V–1.66 \qquad (2)$$

This linear relationship can be ascribed to the fact that the thickness of the anodic oxide film linearly increases with the voltage in forming a compact oxide during the initial stage of tube growth [14]. At higher anodization voltage, larger anodic current during nanotube formation produces longer length of tubes [16]. It is recognized that Eq. (1) and (2) prescribe nanotubes with zero voltage, however the constants are necessary over the 30V-60V range.

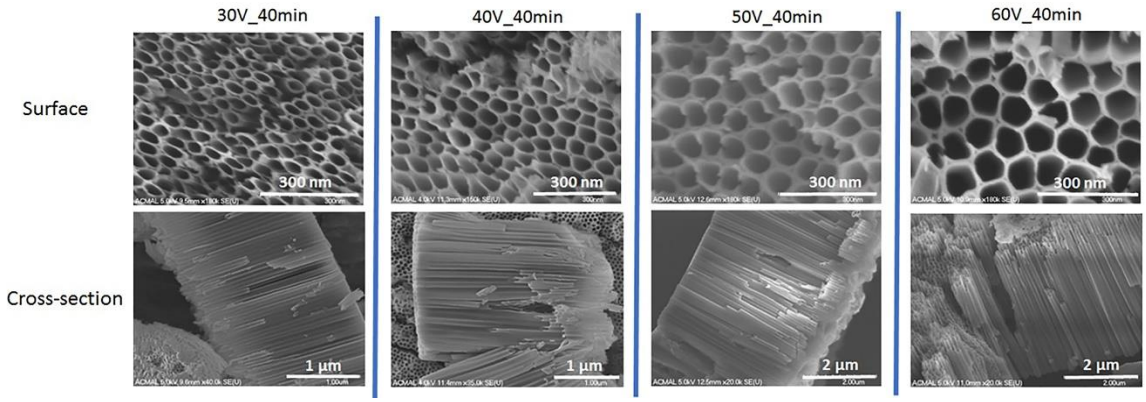

Figure 2.3 Nanotube morphologies obtained with LWHF electrolyte by varying anodization voltage.

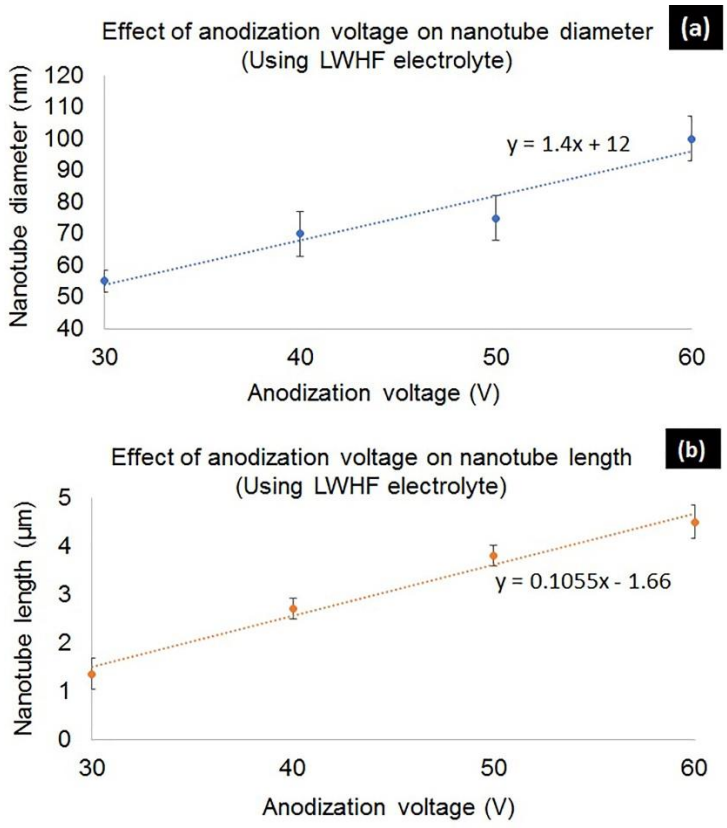

Figure 2.4 Effect of anodization voltage on tube diameter (a) and length (b) using LWHF electrolyte.

2.3.4 Effect of anodization time with LWHF electrolyte

To study the effect of anodization time on nanotube size, another set of experiments was conducted at constant voltage and varying time. The anodization process was at 60V for 25, 30, 35 and 40 minutes. Fig.2.5 shows the FESEM micrographs of nanotube diameters and lengths obtained over the selected range of anodization time. Fig.2.6a summarizes the relationship between anodization time and outer nanotube diameter. For 25, 30, 35 and 40-minute anodization at 60V, the average diameters of 80, 82.5, 82.5 and 95 nm were observed. This variation in nanotube diameter was much less than variation observed with change in anodization voltage indicating that voltage is a stronger factor for diameter than is time. Fig.2.6b summarizes the relationship between anodization time and nanotube length. For 25, 30, 35 and 40-minute anodization at 60V, the average nanotube length of 3.8, 4, 4.3 and 4.7 microns were observed. Again, this variation in nanotube length is much less than the variation observed with changes in voltage. Thus, the anodization voltage has shown more influence on tube dimensions than anodization time.

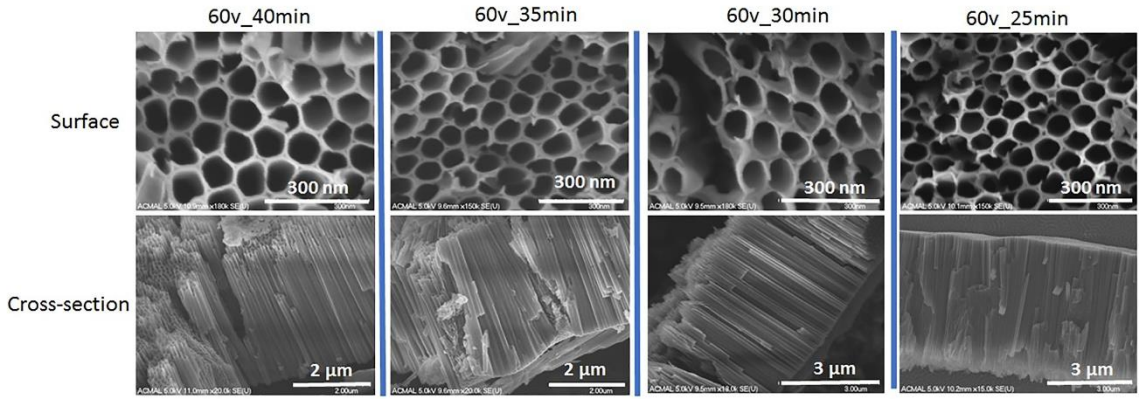

Figure 2.5 Nanotube morphologies obtained with LWHF electrolyte by varying anodization time.

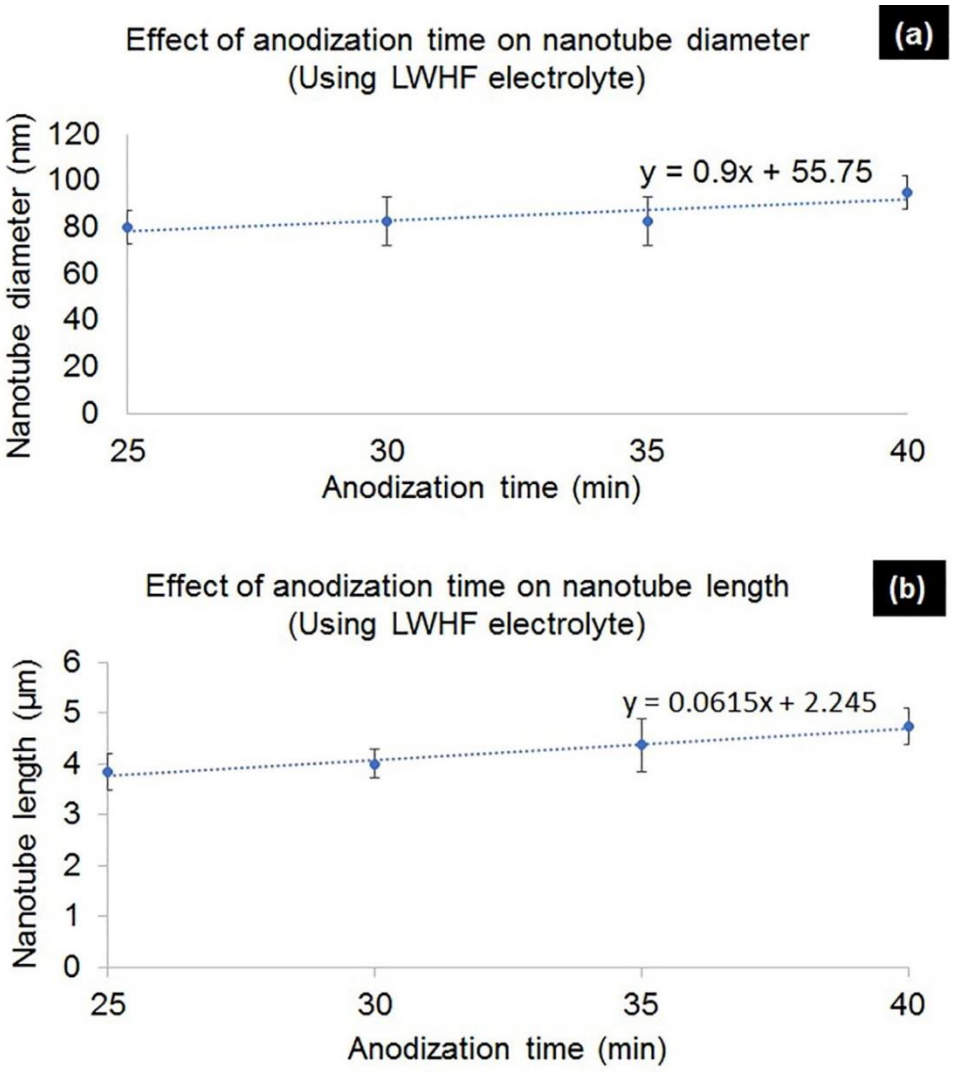

Figure 2.6 Effect of anodization time on tube diameter (a) and length (b) using LWHF electrolyte.

2.3.5 Effect of anodization time with HWLF electrolyte

The effect of variation in anodization time (at 30V) on tube length and diameter using HWLF is shown by FESEM micrographs in Fig.2.7. The relationship between anodization time and outer nanotube diameter is summarized in Fig.2.8a. For 1, 2, 3 and 4h anodization at 30V, the average diameter of 97, 122, 117 and 122 nm were observed. Fig. 8b summarizes the relationship between anodization time and nanotube length. For 1, 2, 3 and 4 h anodization at 30V, the average length of 0.5, 0.7, 1.1 and 1.25 micron were observed.

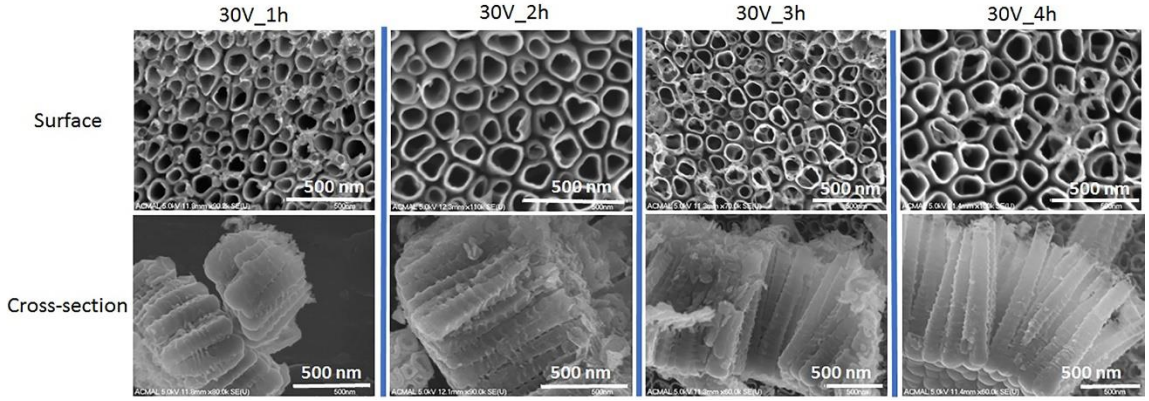

Figure 2.7 Nanotube morphologies obtained with HWLF electrolyte by varying anodization time.

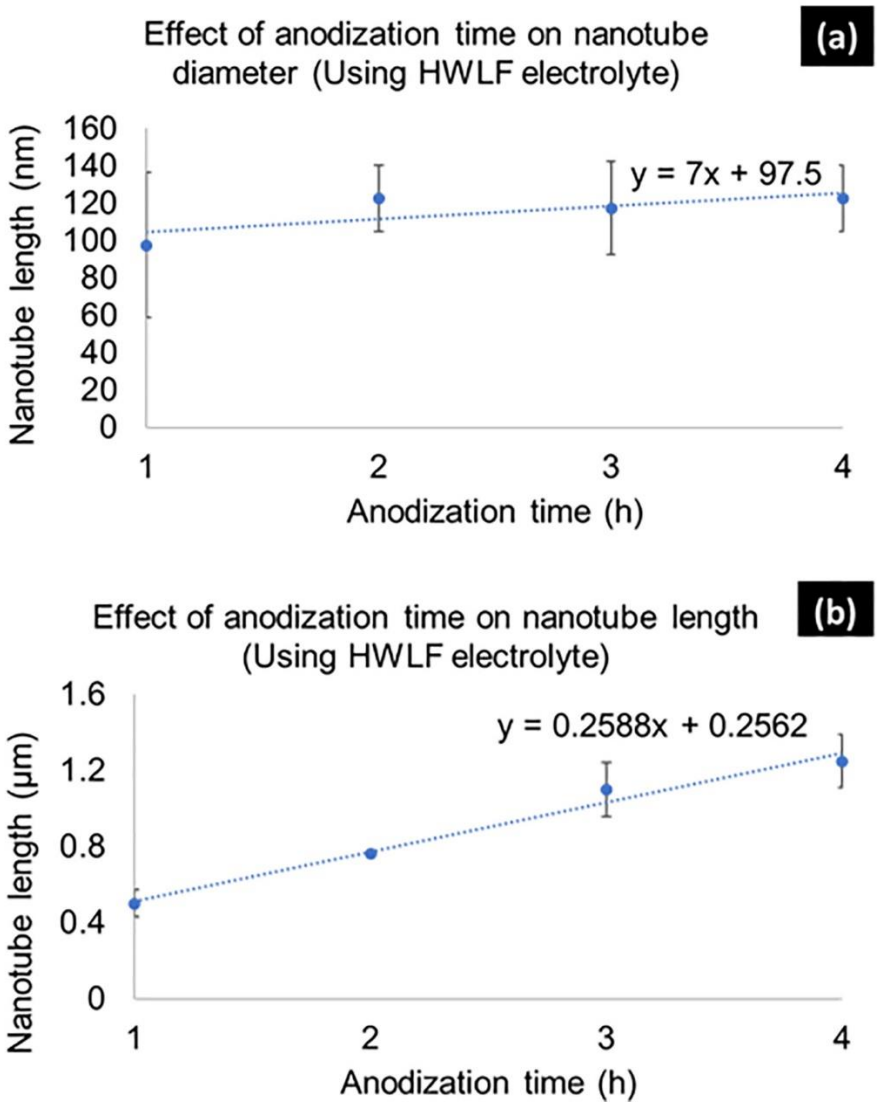

Figure 2.8 Effect of anodization time on tube diameter (a) and length (b) using HWLF recipe.

2.3.6 Effect of electrical conductivity of electrolyte on TiNT morphology

It is reported that, upon reuse of electrolyte, the metal contaminants dissolved during anodization decreases the electrical conductivity of the electrolyte and subsequent current densities lead to change in resulting morphology [17]. The anodization by-products released into the electrolyte are particles of various oxides of titanium, aluminium and vanadium. As this increase in concentration in the electrolyte, the conductivity decreases. Also as fluorine is depleted in the electrolyte, the conductivity further decreases due to reduced ionic strength. The resulting nanostructure morphology also depends on the electrical conductivity of the electrolyte and fluoride ion concentration. To investigate the more influential factor among these two, additional experiments were conducted. To investigate the effect of decreased electrical conductivity due to metals contamination, resistances ranging from 300 Ω to 33 kΩ were added in series. LWHF electrolyte containing 0.6 wt% NH_4F was used for anodization of titanium alloy foils to study the influence of resistances in series (simulated decrease of electrical conductivity of electrolyte) on resulting morphology. Fig.2.9 shows the effect of decreased electrical conductivity of the electrolyte on resulting morphology upon anodization. Only pits and pores of 10 – 20 nm were formed and no tubes were observed with 8.2 kΩ and 33 kΩ resistance. Tube formation initiated with 3.9 kΩ resistance and tube diameters of 50nm was observed. Well defined, self-ordered tubular structures were observed with 1.8 kΩ and 300 Ω resistances. The tube diameters of 65 nm and 85 nm were observed with 1.8 kΩ and 300 Ω resistance, respectively. Although the variation in tube diameter was observed, this indicates that there was sufficient fluorine ion concentration in the electrolyte to provide enough electrical conductivity required for formation of tubular morphology. This also indicates that fluorine concentration in the electrolyte is the more dominating parameter affecting electrical conductivity of the

electrolyte. Thus, as resistance in series was decreased, the increased current density led to formation of tubular structures. From a biological perspective, if nanoporous structures, instead of tubular structures are required, this process can fabricate nanoporous structures of required sizes without changing the electrolyte just by putting appropriate resistance in series.

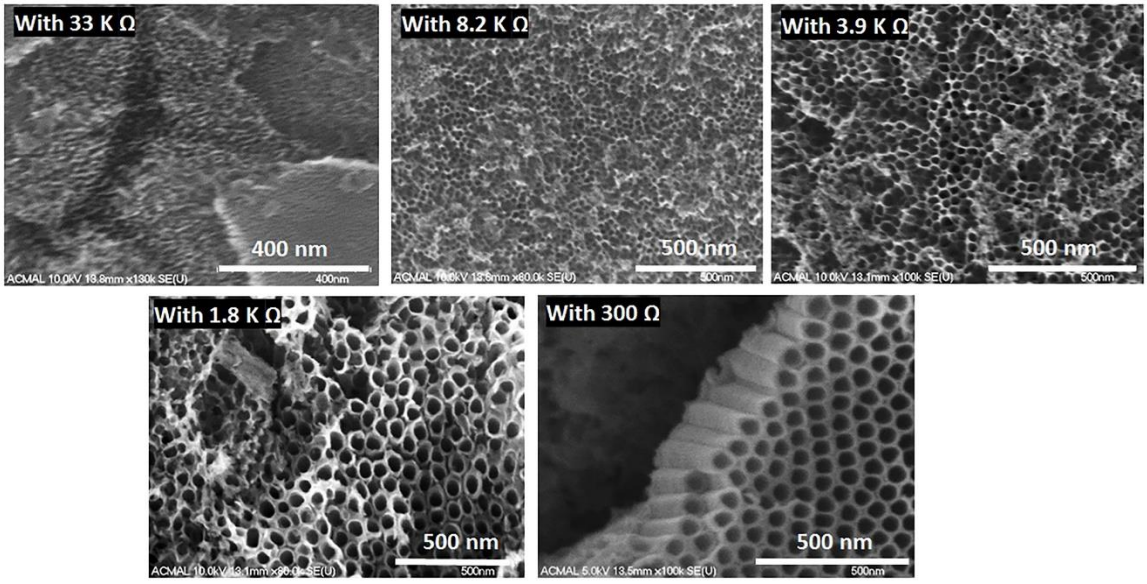

Figure 2.9 Effect of electrical resistances in series on morphology.

2.3.7 Effect of fluoride concentration in electrolyte

To investigate the influence of F^- ion concentration on the electrical conductivity of the electrolyte and resulting morphology, another set of experiments was conducted. LWHF electrolyte containing 2 vol% of DI water with varying concentration of NH_4F was used. FESEM micrographs in Fig.2.10 show the effects of varying F^- ion concentration in the electrolyte on anodized surface morphology. For 0.1 and 0.3 wt% NH_4F, only pores of diameter approximately 25 nm and 80 nm were observed respectively. Whereas using 0.66 wt% NH_4F, the formation of tubular morphology with 100 nm tube diameter was observed. Thus, among two factors viz. resistances in series simulating metals contamination in the electrolyte and varying F^- concentration in the electrolyte causing a decrease in electrical conductivity and current transients during anodization, the F^- concentration was observed to be the more influential factor affecting formation of porous or tubular structures.

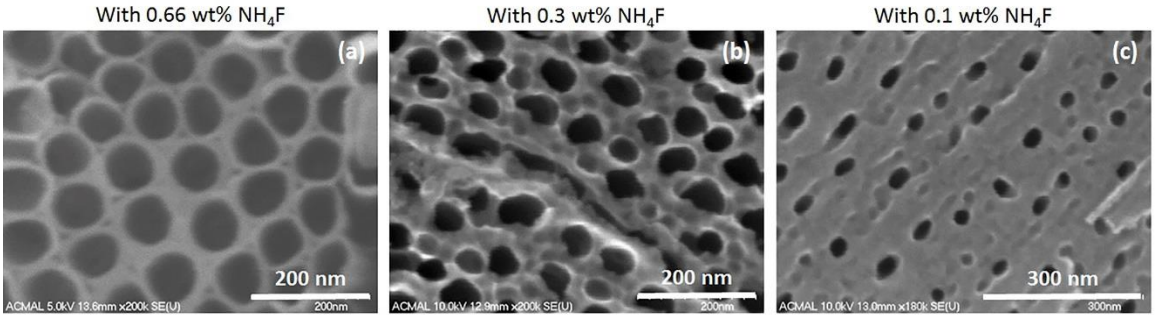

Figure 2.10 Effect of F^- ion concentration in electrolyte on morphology. Resulting structure using 0.6 wt% (a); 0.3 wt% (b); and 0.1 wt% (c); NH_4F in electrolyte solution.

2.3.8 Nanotubes fabricated on powder metallurgically made implants

The porous surfaces made by powder metallurgy (laser-sintered and electron-beam sintered) were anodized using HWLF electrolyte. Anodization voltage and time were varied in two different sets of experiments to obtain the processing conditions for the desired nanotube structure. The laser-sintered surfaces were anodized at 60V for 40 minutes in HWLF electrolyte. The tube diameter observed was 100 ± 10 nm and tube length was 500 nm (Fig.2.11). No nanotube morphologies were detected at 60V after 40 min anodization on electron-beam sintered surfaces (not shown here). Therefore, the electron beam- sintered surfaces were anodized at 30V for 4h. The tube diameter of 90 ± 10 nm and tube length of 450 ± 20 nm were observed (Fig.2.12). In both cases, tubes were observed on all powder particles and other surfaces to which powder particles were attached.

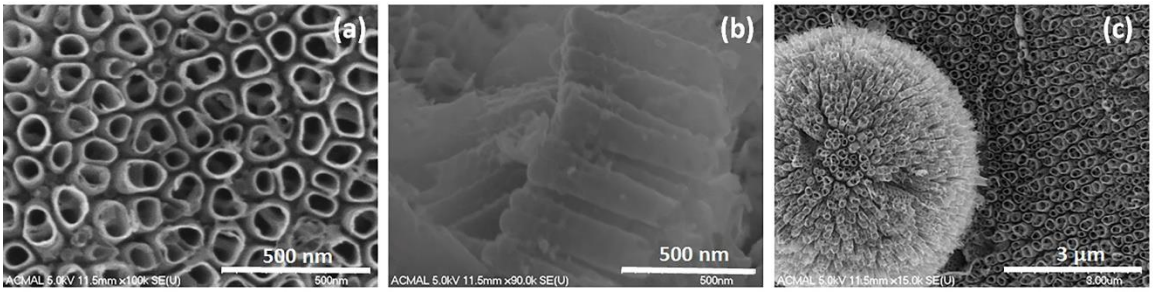

Figure 2.11 FESEM micrographs of nanotube surface formed on powder metallurgically manufactured laser-sintered Ti alloy surface with HWLF at 60V for 40 min. (a) top view of surface; (b) cross-section of nanotube layer; (c) nanotube morphology obtained on powder particles and underneath surface. (Samples were provided courtesy of Nanovation Partners, LLC).

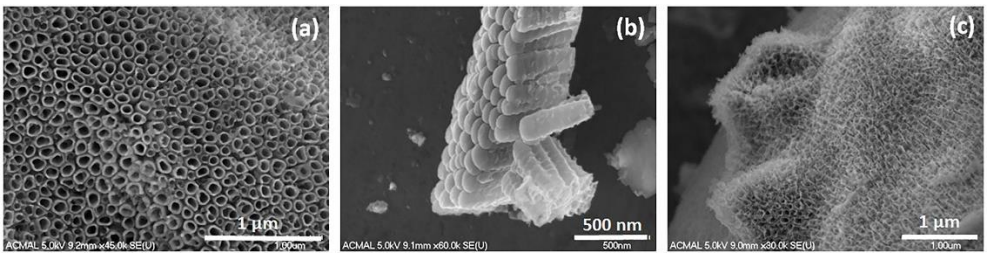

Figure 2.12 Nanotube surface formed on powder metallurgically manufactured electron beam-sintered Ti alloy surface with HWLF at 30V for 4h. (a) top view of surface; (b) cross-section of nanotube layer; (c) nanotube morphology obtained on powder particles and underneath surface. (Samples were provided courtesy of Nanovation Partners, LLC).

2.3.9 Chemistry of TiO_2 nanotubes fabricated on PM porous cylinders

The energy-dispersive X-ray spectroscopy (EDS) results summarized in Table 2.2 indicated the chemical composition of TiNT surfaces fabricated on powder metallurgically manufactured porous cylinders of Ti6Al4V. Residual fluorine of 3.79 and 4.51 wt% was observed in the laser-sintered and electron beam sintered surfaces. The possible source of nitrogen detected could be NH_4F added to make the electrolyte and carbon is detected from carbon tape used mounting the samples for FESEM-EDS examination. Because these materials were formed at high temperature, the chemistry may have changed from the initial alloy powder chemistry, with the possible addition of carbon.

Table 2.2 Comparison of chemical composition of TiNT surfaces on powder metallurgically manufactured titanium alloy surfaces.

Type of surface and anodization conditions	Relative wt% of elements						
	Ti	Al	V	O	F	C	N
Laser-Sintered (60V_40min)	60.76	5.35	1.58	23.41	3.79	0.15	4.97
E-beam Sintered (30V_4h)	56.97	5.54	1.09	26.32	4.51	0.63	4.94

2.3.10 Nanotubes fabricated on thermal plasma sprayed (TPS) titanium alloy surfaces

In vivo studies of thermal plasma sprayed (TPS) implants are reported to show increased bone contact and accelerated bone formation [18]. TPS alloy implant pieces were electrochemically anodized in HWLF electrolyte with two different anodization conditions on different implants to analyze nanotube morphology. Fig.2.13a shows a TiNT surface fabricated at 30V for 4h. The porous surface with an average pore size of 25-30nm was observed. Fig.2.13b shows a TiNT surface fabricated at 60V for 40 minutes. It is evident that the nanotubes were anodized on the entire surface covering all the macroscopic roughness features. Nanotube diameters of 35-40nm and lengths of 500nm were observed with 60V in 40min anodization. The TiNTs on the TPS alloy substrate were vertically oriented, laterally spaced and structurally stable. This porous network of nanotubes showed strong scratch resistance representing good mechanical strength needed to sustain surgical loads.

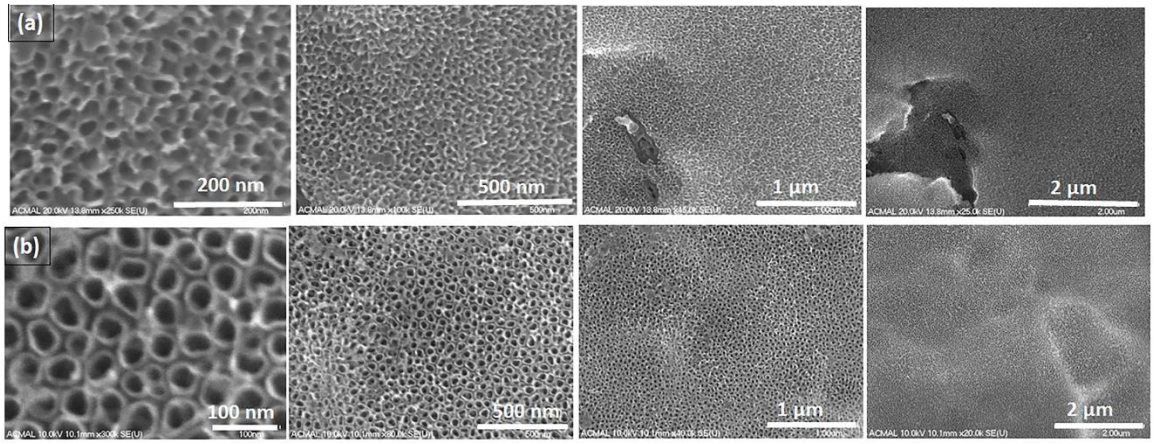

Figure 2.13 FESEM micrographs of nanotube surface formed on TPS titanium alloy with HWLF (a) at 30V in 4h; (b) at 60V in 40min.

2.3.11 Chemistry of TiO_2 nanotubes fabricated on TPS titanium alloy

The energy-dispersive spectroscopy results summarized in Table 2.3 indicated the chemical composition of TiNT surfaces fabricated on TPS Ti6Al4V. Residual fluorine of about 6.25 wt% was observed in nanotube surfaces anodized at 60V in 40 min. This residual fluorine was released upon annealing. In these, and all anodized surfaces, there is a large increase in oxygen indicating the formation of TiO_2 which is the biocompatible layer for titanium implants.

Table 2.3 Chemical composition of as-received and anodized TiNT on TPS titanium alloy surfaces

Type of surface and condition	Relative wt% of elements				
	Ti	Al	V	O	F
As-received TPS	89.04	8.88	2.07	--	--
Nanotube layer anodized on TPS at 60V in 40min	62.45	5.73	3.52	22.05	6.25

2.3.12 Nanotubes fabricated on K-wires

TiNT structures were fabricated on 1mm diameter K-wires of Ti6Al4V using LWHF electrolyte. These were used as femur implants in rats to study the influence of TiNT structure on bone formation and bone-implant stability via *in vitro* experiments as well as an *in vivo* model of femoral intramedullary fixation [19]. It has been demonstrated that osteogenic functions of cultured cells were improved on TiNT surfaces compared to as-received surfaces *in vitro* whereas, increased bone formation on TiNT surfaces was observed *in vivo*. Fig.2.14 shows as received and TiNT morphology achieved with anodization at 60V for 40 min. Tube diameters of 100 nm and length of 1 μm were observed. The chemical composition of as-received and the anodized TiNT surfaces fabricated on K-wires are summarized in Table 2.4. Residual fluorine of about 8.46 wt% was observed in the nanotube surface. Table 2.5. summarizes the surface properties and anodization conditions for different Ti6Al4V substrates.

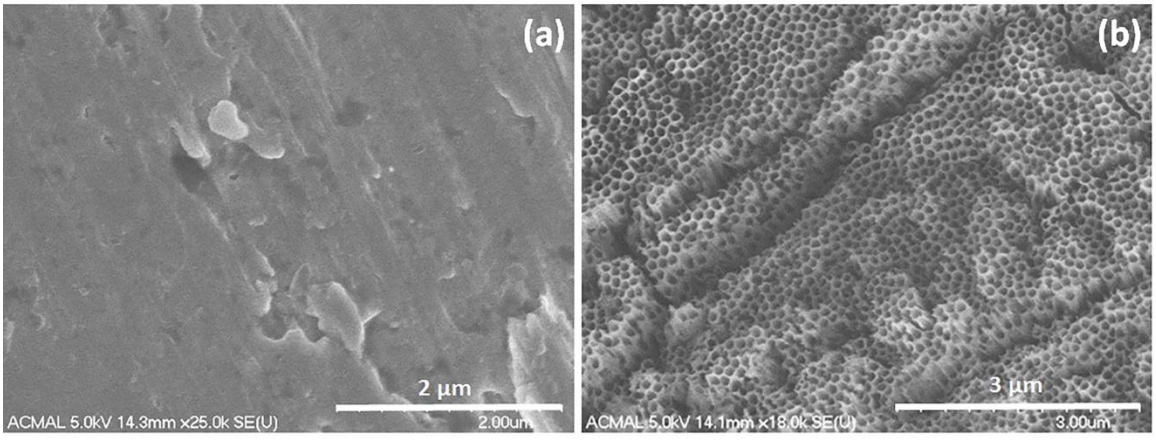

Figure 2.14 Micrographs of K-wires (a) as-received surface; (b) anodized in LWHF at 60V for 40 min showing nanotubes.

Table 2.4 Chemical composition of as-received and anodized TiNT on titanium alloy K-wires

Type of surface and condition	Relative wt% of elements				
	Ti	Al	V	O	F
As-received	89.6	7.13	3.05	0.21	0
TiNT layer anodized at 60V in 40min	58.26	3.81	1.76	27.7	8.46

Table 2.5 Surface properties and anodization conditions for different Ti6Al4V substrates.

Alloy substrate	Electrolyte	Anodization voltage	Anodization time	Tube diameter (nm)	Tube Length (μm)
Foil	LWHF	60V	40min	90 ± 10	4.5
Rod	LWHF	60V	40min	95 ± 5	4.7
Rod	HWLF	30V	4h	122	1.25
K-wire	LWHF	60V	40min	100	1
TPS	HWLF	60V	40min	35 - 40	0.5
TPS	HWLF	30V	4h	25 – 30	--
Laser-sintered PM part	HWLF	60V	40min	100 ± 10	0.5
Electron-beam sintered PM part	HWLF	30V	4h	90 ± 20	0.45

2.4 Conclusions

The present work showed that nanotextured morphology depends on electrolyte composition, and dimensional variation depends on anodization conditions on Ti6Al4V alloy surfaces using different NH_4F and ethylene glycol electrolytes. It was observed that different surfaces of Ti6Al4V need different electrolyte composition and anodization conditions to get nanotubes. This work will help to control morphology and dimensions of titanium oxide nanotubes for potential applications in biomedical implant applications. The much longer tube length of about 4.7 microns obtained in 40 minutes using LWHF electrolyte, compared to 1.25 micron obtained in 4h using HWLF, demonstrates a much more aggressive oxide dissolution rate with higher fluorine concentration in the electrolyte and higher anodization voltage. Resistances in series (simulating metals contamination) and varying F^- concentration in electrolyte caused a decrease in electrical conductivity and current transients during anodization. The F^- concentration was found to be the most influential factor affecting formation of porous nanostructures. This also showed that by inserting resistance in the anodization circuit, porous structures can be formed with the same electrolyte further demonstrating the versatility of this process. It was also shown that commercial TPS, and laser-sintered and electron-beam melted powder implants are easily processed to create nanotube surfaces.

References

[1] Niiomi M. Recent Metallic Materials for Biomedical Applications. Metallurgical and Materials Transactions A. 2002;33A:477-86.

[2] Balasundarama G, Webster TJ. A perspective on nanophase materials for orthopedic implant applications. Journal of Materials Chemistry. 2006;16:3737–45.

[3] Lausmaa J. Surface spectroscopic characterization of titanium implant materials. Journal of Electron Spectroscopy and Related Phenomena. 1996;81:343-61.

[4] Oh S, Daraio C, Chen LH, Pisanic TR, Finones RR, Jin S. Significantly accelerated osteoblast cell growth on aligned TiO_2 nanotubes. J Biomed Mater Res A. 2006;78:97-103.

[5] Jang I, Shim SC, Choi DS, Cha BK, Lee JK, Choe BH, et al. Effect of TiO_2 nanotubes arrays on osseointegration of orthodontic miniscrew. Biomed Microdevices. 2015;17:76.

[6] Zwilling V, Darque-Ceretti E, Boutry-Forveille A, David D, Y. PM, M. A. Structure and Physicochemistry of Anodic OxideFilms on Titanium and TA6V Alloy. Surface and Interface Analysis. 1999;27:629-37.

[7] Gong D, Grimes CA, OOmman KV, Wenchong H, Singh RS, Chen Z, et al. Titanium oxide nanotube arrays prepared by anodic oxidation. Journal of Materials Research. 2001;16:3331-34.

[8] Cai Q, Paulose M, Varghese OK, Grimes CA. The effect of electrolyte composition on the fabrication of self-organized titanium oxide nanotube arrays by anodic oxidation. Journal of Materials Research. 2011;20:230-6.

[9] Xiao X, Ouyang K, Liu R, Liang J. Anatase type titania nanotube arrays direct fabricated by anodization without annealing. Applied Surface Science. 2009;255:3659-63.

[10] Lai YK, Sun L, Chen C, Nie CG, Zuo J, Lin CJ. Optical and electrical characterization of TiO_2 nanotube arrays on titanium substrate. Applied Surface Science. 2005;252:1101-6.

[11] Paulose M, Grimes CA. Anodic Growth of Highly Ordered TiO_2 Nanotube Arrays to 134 μm in Length. Journal of Physical Chemistry Letters B. 2006;110:16179-82.

[12] Friedrich CR, Shokuhfar T. Compositions methods and devices for generating nanotubes on a surface. United States Patent US 20130196128. 2016.

[13] Roy P, Berger S, Schmuki P. TiO_2 nanotubes: synthesis and applications. Angewandte Chemie International Edition Engl. 2011;50:2904-39.

[14] Yasuda K, Schmuki P. Control of morphology and composition of self-organized zirconium titanate nanotubes formed in $(NH_4)_2SO_4/NH_4F$ electrolytes. Electrochimica Acta. 2007;52:4053-61.

[15] Valota A, LeClere DJ, Skeldon P, Curioni M, Hashimoto T, Berger S, et al. Influence of water content on nanotubular anodic titania formed in fluoride/glycerol electrolytes. Electrochimica Acta. 2009;54:4321-7.

[16] Yasuda K, Schmuki P. Formation of Self-Organized Zirconium Titanate Nanotube Layers by Alloy Anodization. Advanced Materials. 2007;19:1757-60.

[17] Bhosle SM, Tewari R, Friedrich CR. Dependence of nanotextured titanium orthopedic surfaces on electrolyte condition. Journal of Surface Engineered Materials and Advanced Technology. 2016;06:164-75.

[18] Darimont GL, Cloots R, Heinen E, Seidel L, Legrand R. In vivo behaviour of hydroxyapatite coatings on titanium implants: a quantitative study in the rabbit. Biomaterials. 2002;23:2569-75.

[19] Vara A, Baker EA, Salisbury M, Fleischer M, Bhosle SM, Friedrich C, et al. Enhancing osseointegration of orthopaedic implants with titania nanotube surfaces. Foot & Ankle Orthopaedics. 2016;1:1.

Chapter 3

Dependence of nanotextured titanium orthopedic surfaces on electrolyte condition†

Sachin M. Bhosle[1,2], Radheshyam Tewari[1], Craig R. Friedrich[1]

[1] *Department of Mechanical Engineering, Multi-Scale Technologies Institute, Michigan Technological University. USA*

[2] *Vidya Pratishthan's Kamalnayan Bajaj Institute of Engineering and Technology, Baramati, India*

Abstract

Electrochemical etching of titanium alloy in a fluoride-containing electrolyte results in ordered nanotextured surfaces. The reproducibility of nanotextured surfaces depends on several process parameters, most notably the fluoride ion concentration in the electrolyte. In the present work, electrochemical etching of Ti6Al4V alloy foils in ethylene glycol containing 0.66 wt% NH_4F and 2% deionized water was carried out at 60V for 45 minutes. This paper describes the depletion of fluoride ion concentration and contamination of electrolyte upon reuse. Inductively coupled plasma-optical emission

**The material contained in this chapter has been published in the Journal of Surface Engineered Materials and Advanced Technology, 2016, 6, 164-175. As the first author of this publication, I have done the fabrication of nanotube surfaces, SEM and EDS characterization, samples preparation for ICP-OES examination, literature review, results analysis and writing the manuscript.*

spectroscopy was used to measure the dissolution of metal oxides in the electrolyte during etching. We found increasing concentration of the alloy elements Ti, Al, V contaminated the electrolyte due to repeated reuse of the electrolyte. The results show an appreciable log-linear depletion of fluoride ion concentration resulting in a changed surface morphology, chemical composition and etched volume. This paper provides an important insight to changes in surface morphology and surface chemistry with extended reuse of the etching electrolyte, useful for regulatory approvals.

3.1 Introduction

Titania nanotubes on orthopedic implants is of scientific interest due to their biocompatibility. Ordered nanotextured titanium surfaces has been an attractive approach as a material for applications in the biomedical field [1]. One of the challenges is to improve bone bonding because of the lack of porosity and ingrowth of apatite deposits in the pores at the bone-implant interface [2]. This results in loosening of the implant due to a lack of osseointegration, or osteolysis, which calls for modifications in implant surface. TiO_2 nanotubes can increase bone-like apatite formation, cell proliferation and osseointegration [3]. TiO_2 tubes can be fabricated on the surface of titanium implants using an electrochemical anodization technique. Ordered nanotubular titania structures can be fabricated in the presence of fluoride ions in an electrolyte using appropriate anodization parameters [4]. The controlled morphology and thickness of porous TiO_2 nanotextured films can be achieved by controlling the anodization parameters [5]. Fabrication of TiO_2 nanotubes during electrochemical anodization is a result of the formation of an anodic

oxide layer followed by field-assisted chemical dissolution [6]. Fabricated nanotubes show compositional and morphological variations as a result of variations in process parameters, including anodization voltage, time, and fluoride concentration. The fluoride ion concentration in the electrolyte is one of the important parameters to achieve repeatability of the etched surface. Fluoride concentration in the electrolyte is reported to be the most influential factor for titania nanotubes etched in ethylene glycol-H_2O electrolyte containing NH_4F [7]. The fluoride ions in the electrolyte are reported to perform two important functions after initial oxide growth on the Ti surface. First, it reacts with dissolved Ti^{4+} ions at the oxide-electrolyte interface and forms soluble $[TiF_6]^{2-}$ complex. Secondly, it chemically dissolves TiO_2 and then forms the $[TiF_6]^{2-}$ complex [8]. Thus, a competition between metal oxide formation and chemical dissolution continues leading to the formation of nanotubes. This sequence of reactions needs to be controlled to repeatedly fabricate highly-ordered nanotubular morphology. Knowing that the chemistry of the process changes with repeated use of the electrolyte, a better understanding of the manufacturing process is the focus of this work. Many studies have addressed the growth mechanism and morphologies of TiO_2 nano-tubular structures. However, less attention has been paid to the morphological changes upon extensive reuse of the electrolyte, which is critical in a manufacturing scenario.

3.2 Materials and Methods

3.2.1 Substrate preparation

Foils of Ti6Al4V alpha/beta titanium alloy of ASTM B 265-11 grade 5 (TIMET, USA) and 0.5 mm thick, were mechanically polished using #150 grit fine crocus cloth and #800 grit ultra-fine sanding cloth. After cleaning in deionized (DI) water followed by acetone, the samples were dried in air at room temperature. Coupons 75 mm x 10 mm x 0.5 mm thick were cut from the foils to etch 1500 mm^2 on each sample, including both sides.

3.2.2 Fabricating nanotubular and nanoporous structures

The nano-structures were etched by electrochemical anodization of Ti6Al4V alloy using a DC power source (Protek 3006B), with direct current (DC) output 0 – 60V, 1.5 A. Electrolyte containing 98% ethylene glycol, 2% DI water and 0.66 wt % of NH_4F was used for etching. The surfaces were electrochemically anodized at room temperature and 60V for 40 minutes with a graphite rod as the cathode and the titanium alloy foil as the anode.

3.2.3 Morphological and compositional characterization

Characterization of the anodized surfaces was done using field emission scanning electron microscopy (FE-SEM, Hitachi S-4700). The chemical composition of the TiNT surfaces used energy dispersive spectroscopy (EDS) with standardless quantitative analysis on the FESEM at 10 kV. Topographical analysis of the surface texture was conducted using white light interferometric microscopy with nanometer vertical resolution and submicron lateral resolution to measure the volume of the alloy removed upon etching.

3.2.4 Measurement of fluoride-ion concentration

A fluoride ion sensitive electrode ISE (Oakton Instruments, USA) was used for determination of the fluoride concentration in electrolyte samples by direct measurement of fluoride ions after electrode calibration. The electrolyte was mixed by a magnetic stirrer. The pH and fluoride concentration were measured in the bulk electrolyte prior to anodization of each coupon, and after anodization of each coupon by removing 1ml of electrolyte and adding 4.5ml TISAB I buffer solution (Sigma-Aldrich). All measurements were carried out 24 ± 4ºC.

Before the measurements, 1x and 10x NaF standard solutions in 50 ml DI H_2O+50 ml TISAB I was prepared. These standard solutions were used before starting the experiment for a slope check of the ISE to ensure performance within calibration limits. Additionally, standard solutions using 1, 10, 100, 1000 and 5000 ppm concentrations of NaF (with TISAB I) and NH_4F (with TISAB I and w/o TISAB I) were used to prepare calibration plots. One calibration plot was prepared using NaF + TISAB I + DI water as the fluoride standard solution. The other two calibration plots were prepared using standard solutions of NH_4F + DI water + ethylene glycol (with TISAB I and w/o TISAB I). While preparing the NH_4F standard solutions, it was ensured that the molarity of F^-ions was between 10^{-1} and 10^{-5} and the pH was between 5 and 9 to avoid interference of hydroxide ions on electrode response. TISAB I was added to avoid hydroxide interferences or the formation of hydrogen complexes of fluoride and thus to maintain pH of standard solution and the 1 ml electrolyte samples.

3.2.5 ICP-OES trace metal analysis

An inductively coupled plasma-optical emission spectrometer (Perkin Elmer, Optima 7000 DV, USA) was used with 1400 Watts RF power to measure Ti, Al, and V trace metal elements in the electrolyte. Wavelengths of 334.940 nm for Ti (II), 396.153 nm for Al (I) and 292.464 nm V (II) were used. For determination of dissolved metals in the electrolyte after each coupon was anodized, a 10ml sample form the bulk electrolyte was dried at 250ºC in Teflon evaporating dishes with subsequent addition of 10 ml 2% nitric solution. All analyses were performed in one replicate of each element and the average values have been reported. The standard measurements ranged from 0.1-20.0 mg/L. For the Ti analysis, a 1:10 dilution was made prior to analysis so that the samples fell within the calibration range.

3.3 Results and Discussion

3.3.1 Morphological analysis

A distinct fluoride rich layer exists between the tube-walls at the triple point of ordered TiO_2 nanotubes etched in the electrolyte [9]. The morphological transition from pores to tubes as a result of increased fluoride concentration occurs due to chemical solubility of the triple point cell boundaries where a fluoride rich layer accumulates [10]. The transition from pores to tubes is due to high chemical dissolution occurring in the fluoride rich layer [6]. The fluoride rich boundaries get suppressed in viscous electrolytes which results in formation of nano-pores instead of tubes [11]. Thus, the process of

morphology transition from pores to tubes is favored by the fluoride rich layer formed between the nanotube cell boundaries.

The morphological changes in surface aggregate from tubular nano-grass to porous film formation on the top of the surface aggregate was observed with depleting fluoride con-centration upon extended use of the electrolyte. Depending on the F^- concentration, morphologically different structures were obtained. With fresh electrolyte, distinct nanotubes were fabricated. With well-used electrolyte after 20 coupons, the morphology was much more porous and roughened. The authors hypothesize that upon extended reuse of the electrolyte, the decreased F^- ion concentration lowered the ionic migration. Surfaces obtained from electrochemical etching of Ti6Al4V alloy foils in EG-based electrolyte are shown in Fig.3.1 and 3.2. Fig.3.1a shows the as-anodized surface aggregate which shows a tubular nano-grass obtained in fresh electrolyte. The as-anodized surfaces were always covered with this oxide layer which can be removed with ultrasonication. Fig.1b. shows the sonicated surface revealing close packed, well-rounded, open-tubular morphology after removal of the nano-grass. The tubes have smooth walls and are well-ordered. In Fig.3.2, the morphological variation obtained with reused electrolyte in the form of a porous-film on the top of surface aggregation is shown after 22 anodization cycles on 22 different coupons. Thus, a change in morphology of the surface aggregate occurred, but no significant difference in the tubular morphology underneath was observed with fresh or reused electrolyte. This implies that after anodizing the 22 coupons, there is still enough fluorine in the electrolyte to produce ordered tubular morphology and the minimum

concentration of fluoride is not reached which may affect the etched tubular structures underneath.

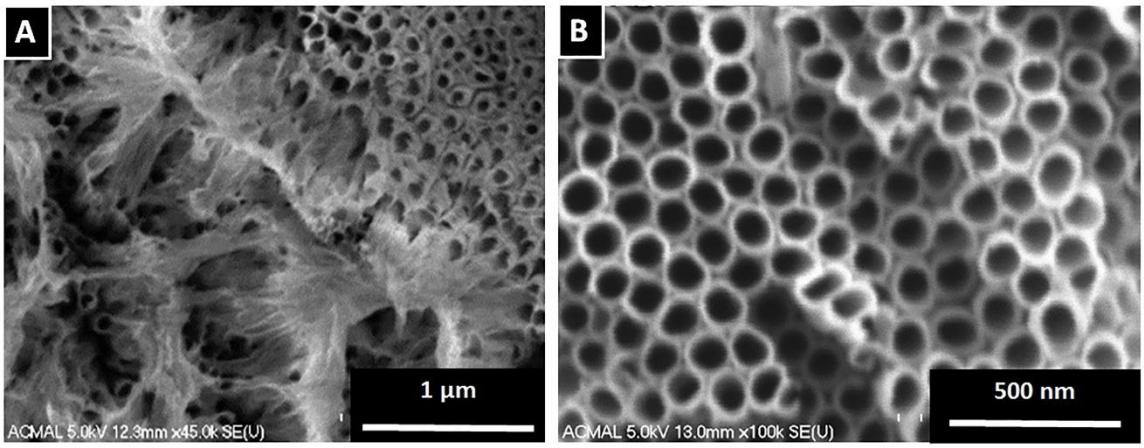

Figure 3.1 FESEM top view of the nanotextured surface fabricated with fresh electrolyte: (a) As-anodized oxide surface (tubular nano-grass) on top of nanotubes, (b) Ordered network of well-rounded TiO_2 nanotubes after ultrasonic agitation.

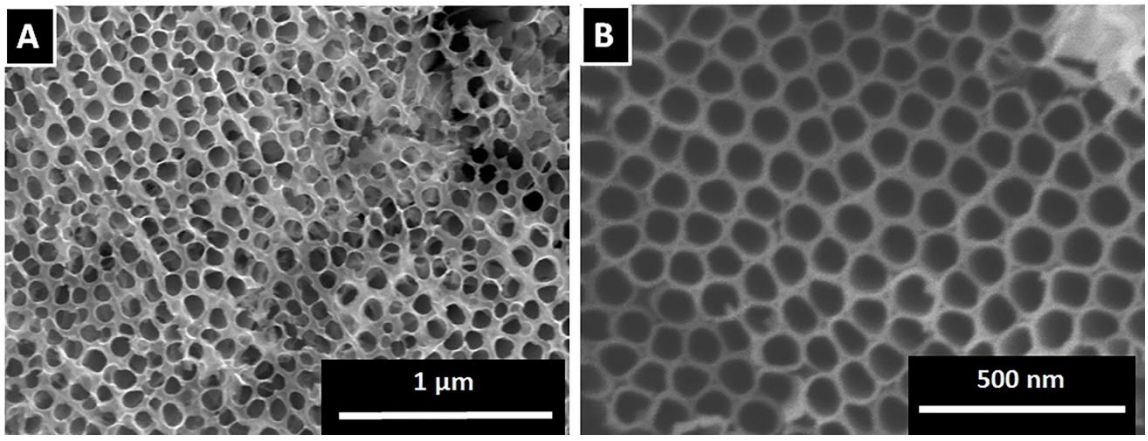

Figure 3.2 FESEM top view of the nanotextured surface fabricated with reused (aged) electrolyte: (a) As-anodized porous film on the top of surface aggregation, (b) Ordered network of well-rounded TiO_2 nanotubes after ultrasonic agitation.

3.3.2 Depletion of fluoride concentration Vs cumulative area etched

The fluoride concentration in the electrolyte is an important parameter for controlled electrochemical anodization. A higher fluoride concentration creates higher current densities during anodization [12]. A total of 36000 mm^2 was etched by anodizing 24 coupons each with 1500 mm^2 area on each sample. Fig.3.3a summarizes the depleted F^- concentration corresponding to the cumulative etched area upon reuse of the electrolyte. The fluoride concentration in the fresh electrolyte was 3033 ppm, and decreased to 333 ppm after etching 36000 mm^2. It is evident from these measurements and SEM images that a fluoride concentration control strategy must be advanced. Our results showed a log-linear depletion of F^-concentration as a function of area anodized which can be used to effectively adjust the fluorine by periodic addition to the electrolyte. If the F^- concentration in the electrolyte reduces below 0.3 wt% of NH_4F, it can affect the resulting morphology. Fig.3.3b summarizes the log-linear relation corresponding to the cumulative etched area upon reuse of the electrolyte. As this technology moves toward integration with current implants, it is required to understand and control the manufacturing process to ensure reproducible results on a large scale and with different sizes of implants based only on the implant surface area.

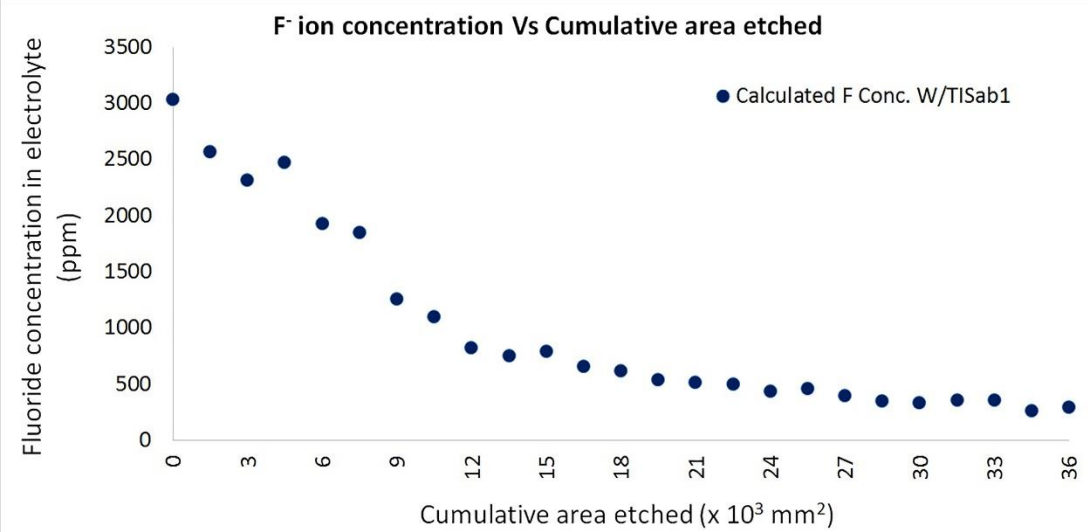

Figure 3.3a F^- concentration measurement using ion sensitive electrode from electrolyte samples with TISAB I.

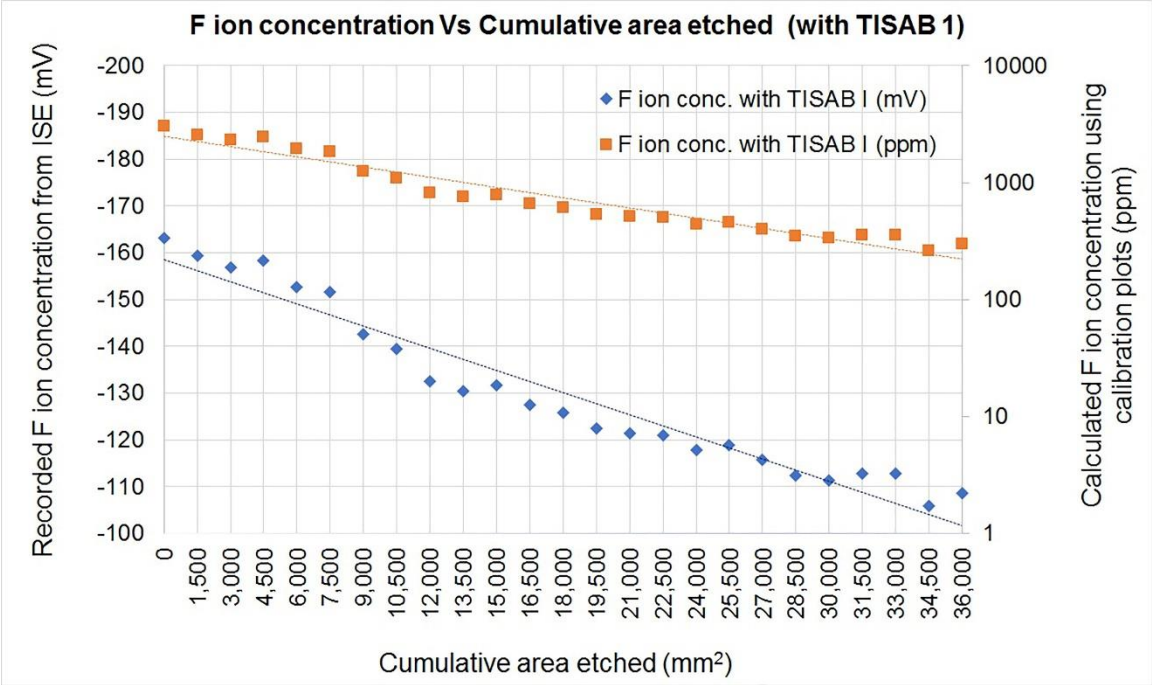

Figure 3.3b F^- concentration measurement (log-linear relation between the F^- concentration and the area anodized).

3.3.3 Effect on current transients

TiNT formation is a reflection of current-time transient analysis [6]. The current-time profile reflects film growth leading to the corresponding morphologies [13]. Variation in current densities affects the etching rate which also causes variation in tube diameters [14]. The higher diffusibility and concentration of ions in aqueous electrolytes gives much higher current densities compared to organic electrolytes [15]. The oxidation of titanium and chemical dissolution creates changes in the electrolyte chemistry. Fig.3.4 shows three distinct stages of the current-time transient recorded at 60 V during anodization. Three stages (I, II, III) were observed for samples 2, 10 and 20 etched in the same electrolyte solution. Each sample had an etched area of 1500 mm^2. At the start of anodization, when the potential is applied, the initial anodic current reached maximum. This initiated the formation of oxide on the metal foil anode. Then, the current quickly dropped showing formation of the oxide layer. During stage II, the resistance of the anodic film decreased and the current density increased demonstrating the pore nucleation due to selective dissolution of oxide by fluoride species. This local breakdown of an initially formed oxide layer caused eventual development of tiny pits and pores in the compact oxide film. This facilitated ion transport causing a slight increase in anodic current [13]. The continued deepening of pores causes the inter-pore sites to become high surface energy regions which attracts more F^- ions leading to faster dissolution of oxides there [16]. Finally, at stage III, a slowly decreasing current value was attained over the entire anodization time demonstrating steady state formation of nanostructures by field-assisted oxidation and dissolution of metal oxides into the electrolyte. The slight step in sample 2 near 1200

seconds is an artifact of the etching experiment and may have been due to a slight movement of the cathode causing a temporary change in etching rate. This was not seen in any other experiments.

Higher fluoride concentration in the electrolyte creates higher current densities during anodization [12]. Our results show that, the first current peak was observed in approximately the same position for all fluoride concentrations. Just after the first peak, decreased current shown by a distinct second peak demonstrated morphological changes. Thus, decreased current densities are the result of depleted fluoride in the electrolyte upon reuse. The formation of fluoride complexes at cell boundaries is an essential condition for higher chemical dissolution of metals to achieve tubular morphology. Hence suppressed dissolution of F^- rich layer resulted in morphological variation.

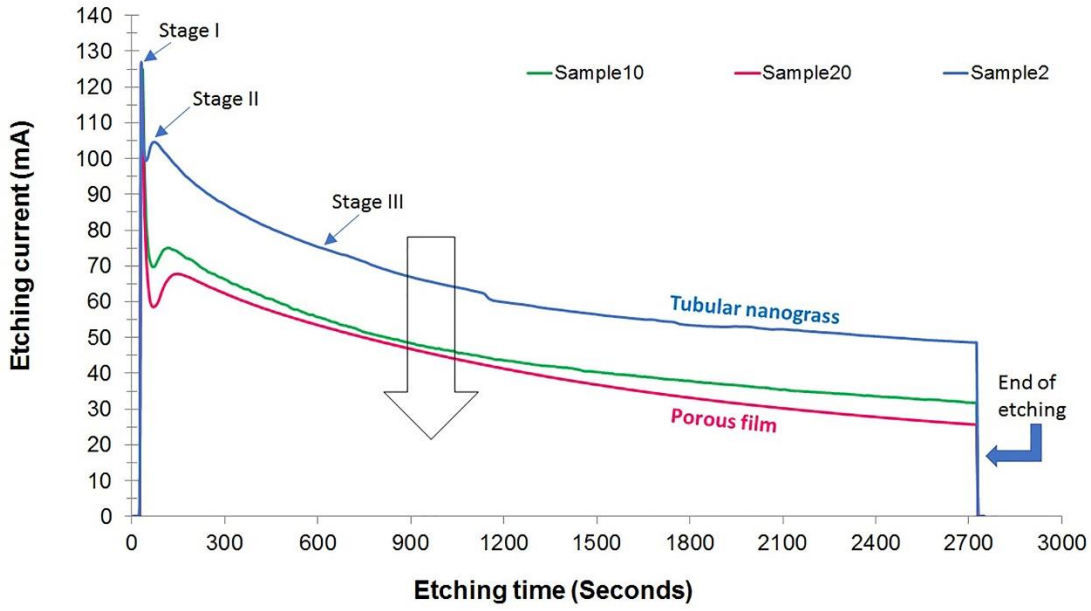

Figure 3.4 Current-time profile recorded during anodization.

3.3.4 Effect on macroscale volume removal

Fig.3.5 shows the estimated etched volume of the anodized surfaces using white light interferometric microscopy to evaluate volume removed upon etching with respect to cumulative etching time. It was observed that anodization roughens the surfaces. The volume removed during anodization was calculated from the difference between baseline volume of an unetched area and the final volume of the etched area. The decrease in volume removed during the same anodization duration can be attributed to the depleted fluorine. The variation of the surface topographies due to depleted fluorine is tabulated in Table 3.1.

Table 3.1 3D topographic parameters of 400 µm x 400 µm scanning area.

Sample #	Cumulative Etching Time (Hrs.)	Final Volume (Etched Area) (x 10^6 µm^3)	Baseline Volume (Unetched Area) (x 10^5 µm^3)	Volume Removed (Final – Baseline) (x 10^5 µm^3)
2	1.5	3.027	2.357	27.913
10	7.5	2.328	2.452	20.828
20	15	1.313	2.689	10.441

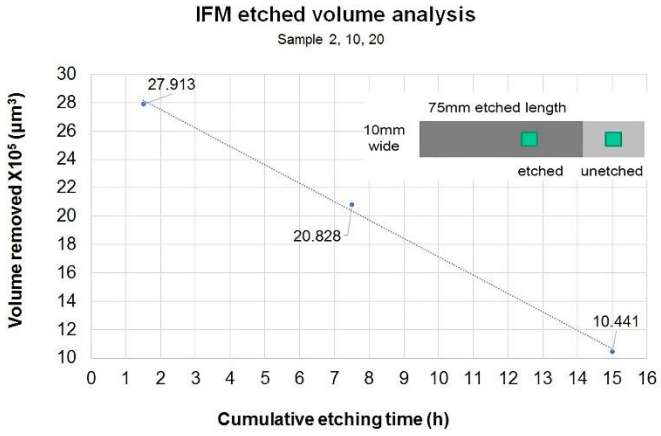

Figure 3.5 Estimation of volume removed during etching.

3.3.5 Electrolyte contamination due to metals dissolution

The higher electric field intensity during the initial stage of anodization leads to larger oxide breakdown sites resulting in larger diameter nanotubes. The dissolution rate of oxide formation is affected by the pH of the electrolyte [17]. More acidic pH linearly increases the dissolution rate [18]. Fig.3.6a and 3.6b shows ICP-OES measurements of the dissolved titanium, aluminum, and vanadium in the electrolyte. Our results show that reuse of the electrolyte led to a linear increase in metals as would be expected. This analysis provides guidelines for the control of the electrolyte chemistry, for both remaining fluorine and metals contamination, to ensure repeatable results when the electrolyte is reused instead of disposed of reducing environmental impact for large scale manufacturing.

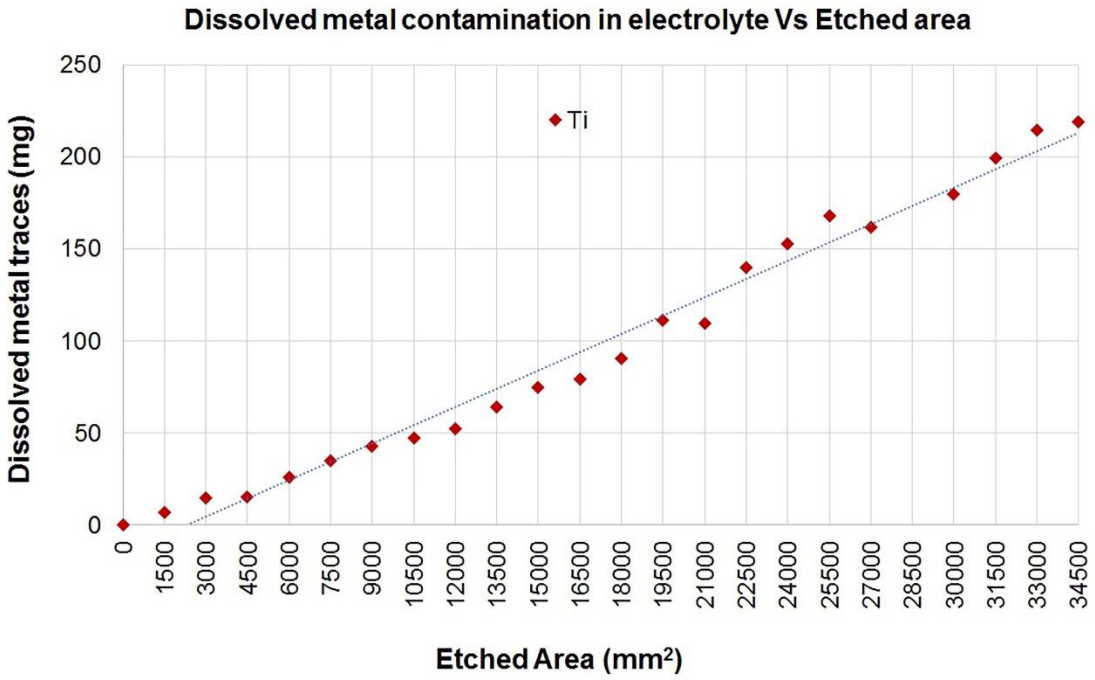

Figure 3.6a ICP-OES analysis of titanium contamination in electrolyte.

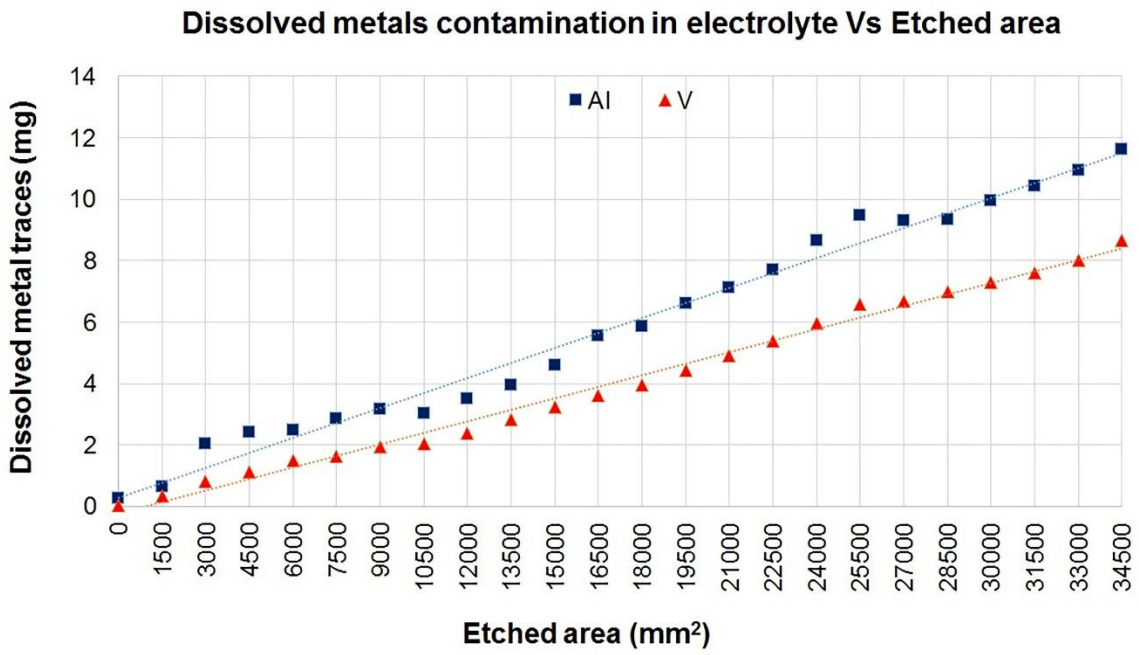

Figure 3.6b ICP-OES analysis of aluminum and vanadium contamination in electrolyte.

In Fig.3.4, the current amplitude of sample 2 represents new electrolyte with a higher level of fluorine and fewer non-conductive metal oxide particles distributed in the electrolyte. As cumulative etching progresses, the current decreases in an asymptotic fashion which follows the similar fluorine depletion shown in Fig.3.3a. Additionally, the introduction into the electrolyte of the etched oxides of titanium, aluminum, and vanadium shown in Fig.3.6a and 3.6b reduces the electrical conductivity of the electrolyte further reducing etching current. These two combined effects cause the progressive etching current to reduce exponentially to an asymptotic condition similar to Fig.3.3a. This is the reason the current traces of samples 10 and 20 are similar and nearer in magnitude than sample 2.

The decreasing trend of the etching current over time for a particular sample is primarily due to the formation of the nanotubes that have a relatively high aspect ratio,

depth to diameter. Fluorine is the element responsible for etching and as the nanotube is deepened, the local etch rate is diffusion-limited by the ability to introduce fluorine at the inside bottom of the nanotube. As the nanotube grows deeper, the fluorine concentration at the bottom reduces due to this diffusion-limited effect and the overall etch rate, and therefore etching current reduces. Thus, besides F depletion, the other subsequent effects such as decrease in etching current occurred because of eventually dissolved metals contamination are also important.

3.3.6 EDS analysis

Chemical compositional analysis of the anodized surfaces by EDS was also undertaken and typical results are shown in Table 3.2. The structures were characterized to compare the effect of the fresh and reused electrolyte. The greatly increased oxygen content represents the formation of the stable oxide during anodization. The structures obtained using fresh electrolyte shows 35wt% oxygen and 12wt% residual fluorine, whereas the structure obtained using aged electrolyte shows 27wt% oxygen and 9wt% residual fluorine. The lower residual fluorine with the reused reflects the depleted fluorine in the electrolyte. During anodization, the growth of nanotubes leads to the formation of hexafluorotitanate complex TiF_6^{2-} by fluorine diffusion from electrolyte to titanium [4]. The presence of fluorine in the anodized surfaces is indicative of the diffused TiF_6^{2-} during etching rather than free fluoride ions. The decreased fluorine wt% observed in nanotextured surfaces can be attributed to fewer TiF_6^{2-} complexes formed.

Table 3.2 Relative chemical composition of control and as-anodized surfaces.

TiNTs and TiNPs on alloy	wt % of elements				
	Ti	Al	V	F	O
Control	88.68	7.27	3.90	0	0.15
Tubular nano-grass (sample #1)	47.51	3.64	2.57	11.99	34.29
Porous nano-film (Sample #23)	56.30	3.51	2.76	9.46	27.98

3.4 Conclusions

The experimental results of reusing the electrolyte for many samples, rather than disposing the electrolyte after each use, leads to several important conclusions from a manufacturing perspective. First, the amount of fluorine removed from the electrolyte is accounted for by its presence in the anodized surface. This fluorine may be of benefit as the hydroxyapatite of bone contains fluorine. However, this effect is still to be determined from a biological perspective. From a manufacturing control perspective, the reduction of fluorine in the electrolyte available for repeatable anodization of nanostructures reduces in a log-linear fashion, in this case from an initial value of approximately 3000ppm to approximately 300ppm after 34,500mm^2 was etched. Such a behavior leads to a relatively easy prediction of the remaining fluorine concentration as a function of implant area etched, knowing the initial concentration. This strategy would replenish fluorine periodically depending on the total or incremental area of implants anodized. This control is important as we have shown that the volume of the implant removed varies as the electrolyte is reused, leading to a variable morphology progressing from distinct nanotubes to a simpler porous surface. By knowing *a priori*, the area of each duplicate or different

implant in a manufacturing process, the fluorine content in the electrolyte could be controlled.

The metal removed from the surface during anodization is accounted for in the electrolyte. Again, the presence of each alloying element in the electrolyte increases in a linear fashion. EDS has been conducted on the cathode used in the process and there are no metals present so the electrolyte represents all metal removed. With this well-behaved increase in metals in the electrolyte, removal of those metal particles by batch centrifugation or continuous filtration, will provide for easy process control.

Acknowledgements

This work performed under the M-TRAC program was supported by Grant Case-48161 of the 21st Century Jobs Trust Fund received through the Michigan Strategic Fund from the State of Michigan. The M-TRAC program is funded by the Michigan Strategic Fund with program oversight by the Michigan Economic Development Corporation.

References

[1] Macak JM, Tsuchiya H, Taveira L, Ghicov A, Schmuki P. Self-organized nanotubular oxide layers on Ti-6Al-7Nb and Ti-6Al-4V formed by anodization in NH_4F solutions. J Biomed Mater Res A. 2005;75:928-33.

[2] Liang B, Fujibayashi S, Neo M, Tamura J, Kim H-M, Uchida M, et al. Histological and mechanical investigation of the bone-bonding ability of anodically oxidized titanium in rabbits. Biomaterials. 2003;24:4959-66.

[3] Li B, Li Y, Li J, Fu X, Li C, Wang H, et al. Improvement of biological properties of titanium by anodic oxidation and ultraviolet irradiation. Applied Surface Science. 2014;307:202-8.

[4] Macak JM, Tsuchiya H, Ghicov A, Yasuda K, Hahn R, Bauer S, et al. TiO_2 nanotubes: Self-organized electrochemical formation, properties and applications. Current Opinion in Solid State and Materials Science. 2007;11:3-18.

[5] Yin H, Liu H, Shen WZ. The large diameter and fast growth of self-organized TiO_2 nanotube arrays achieved via electrochemical anodization. Nanotechnology. 2010;21:035601.

[6] Regonini D, Bowen CR, Jaroenworaluck A, Stevens R. A review of growth mechanism, structure and crystallinity of anodized TiO_2 nanotubes. Materials Science and Engineering: R: Reports. 2013;74:377-406.

[7] Robin A, Bernardes de Almeida Ribeiro M, Luiz Rosa J, Zenhei Nakazato R, Borges Silva M. Formation of TiO_2 nanotube layer by anodization of titanium in ethylene glycol-

H_2O electrolyte. Journal of Surface Engineered Materials and Advanced Technology. 2014;04:123-30.

[8] Parcharoen Y, Kajitvichyanukul P, Sirivisoot S, Termsuksawad P. Hydroxyapatite electrodeposition on anodized titanium nanotubes for orthopedic applications. Applied Surface Science. 2014;311:54-61.

[9] Berger S, Albu SP, Schmidt-Stein F, Hildebrand H, Schmuki P, Hammond JS, et al. The origin for tubular growth of TiO_2 nanotubes: A fluoride rich layer between tube-walls. Surface Science. 2011;605:L57-L60.

[10] Roy P, Berger S, Schmuki P. TiO_2 nanotubes: synthesis and applications. Angewandte Chemie International Edition. 2011;50:2904-39.

[11] Ali G, Chen C, Yoo SH, Kum JM, Cho SO. Fabrication of complete titania nanoporous structures via electrochemical anodization of Ti. Nanoscale Res Lett. 2011;6:332.

[12] Macak JM, Hildebrand H, Marten-Jahns U, Schmuki P. Mechanistic aspects and growth of large diameter self-organized TiO_2 nanotubes. Journal of Electroanalytical Chemistry. 2008;621:254-66.

[13] Liu H, Tao L, Shen W. Controllable current oscillation and pore morphology evolution in the anodic growth of TiO_2 nanotubes. Nanotechnology. 2011;22:155603.

[14] Tsuchiya H, Macak JM, Ghicov A, Räder AS, Taveira L, Schmuki P. Characterization of electronic properties of TiO_2 nanotube films. Corrosion Science. 2007;49:203-10.

[15] Tsuchiya H, Macak JM, Taveira L, Balaur E, Ghicov A, Sirotna K, et al. Self-organized TiO_2 nanotubes prepared in ammonium fluoride containing acetic acid electrolytes. Electrochemistry Communications. 2005;7:576-80.

[16] Cao C, Li J, Wang X, Song X, Sun Z. Current characterization and growth mechanism of anodic titania nanotube arrays. Journal of Materials Research. 2011;26:437-42.

[17] Indira K, Mudali UK, Nishimura T, Rajendran N. A review on TiO_2 nanotubes: Influence of anodization parameters, formation mechanism, properties, corrosion behavior, and biomedical applications. Journal of Bio- and Tribo-Corrosion. 2015;1.

[18] Macak JM, Tsuchiya H, Schmuki P. High-aspect-ratio TiO_2 nanotubes by anodization of titanium. Angewandte Chemie International Edition Engl. 2005;44:2100-2.

Chapter 4

Wetting behaviour and chemistry of titanium nanotubular orthopedic surfaces: Effect of aging and thermal annealing*

Sachin M. Bhosle[1,2], Craig R. Friedrich[1]

[1] *Department of Mechanical Engineering, Multi-Scale Technologies Institute, Michigan Technological University. USA*

[2] *Vidya Pratishthan's Kamalnayan Bajaj Institute of Engineering and Technology, Baramati, India*

Abstract

In the present work, the wetting behaviour and chemical composition of anodized titanium nanotubular surfaces for orthopedic implants was investigated. The wetting behaviour of the nanotubes by alternating UV irradiation and dark storage is reported. This study suggests that hydrophobicity due to aging in air can be restored by annealing, and release of residual fluorine was observed as a function of annealing time, which is important considering side-effects of fluorosis. Fabrication of nanotubes on thermal plasma sprayed implants and super-hydrophilic behaviour of these nanotubular surfaces needed for enhanced bioactivity was demonstrated.

---

* *The material contained in this chapter is in preparation for submission to a journal. As the first author of this publication, I have done the fabrication of nanotube surfaces, SEM and EDS characterization, water contact angle measurements, literature review, results analysis and writing the manuscript.*

4.1 Introduction

Surfaces capable of promoting osseointegration will be beneficial for orthopedic implants. Increasing the surface wettability of titanium nanotube surfaces by post-anodization annealing has been shown to enhance *in vitro* osteoblast proliferation. The hydrophilic to hydrophobic transition of Ti-based nanotubular surfaces due to aging in air is well known [1]. Enhanced osteoblast adhesion and proliferation is influenced by surface morphology, topography and chemistry. *In-vivo* experimental studies in the frontal skull of pigs demonstrated that nanotube surfaces gave enhanced bone formation and bone development with better osteoblast function compared to bare titanium surfaces [2]. The *in vivo* experimental studies in the femora with titania nanotubular surfaces in rats demonstrated increased bone formation, at 4 week and 12 week time points [3]. Wettability is an important property for biological functions. As-anodized TiO_2 nanotubes show super-hydrophilic behaviour which becomes hydrophobic after aging in air. As the reaction of stabilization from $Ti(OH)_4$ to TiO_2 occurs, the hydroxyl groups disappear in air. In biomedical applications of titanium, alteration of wetting properties of the surface is important [4]. The hydrophobic transition can also be achieved by coating nanotubular surface with octadicylsilane and octadecylphosphonic acid molecules which can be reversed to hydrophilic by UV illumination [5]. One approach to enhance osseointegration, cell adhesion, proliferation and biocompatibility is to increase hydrophilicity by introducing Ti-OH groups on nanostructured commercially pure titanium (Cp Ti) surfaces [6]. Biocompatibility is governed by factors including material of the implant, structure and chemistry of the implant surface and micro/nanostructured topography. A TiO_2

nanotube (TiNT) layer, as nanophase material on orthopaedic implants, have been demonstrated to improve bonding with surrounding bone [7]. TiNTs create research interest due to better osseointegration as nanotubes provide numerous anchoring sites for cells.

During the past few years, researchers have investigated optical, chemical, electrical, and wettability properties of organized TiNT surfaces on orthopedic implants, while there are few literature reports on controlled wettability and chemical composition of the TiNT surfaces needed for orthopedic implant applications [8]. Therefore, the goal of the present work was to quantify these promising characteristics of TiNT surfaces with controlled wettability and chemical composition.

In the first part of this study the wetting condition of TiNT surfaces was analyzed to evaluate hydrophobicity induced due to surface aging during dark storage. This analysis can be useful from a shelf life perspective for orthopedic implants with TiNT surfaces. For this analysis two types of Cp TiNT surfaces anodized using two different electrolytes were used. Comparison of two Cp TiNT morphologies for their ability to retain hydrophilicity was made. A previous study reported that UV irradiation of 1.0$\mu W/cm^2$ for 240 minutes can improve the surface wettability of annealed and unannealed Cp TiNT surfaces [9]. In order to study the effect of more intense UV irradiation for comparatively shorter duration on the wettability, unannealed alloy TiNT surfaces were UV irradiated. The aim was to determine the possibility of restoring hydrophilicity of aged amorphous alloy TiNT surfaces in less time.

Crystallinity and chemistry of TiNT surfaces could be other factors that affect bio-performance [10]. Wettability can be improved by changing the chemistry and crystallinity

of the surfaces. Thermal annealing can make anodized surfaces super-hydrophilic partly because of the formation of the anatase phase [9]. Therefore, the latter part of this chapter focuses on post-anodization thermal annealing of TiNT surfaces to identify if the residual fluorine in the TiNT surfaces can be controlled in addition to restoring wettability. Lastly, a procedure for fabricating nanotubes on thermal plasma sprayed (TPS) surfaces was also investigated.

4.2 Material and Methods

4.2.1 Substrate preparation

Strips of commercially pure titanium (CpTi) AMS 4902 J grade 2 with 99.7 wt% purity (TIMET, USA) and Ti6Al4V alpha/beta titanium alloy of ASTM B 265-11 grade 5 (TIMET, USA), were mechanically polished using #150 grit fine crocus cloth and # 800 grit ultra-fine sanding cloth. After cleaning in deionized (DI) water followed by acetone, the samples were dried in air at room temperature. The samples were 12mm x 12mm x 0.5mm thick cut from strips. Thermal Plasma Sprayed CpTi surfaces were cleaned as received with no further preparation.

4.2.2 Fabricating nanotubes

The TiNTs were fabricated by electrochemical anodization of Cp Ti and alloy using a DC power source (Protek 3006B), with direct current (DC) output 0-60V, 1.5A. Two electrolyte recipes used to anodize the nanotubes with specific compositions, as listed in Table 4.1, are hereafter abbreviated as LWHF (low-water, high-fluorine) and HWLF (high-water, low-fluorine). To fabricate the TiNTs, the surfaces were electrochemically anodized

at room temperature with a graphite rod as the cathode and the titanium strip as the anode. The anodized samples were further categorized whether they were as-anodized or included 5 minutes of sonication in deionized water after anodization. The purpose of sonication for a short time was to clean the top surface of nanotubular layer by removing the surface aggregation formed during anodization without affecting the nanotubes. This was confirmed with scanning electron microscopy.

Table 4.1 Anodization conditions used for fabrication of TiNT surfaces.

TiNT surface	Electrolyte solution	Potential (V)	Anodization time (minutes)
Cp TiNT	LWHF - 98% EG + 2% DI water + 0.6 wt% NH_4F	60	40
Cp TiNT	HWLF - 60% EG + 40% DI water + 0.2wt% NH_4F	30	240
Alloy TiNT	LWHF - 98%EG + 2% DI water + 0.6 wt% NH_4F	60	40

4.2.3 Surface characterization

Characterization of the anodized surfaces was performed by field emission scanning electron microscopy (FESEM, Hitachi S-4700). The wt% chemical compositional analysis of TiNT surfaces was done by energy dispersive spectroscopy (EDS) with standardless quantitative analysis on the FESEM at 10kV.

4.2.4 Thermal treatment protocol

The post-anodization thermal annealing was performed at 350ºC for 3h in air using a programmable automatic heating chamber (Fisher Scientific Isotemp® Programmable Muffle Furnace). The heating rate chosen was 7.5ºC/min and the slow cooling to room

temperature was obtained inside the chamber.

4.2.5 Contact angle imaging and measurements

An air displacement micro-pipette (Eppendorf Research Plus adjustable from 0.5-10μL) was used to deposit 1μL droplets. Phosphate-buffered saline (PBS) solution of pH 7.4 was used to simulate the body fluid interaction with alloy TiNT and DI water of pH 7 alone was used for Cp TiNT. Images were acquired using a Kohler illumination system and microscope integrated camera in ambient conditions. In this work, the advancing contact angle of the droplet at the air-liquid-solid interface was recorded each second for 30 secs total. Images corresponding to 10 seconds after putting a droplet were considered as stable. The water contact angle (WCA) measurements were performed by the drop shape analysis method for angles more than 15º and by the tangent method for angles less than 15º of the spherical crown of the droplet.

4.2.6 Wetting behaviour by alternating UV irradiation and dark storage

To analyze hydrophobic conversion from as-anodized hydrophilic Cp TiNT surfaces due to aging, the two types of Cp TiNT surfaces were kept in dark storage for 2, 20, 40 and 60 days under ambient condition. Two types of Cp TiNT surfaces anodized using HWLF and LWHF electrolyte were used for this purpose to compare the aging effect on two different morphologies. After each storage time interval, the contact angle was measured.

To investigate photo-induced hydrophilicity, only alloy TiNT surfaces were used in additional set of experiments. The alloy TiNT samples were exposed to UV irradiation before and after dark storage at different time intervals under ambient conditions. The UV

light (λ = 365nm, 450μW/cm^2 intensity) was used for 30 minutes to study the effect of high intensity UV irradiation for a short duration on wettability. The purpose was to determine whether hydrophobicity of alloy TiNT surface due to aging could be reversed to a more hydrophilic state. After each irradiation time interval, the contact angle was measured. After initial irradiation, the alloy TiNT samples were kept in dark for 2, 20, 40 and 60 days. After aging, the samples were again irradiated under UV light for 30 minutes to investigate the possibility of UV-induced wettability. Each contact angle measurement was repeated twice at different places on the sample surface.

4.2.7 Statistical analysis

The EDS spectra were collected at three different locations on each surface for compositional characterization using standardless quantitative analysis on FESEM and the data were reported as an average. For all contact angle measurements, the uncertainty of the measurements is +/- 3º. This is based on the ability to reproducibly determine a tangent line or elliptical shape at the solid-liquid-vapour contact while doing contact angle measurements.

4.3 Results

4.3.1 Surface morphology – SEM analysis

The morphology of the TiNT structures showed a strong dependence on electrochemical anodization potential and anodizing time. FESEM images in Fig.4.1 show representative TiNT surfaces. The alloy and pure nanotubes produced in the LWHF electrolyte (40 minutes) were found to have a length of ~1.5μm with a honeycomb-like

tightly bound vertically aligned structure and smooth walls. These tubes present an ordered and well packed structure. In contrast, the pure nanotubes produced in the HWLF electrolyte (240 minutes) were found to have a shorter length of ~1.0μm with cantilever-like, well-spaced individual-vertically aligned structures. These tubes showed ripples in their side walls, which introduce a small-scale surface component. Table 4.2 summarizes the characteristic mean vales of tube dimensions.

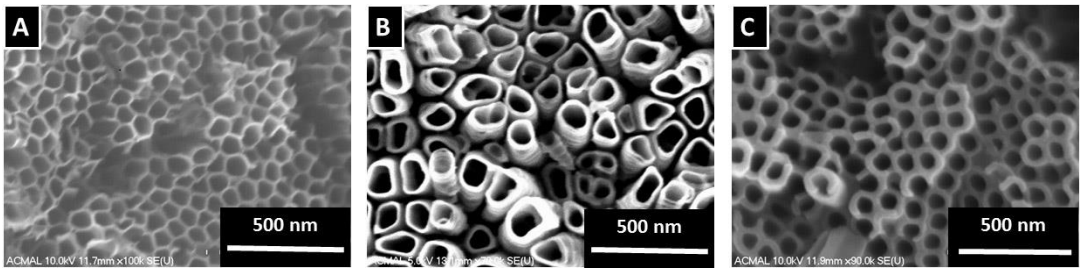

Figure 4.1 SEM images of the surfaces (a) alloy TiNT anodized in LWHF electrolyte, (b) Cp TiNT anodized in HWLF electrolyte and (c) Cp TiNT anodized in LWHF electrolyte.

Table 4.2 Morphological parameters of alloy TiNT and Cp TiNT: tube inner diameter (D), length (L), wall thickness (w), intertubular spacing (χ) obtained by SEM and approximate number density (ρ).

SEM Results					
Sample	D (nm)	L (μm)	w (nm)	χ (nm)	ρ (μm^{-2})
Alloy TiNT_LWHF	70	1.5	10	0	260
Cp TiNT_HWLF	150	1	20	20	56
Cp TiNT_LWHF	100	3	25	5	172

4.3.2 Chemical composition of as-anodized structures

The chemistry of an implant surface is vital in biological events after implantation. Surfaces with a mechanical similarity to bone and controlled chemistry at the nanometer scale can promote spreading and attachment of osteoblasts on the implant surface [11]. Only a few studies have provided details on the residual chemistry of TiO_2 nanotubular surfaces.

The TiNTs were characterized to compare the effect of the electrolyte composition and anodization process on chemical composition of TiNTs (Table 4.3). The oxygen content in TiNTs during anodization, represents the formation of the oxides. The nanotubes show 33 wt% of oxygen. The lower oxygen content can be justified by the presence of TiOH on the nanotube surface. During anodization the diffusion controlled growth of nanotubes leads to formation of hexafluorotitanate complex TiF_6^{2-} by fluorine diffusion from electrolyte to titanium [4]. The presence of fluorine in the anodized surfaces is indicative of the diffused TiF_6^{2-} during anodizing rather than free fluoride ions.

Table 4.3 Comparison of chemical composition of control (non-anodized) and TiNT (as-anodized) surfaces using EDS.

Sample	Relative weight % of elements elements				
	Ti	Al	V	F	O
Control Cp Ti	99.13	0	0	0	0.87
Control Alloy	89.97	7.42	2.61	0	0
Alloy TiNT_LWHF	50.44	3.94	1.62	11.64	32.37
Cp TiNT_HWLF	62.40	0	0	4.11	33.39
Cp TiNT_LWHF	57.45	0	0	8.28	34.27

4.3.3 Wetting condition analysis

The wettability originates from the surface hydroxyls. These surface hydroxyls combine with water molecules forming hydrogen bonds which further results in increased wettability. The mechanism of hydrophobic to hydrophilic transition of the surface upon UV irradiation is explained by the excitation of oxide with reduction of Ti^{4+} by surface trapped electrons [12]. This forms oxygen vacancies. Thus, when a water droplet is placed on the surface, it reacts with oxygen vacancies resulting in complete spreading of the water droplet.

Fig.4.2 shows the trends of the WCA variations on Cp TiNT surfaces prepared using LWHF and HWLF electrolytes. Initially, 2 days after anodization, the two different Cp TiNT morphologies showed similar hydrophilicity. This later showed variation in the hydrophilic to hydrophobic transition as a function of aging. In the case of nanotubes prepared using HWLF electrolyte, the surface became hydrophobic after 20 days. On the contrary, nanotubes prepared using LWHF electrolyte maintained hydrophilicity after 20 days. The non-anodized control Cp Ti foil surfaces showed a WCA of 64º (not shown in figure) which reduced to 14º on both types of nanotubular surfaces representing hydrophilic behaviour upon anodization. This reduction in WCA after fabrication of the nanotubes could also be because of the increased surface area of the separated nanotubes along with formation of TiOH on the surface.

Previous studies reported that, reversible switching between hydrophobic and hydrophilic states is an effect defined by surface chemical composition and roughness [13]. The chemical composition provides a photosensitive surface, which can be switched

between the two wetting states. Fig.4.3 shows representative pictures of droplets on non-sonicated and sonicated alloy TiNT surfaces. The trends of the contact angle variations are presented in Fig.4.4. The contact angle measurements were conducted before and after irradiating with UV light. The effect of indirectly induced UV photocorrosion was not considered within the scope of this study and the possibility of oxygen vacancy formation which directly affects the hydrophobicity was considered. The following phenomena were observed. The first, in the case of non-sonicated alloy TiNTs, the wetting transition from hydrophilic to hydrophobic is mildly irreversible with the largest effect after 60 days aging. The second is, the aging effect dominated in sonicated alloy TiNTs as compared to non-sonicated, due to oxidation of TiNTs in ambient conditions during storage. These results suggest that with more intense UV irradiation the photo-induced wettability effect cannot be achieved with short duration. The sharp increase in contact angle in non-sonicated alloy TiNT surfaces, represented a much faster hydrophobic transition between 40 and 60 days. Whereas in case of sonicated alloy TiNT surfaces, a much faster transition occurred in first 20 days.

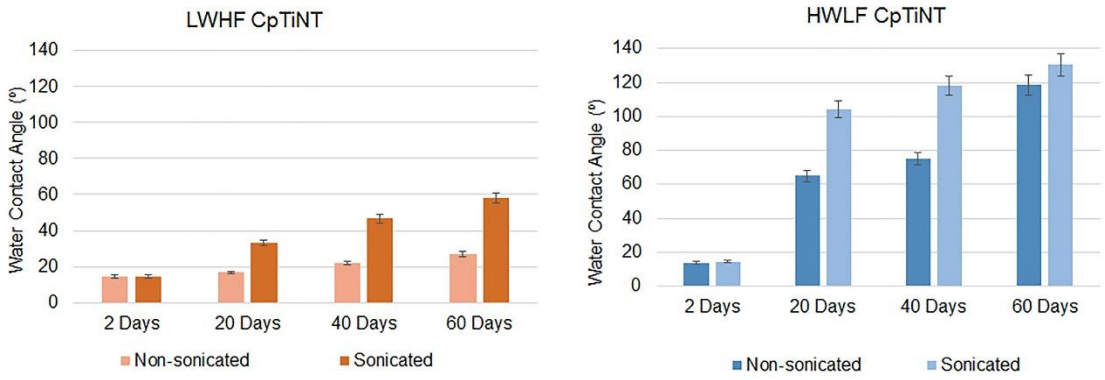

Figure 4.2 Wetting condition of Cp TiNT surfaces during dark storage.

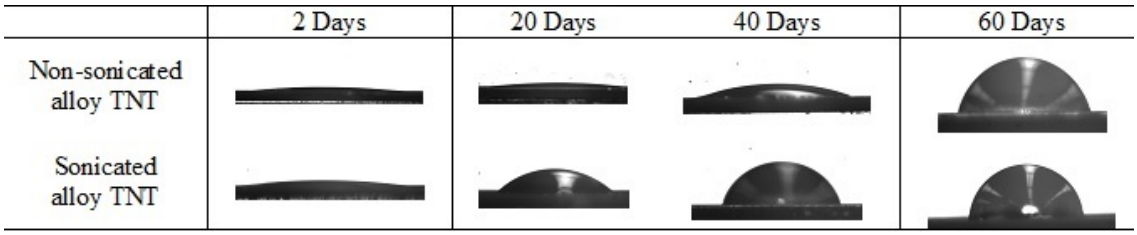

Figure 4.3 Representative pictures of changes in wettability as function of time.

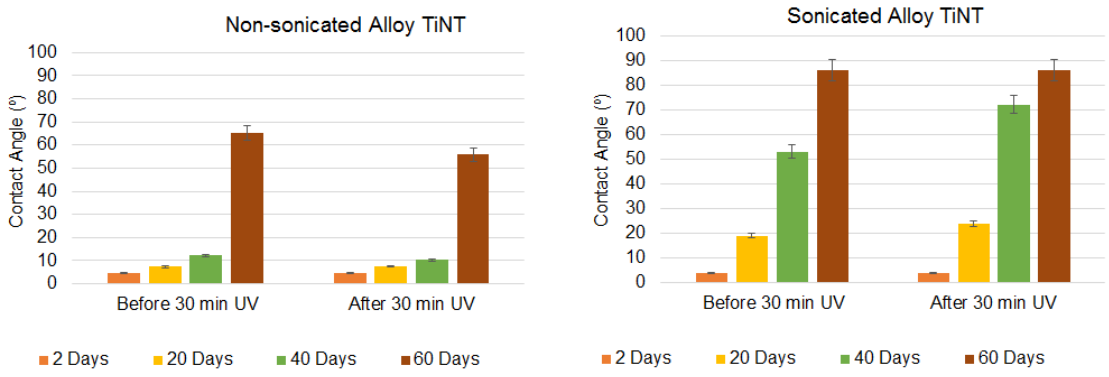

Figure 4.4 Wetting condition of alloy TiNT surfaces by alternating UV irradiation and dark storage.

4.3.4 Effect of thermal annealing on chemical composition and wettability

The compositional and wettability changes of TiNT surfaces upon annealing were studied. The TiNT surfaces were annealed at 350ºC to achieve the amorphous to anatase phase transformation. As-anodized TiNTs showed strong residual fluorine content. Reduction or elimination of fluorine may be advantageous because the presence of fluorine could alter the properties of the surface in biomedical devices [14]. Excessive levels of fluorine can also lead to skeletal fluorosis with the first indications being increased bone density and loss of calcium.

For Cp TiNTs anodized with HWLF electrolyte, which could also produce nanotubes on thermal plasma sprayed implants, the chemical composition was studied before and after annealing for 1, 2, 3, and 4h at 350ºC. From EDS wt% data, the graph in Fig.4.5 shows the decreasing trend of fluorine in TiNTs with respect to annealing time. The fluorine concentration gradually decreased from 4.11wt% in as-anodized TiNTs to 0.77wt.% upon annealing for 4h.

Fig.4.6 Shows wettability changes after annealing at 350ºC for 3h on control and TiNT surfaces. The alloy and Cp TiNT surfaces became superhydrophilic upon annealing. In the case of unannealed amorphous nanotubes, the contribution of tube-walls to generate photocurrent is very less [15]. The reason is the amorphous structure of tubes possess more defects. Whereas the annealed nanotubes represents better photocurrent, because by conversion to anatase, the tube walls become activated and contribute to photocurrent [15]. These annealed surfaces can become hydrophobic upon aging and these can be exposed to UV, to make them hydrophilic again.

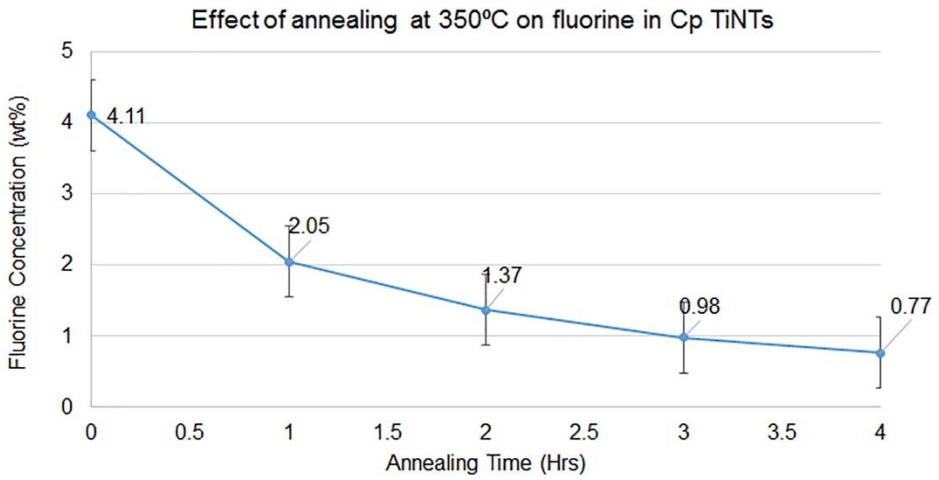

Figure 4.5 Effect of annealing at 350ºC on decreasing fluorine concentration wt% in CpTiNT surfaces fabricated with HWLF electrolyte.

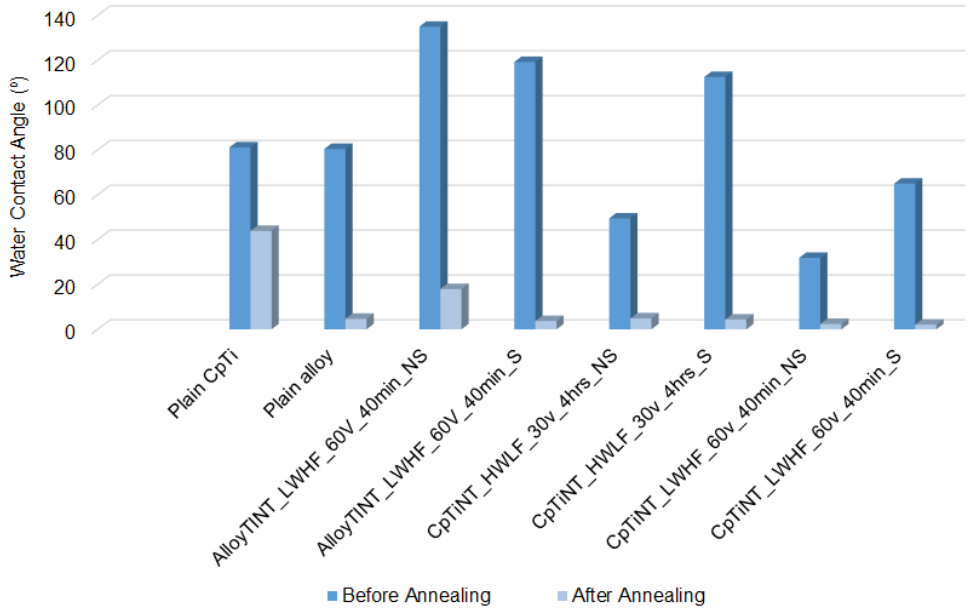

Figure 4.6 Effect of annealing on wettability.

4.3.5 TiNT on Cp TPS implant surfaces

Nanotubular implant surfaces, providing nanoscale 3-D topographies with more surface area than flat surfaces, demonstrated enhanced osseointegration in rats [16]. *In vivo* studies of hydroxyapatite (HA) and thermal plasma sprayed (TPS) implants in a rabbit model showed higher percentage of bone contact, accelerated bone formation and extremely high bonding strength with the HA coated implant compared to the TPS [17].

In this study, TPS implant surfaces were anodized in HWLF electrolyte with two different anodization conditions on different implants to analyze nanotube morphology and their wetting behaviour. Figs.4.7a-d show the TiNT surfaces fabricated at 30V for 4h. Figs.4.7e-h show TiNT surfaces fabricated at 60V for 40 minutes. It is evident that the nanotubes were anodized on the entire surface covering all the macroscopic roughness features. The TiNTs on the TPS substrate were vertically oriented, laterally spaced, and structurally stable. This porous network of nanotubes showed strong scratch resistance representing good mechanical strength needed to sustain surgical loads. The nanotubes were approximately 80 to 100nm in diameter. The intertubular spaces between nanotube walls were ~10nm. A similar type of nanotube morphology has been reported to have potential for bone implant material because of their ability to induce more osteoblast elongation with higher alkaline phosphate activity [18]. This type of morphology with interstitial spaces between tubes, even after cell adhesion, is reported to allow continued fluid flow of culture media and increased exchange spaces between tube walls for gas nutrients and cell signalling molecules, leading to enhanced performance of bioactivity on implant [19].

Controlled dimensional variation in tube diameter and length can be achieved using this HWLF electrolyte by changing anodization conditions.

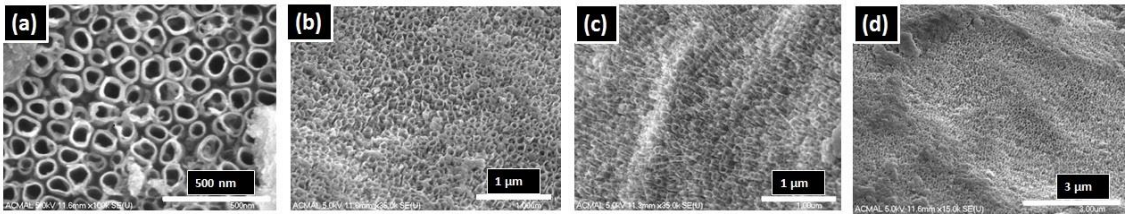

Figure 4.7a-d Nanotubular surface fabricated on Cp TPS implant at 30V for 4h in HWLF electrolyte.

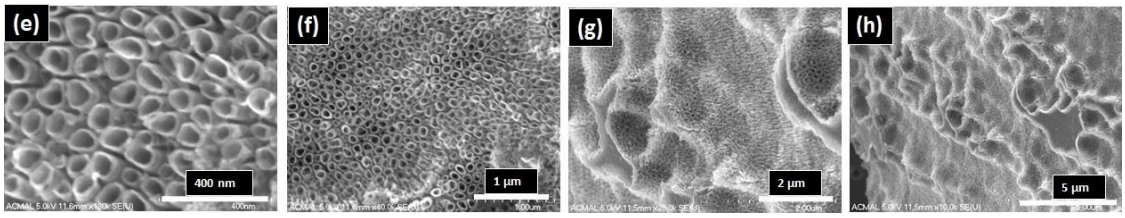

Figure 4.7e-h Nanotubular surface fabricated on Cp TPS implant surface at 60V for 40 minutes in HWLF electrolyte.

Another desirable property of nanotubular structure is hydrophilicity for effective bioactivity. The greater cell adhesion by TiNTs, as compared to flat smooth control surfaces is partly because of nano-topography and partly because of hydrophilicity of the TiNTs [19, 20]. Table 4.4 shows the water contact angle (WCA) measurements on as-received and TiNT anodized surfaces of CpTPS implants using 1µL DI water. The TiNT surfaces fabricated at 30V for 4h demonstrated retention of hydrophilicity even after aging up to 40 days whereas nanotubes fabricated at 60V for 40 minutes became hydrophobic after 20 days. The annealed TiNT surfaces on CpTPS implants demonstrated a decrease in residual fluorine up to 85% to 93% compared to unannealed TiNT surfaces (Table 4.5).

Table 4.4 Wettability of TiNTs on Cp TPS implant

WCA measurement on as-received and anodized Cp TPS implant surface			
Aging time	Control Cp TPS surface	TiNTs anodized with HWLF_30V_4h	TiNTs anodized with HWLF_60V_40min
As-received Control Cp TPS surface	94°	--	--
2 days	--	0°	0°
20 days	--	0°	106°
40 days	--	0°	119°

Table 4.5 Comparison of chemical composition of TiNT surfaces on Cp TPS implants

TiNTs on Cp TPS Implant		Relative wt% of elements		
		Ti	F	O
HWLF_30V_4h	As-Anodized	52.61	6.58	40.82
	Annealed	68.25	0.48	31.27
HWLF_60V_40min	As-anodized	75.64	2.84	21.51
	Annealed	63.59	0.36	36.05

4.4 Discussion

The morphological analysis of TiNTs indicates that as the ratio of NH_4F to DI water was decreased, the nanotube density decreased and spacing between the nanotubes increased (Table 4.2). The shape and dimensions of nanotubes showed a strong correlation with composition of electrolyte. It is also interesting to note that the difference in the fluorine concentration in the two electrolytes has a pronounced effect on the amount of residual fluorine in the TiNT surfaces (Table 4.3).

The presence of TiOH on nanotube surface makes the surface hydrophilic in the as-anodized condition. The aging in air causes atmospheric contamination during dark storage which makes the nanotubular surfaces more hydrophobic. In alloy TiNTs, much faster

hydrophilic to hydrophobic transition of sonicated alloy TiNT surfaces in 20 days as compared to non-sonicated surfaces which occurred in 40 days (Fig.4.4b) indicates that, the surface aggregation of the non-sonicated TiNT surfaces has apparently protected the underlying nanotubes delaying TiO_2 stabilization and slower aging. Our results show that the rate of hydrophilic to hydrophobic transition (increase in contact angle values) was observed to be only 12% up to 40 days of dark storage in the case of non-sonicated alloy TiNT. This slower transition and retention of hydrophilicity up to 40 days, compared to sonicated alloy, could be important from a manufacturing, packaging, and shelf life perspective for orthopedic implants with TiNT surfaces.

The UV-induced hydrophilic effect was not observed in alloy TiNT surfaces that were non-sonicated and sonicated. This could be explained by the presence of aluminium and vanadium oxides, having higher band gap energy than titanium, along with corresponding intermetallic compounds. This could not lead to reduction of metal ions and thus affected the process of formation of surface hydroxyls Ti(OH) upon UV.

In the case of TPS implant surface, the TiNTs fabricated with HWLF electrolyte at 60V for 40 minutes showed major hydrophilic to hydrophobic transition in the first 20 days. This information is useful to determine short-term shelf life of Cp Ti nanotextured implant surfaces. The compositional and functional changes of TiNT surfaces upon annealing were studied. Our results showed that the residual fluorine in the TiNTs could be eliminated upon annealing.

4.5 Conclusions

The wetting transition from hydrophilic to hydrophobic is irreversible for amorphous TiNTs using UV irradiation. The wettability of nanotubes is dominated by the aging effect. Successful fabrication of superhydrophilic nanotubes on Cp TPS implant was achieved, establishing a reliable procedure for reproducible nanotubular surfaces needed for enhanced bioactivity. The elimination of residual fluorine by thermal annealing of the TiO_2 nanotubes was shown. As a result of annealing at 350^{o}C, release of fluorine was observed as a function of annealing time.

Acknowledgments

This work performed under the M-TRAC program was supported by Grant Case-48161 of the 21st Century Jobs Trust Fund received through the Michigan Strategic Fund from the State of Michigan. The M-TRAC program is funded by the Michigan Strategic Fund with program oversight by the Michigan Economic Development Corporation.

References

[1] Shin DH, Shokuhfar T, Choi CK, Lee SH, Friedrich C. Wettability changes of TiO_2 nanotube surfaces. Nanotechnology. 2011;22:315704.

[2] Von Wilmowsky C, Bauer S, Lutz R, Meisel M, Neukam FW, Toyoshima T, et al. In vivo evaluation of anodic TiO_2 nanotubes: An experimental study in the pig. J Biomed Mater Res B Appl Biomater. 2009;89:165-71.

[3] Alexander Vara EAB, MS, Meagan Salisbury, Mackenzie Fleischer, Sachin M. Bhosle, MS, Craig Friedrich, Paul, Fortin M. Enhancing osseointegration of orthopaedic implants with titania nanotube surfaces. Foot & Ankle Orthopaedics,. 2016;1.

[4] Macak JM, Tsuchiya H, Ghicov A, Yasuda K, Hahn R, Bauer S, et al. TiO_2 nanotubes: Self-organized electrochemical formation, properties and applications. Current Opinion in Solid State and Materials Science. 2007;11:3-18.

[5] Balaur E, Macak JM, Taveira L, Schmuki P. Tailoring the wettability of TiO_2 nanotube layers. Electrochemistry Communications. 2005;7:1066-70.

[6] Li B, Li Y, Li J, Fu X, Li C, Wang H, et al. Improvement of biological properties of titanium by anodic oxidation and ultraviolet irradiation. Applied Surface Science. 2014;307:202-8.

[7] Ganesan B, Webster TJ. A perspective on nanophase materials for orthopedic implant applications. Journal of Materials Chemistry. 2006;16:3737-45.

[8] Indira K, Mudali UK, Rajendran N. In-vitro biocompatibility and corrosion resistance of strontium incorporated TiO_2 nanotube arrays for orthopaedic applications. J Biomater

Appl. 2014;29:113-29.

[9] Yang L, Zhang M, Shi S, Lv J, Song X, He G, et al. Effect of annealing temperature on wettability of TiO_2 nanotube array films. Nanoscale Res Lett. 2014;9:621.

[10] Mazare A, Dilea M, Ionita D, Titorencu I, Trusca V, Vasile E. Changing bioperformance of TiO_2 amorphous nanotubes as an effect of inducing crystallinity. Bioelectrochemistry. 2012;87:124-31.

[11] Le Guehennec L, Soueidan A, Layrolle P, Amouriq Y. Surface treatments of titanium dental implants for rapid osseointegration. Dent Mater. 2007;23:844-54.

[12] Kontos AG, Kontos AI, Tsoukleris DS, Likodimos V, Kunze J, Schmuki P, et al. Photo-induced effects on self-organized TiO_2 nanotube arrays: the influence of surface morphology. Nanotechnology. 2009;20:045603.

[13] Papadopoulou EL, Zorba V, Pagkozidis A, Barberoglou M, Stratakis E, Fotakis C. Reversible wettability of ZnO nanostructured thin films prepared by pulsed laser deposition. Thin Solid Films. 2009;518:1267-70.

[14] Regonini D, Jaroenworaluck A, Stevens R, Bowen CR. Effect of heat treatment on the properties and structure of TiO_2 nanotubes: Phase composition and chemical composition. Surface and Interface Analysis. 2010;42:139-44.

[15] Beranek R, Tsuchiya H, Sugishima T, Macak JM, Taveira L, Fujimoto S, et al. Enhancement and limits of the photoelectrochemical response from anodic TiO_2 nanotubes. Applied Physics Letters. 2005;87:243114.

[16] Smith GC, Chamberlain L, Faxius L, Johnston GW, Jin S, Bjursten LM. Soft tissue response to titanium dioxide nanotube modified implants. Acta Biomater. 2011;7:3209-15.

[17] Darimont GL, Cloots R, Heinen E, Seidel L, Legrand R. In vivo behaviour of hydroxyapatite coatings on titanium implants: a quantitative study in the rabbit. Biomaterials. 2002;23:2569-75.

[18] Brammer KS, Oh S, Cobb CJ, Bjursten LM, van der Heyde H, Jin S. Improved bone-forming functionality on diameter-controlled TiO_2 nanotube surface. Acta Biomater. 2009;5:3215-23.

[19] Brammer KS, Frandsen CJ, Jin S. TiO_2 nanotubes for bone regeneration. Trends Biotechnol. 2012;30:315-22.

[20] Hamlekhan A, Butt A, Patel S, Royhman D, Takoudis C, Sukotjo C, et al. Fabrication of anti-aging TiO_2 nanotubes on biomedical Ti alloys. PLoS One. 2014;9:e96213.

Chapter 5

Rapid heat treatment for anatase conversion of titania nanotube orthopedic surfaces*

Sachin M. Bhosle[1,2], Craig R. Friedrich[1]

[1] *Department of Mechanical Engineering, Multi-Scale Technologies Institute, Michigan Technological University. USA*

[2] *Vidya Pratishthan's Kamalnayan Bajaj Institute of Engineering and Technology, Baramati, India*

Abstract

The amorphous to anatase transformation of anodized nanotubular titania surfaces has been studied by X-ray diffraction and transmission electron microscopy. A more rapid heat treatment for conversion of amorphous to crystalline anatase favorable for orthopedic implant applications was demonstrated. Nanotube titania surfaces were fabricated by electrochemical anodization of Ti6Al4V in an electrolyte containing 0.2 wt% NH_4F, 60% ethylene glycol and 40% deionized water. The resulting surfaces were systematically heat treated in air with isochronal and isothermal experiments to study the temperature and time

* *The material contained in this chapter is in preparation for submission to a journal. As the first author of this publication, I have done the fabrication of nanotube surfaces, SEM and EDS characterization, XRD measurements, literature review, results analysis and writing the manuscript.*

dependent transformation respectively. Analysis shows that the anatase phase transformation of TiO_2 in the as-anodized amorphous nanotube layer can be achieved in as little as 5 minutes at 350C in contrast to reports of higher temperature and much longer time. The crystallinity analysis at different temperatures and times yield transformation rate coefficients and activation energy for crystalline anatase coalescence.

5.1 Introduction

Titanium surfaces, electrochemically modified to produce titania nanotubes, have been reported to demonstrate enhanced osteoconductivity by providing anchorage sites for osteoblast filopodia extensions leading to early differentiation and significant proliferation [1]. Titania nanotube structures (TiNTs) have been researched for potential implant applications in recent years, but less attention has been paid towards conversion of amorphous to crystalline anatase structures at lower temperatures and in minimum time for more favorable inclusion in implant manufacturing processes. The morphological parameters of titania nanotubes (diameter and length) can be controlled by using different electrolytes and anodization conditions [2-5]. The surface properties of biomaterials can influence cell function in the biological environment hence, along with morphology and chemistry, the crystallinity is another important factor [6]. To achieve crystalline TiNTs, the most reliable approach to date is post-anodization heat treating [7]. It is a straight forward way to change the electro-chemical [8], and the structural and physical properties of TiNTs. The crystallization improves electric, optical, and catalytic properties along with enhanced mechanical strength of as-anodized amorphous TiNTs [9]. Osteoblast adhesion and proliferation on anatase titania films is enhanced as compared to rutile and amorphous

films [10]. The as-anodized nanotube surfaces containing electrochemically induced anatase produced by high voltage anodization (120 V compared to 30 V in present study) inhibits antibacterial activity, and promotes osteoblasts and fibroblasts proliferation [11]. Heat treated TiO_2 nanotubes, on commercially pure Ti and Ti6Al7Nb with a specific anatase to rutile ratio, shows increased hydrophilicity and better biocompatibility by enhanced bone adhesion due to high surface reactivity, and favorable osteoblastic differentiation and gene expression with improved electrochemical stability [6]. Thus, a quick and low cost process for anatase conversion can be promising for titanium nanotube-based orthopedic implants.

The anatase conversion heat treatment is a decisive protocol that induces crystallite formation in the oxide layer and needs to be qualified to help reduce eventual implant manufacturing costs. In this study, the amorphous to crystalline phase transformation in nanotube surfaces during post-anodization heat treatment was investigated. The novelty of this work is the demonstration of a more rapid and lower temperature heat treatment for conversion of amorphous TiNTs to anatase. We synthesized anatase-rich crystalline TiNTs at lower temperatures and in much less time than what has been reported in the literature with temperatures as high as 500C and as long as 3-4 hours. For the present study, time and temperature dependent crystallinity transformation analysis was performed using isochronal and isothermal heat treatments on amorphous TiNTs. This led to the validation of a quick technique useful in manufacturing for improved bio-performance of nanotube titanium implant surfaces. The analysis yielded transformation rate coefficients, activation

energy for crystallite coalescence, and crystallite sizes. The related transient temperature profile as a function of depth in a typical orthopedic hip stem implant is also presented.

5.2 Materials and Methods

5.2.1 Substrate preparation

Foils of 0.5 mm thick Ti6Al4V alpha/beta titanium alloy, ASTM B 265-11 grade 5 (TIMET, USA) were mechanically polished using #150 grit fine crocus cloth and #800 grit ultra-fine sanding cloth. After subsequent cleaning in deionized (DI) water followed by acetone, the samples were dried in air at room temperature. Coupons 30 mm x 30 mm were cut from the foils to anodize.

5.2.2 Fabricating nanotubes

The nanotubes were fabricated by electrochemical anodization using a DC power source (Protek 3006B), with direct current (DC) output 0 – 60 VDC, 1.5 A capacity. Electrolyte containing 60% ethylene glycol, 40% DI water both by volume, and 0.2 wt% of NH_4F was used for etching. The surfaces were electrochemically anodized at 30 V for 4 hours with a graphite rod as the cathode and the titanium alloy foil as the anode at room temperature. The as-anodized foils were sonicated in deionized water for 5 minutes to remove possible surface aggregation formed during anodization.

5.2.3 Heat treatment protocol

For the isochronal experiments, the post-anodization heat treatment was performed by heating the sonicated TiNT foils at 300C, 325C, 350C, 400C, 450C and 500C for 5

minutes in air using a hot plate. The TiNT samples were placed directly onto the hot plate which was first heated and maintained at the specified temperature to ensure a constant temperature during the 5 minutes. The TiNT samples were under an inverted glass beaker to minimize convective heat losses from the top surface. The hot surface was many times larger than the samples to ensure adequate thermal inertia. For the isothermal experiments, the TiNT samples were heated on the hot plate as described at 350C for 2, 5, 20 and 40 minutes. The heat treatment conditions (temperature and time) were chosen to promote the complete formation of the anatase crystalline phase and to determine the minimum temperature and time that resulted in anatase formation. After each treatment at the specific temperature and time, the TiNT sample was removed from the hot plate and cooled to room temperature in air.

5.2.4 Surface and nanotube characterization

Inspection of the anodized and heat treated surfaces was performed using field emission scanning electron microscopy (FESEM, Hitachi S-4700). The wt% chemical compositional analysis of the TiNT surfaces was obtained by energy dispersive spectroscopy (EDS) with standardless quantitative analysis at 10 kV. X-ray diffraction patterns of the heat treated and non-heat treated control samples were taken to identify phase structures using an X-ray diffractometer (Scintag XDS 2000). Diffraction patterns were collected in the range of 23-29º with a scan rate of 0.0015º/min, with a step size of 0.03º, and X-ray radiation of Cu-Kα (λ - 1.540562 Å) where the tube parameters was set at 45kV and 35mA. This range of diffraction angles is the dominant region for crystalline

anatase. The crystallite size was calculated using the Scherrer equation for the full-width, half-maximum of the (101) peak for anatase and the (110) peak for rutile. Transmission electron microscopy (TEM) analysis of TiO_2 nanotubes was performed at University of Illinois - Chicago on a JEOL-3010 TEM at an accelerating voltage of 300kV. A single-tilt TEM holder was used. Selected area diffraction patterns (SAED) were obtained from the side and top opening of the nanotubes to examine their crystallinity. To prepare the TEM samples, the TiO_2 nanotubes were scratched off the substrate, dissolved in isopropyl alcohol (IPA), dipped on a Lacey-carbon TEM grid, and fully dried in air.

5.3 Results and Discussion

To compare our work with conventional annealing treatments, TiNT samples were annealed for 1h and 3h at 350C, since 350C was the lowest temperature at which anatase presence was measured. Fig.5.1 shows the XRD profiles for; 1h annealed plain Ti6Al4V foil, TiNTs unannealed, and TiNTs annealed for 1h and 3h. It is evident from Fig.5.1 that anatase phase transformation upon annealing occurs only in the presence of TiNTs and not on plain Ti6Al4V foil (bottom profile compared with top 2 profiles). Fig.5.1 also shows no discernible difference between 3h and 1h annealing times, but obvious anatase formation compared with unannealed TiNT. To compare the effect of annealing time on anatase conversion, we compared annealed TiNTs at 350C for 5min, 1h and 3h. Fig.5.2 shows the XRD profiles of these samples. No significant difference in anatase peak intensity is observed for 1h and 3h annealed samples, whereas 5 min annealed TiNTs showed slightly lower anatase peak intensity. For crystallinity based on measuring the area under the

anatase peak, the 5min annealing yielded 79 to 81% of the amount of anatase compared to 1h and 3h annealed TiNTs. This suggests that at a certain temperature required for amorphous to anatase transformation, longer heating times do not significantly contribute further to anatase conversion and the time required to achieve maximum possible anatase conversion at specific temperature (350C here) could be less than one hour.

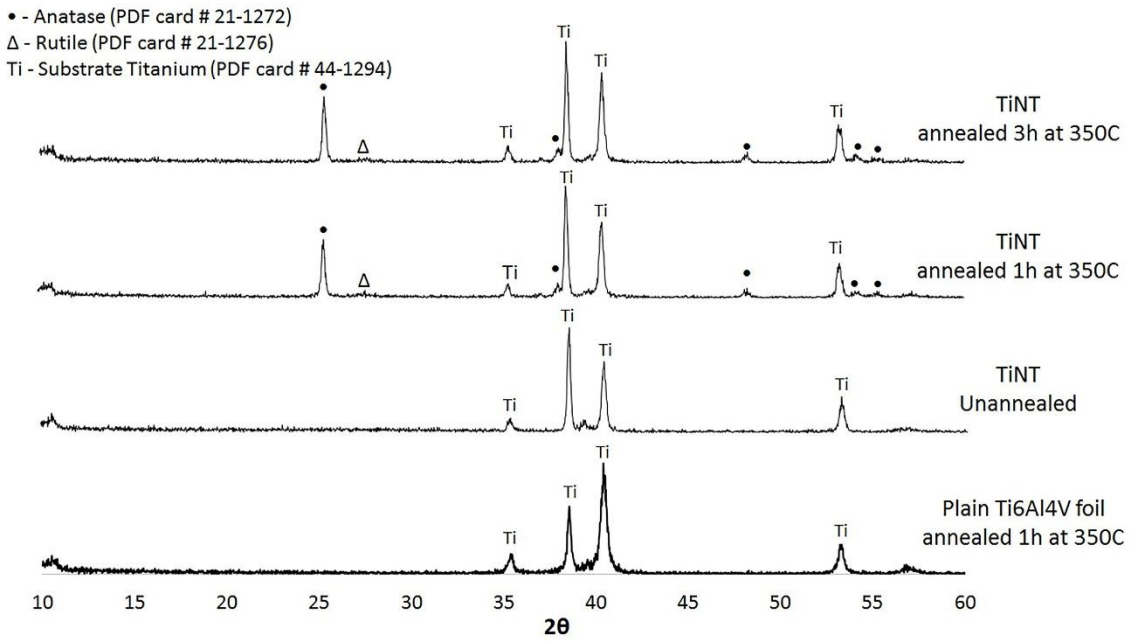

Figure 5.1 XRD profiles of 1h annealed plain foil (bottom), unannealed TiNTs and TiNTs annealed for 1h and 3h at 350C

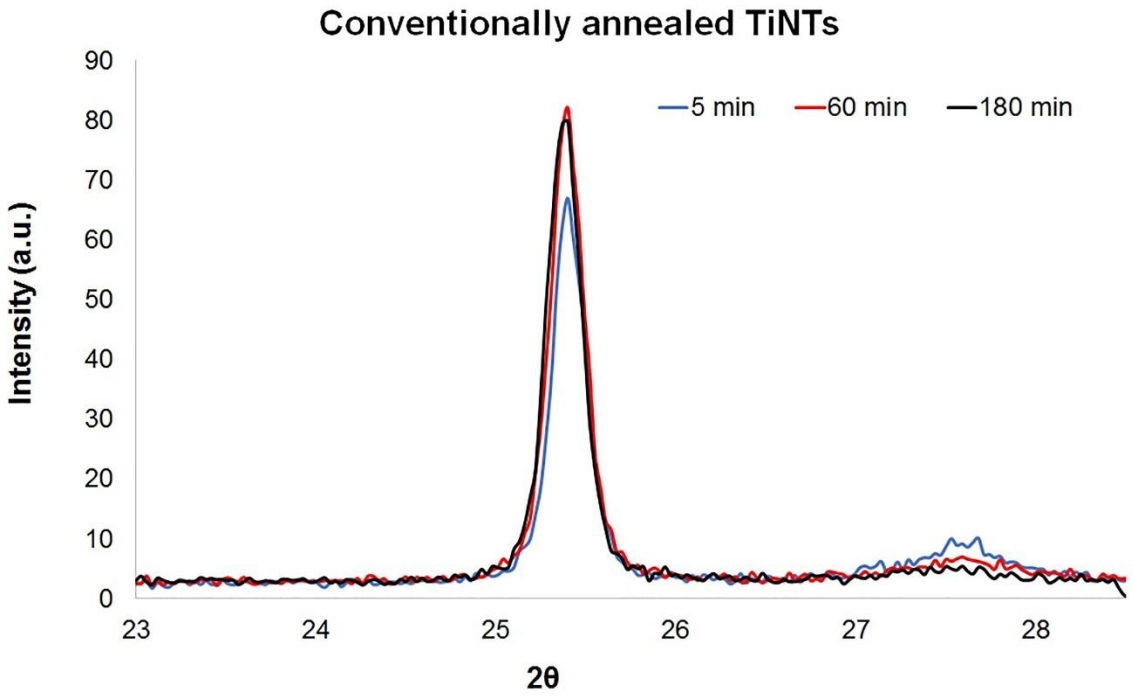

Figure 5.2 XRD profiles of TiNTs annealed for 5 minutes, 1h and 3h at 350C.

5.3.1 Isochronal experiments - Temperature dependent crystallinity transformation

The transition from amorphous to anatase depends on various factors, including time, temperature, and chemical environment and there is insufficient data on the minimum temperature required for transition of TiNTs specifically prepared in an NH_4F, EG and DI water electrolyte. Therefore, to study the temperature dependent anatase transformation of TiNT surfaces subjected to post-anodization isochronal heat treatment, XRD measurements were performed. The sonicated TiNT foils were heat treated in the range 300C to 500C for 5 minutes each in air, before XRD measurements. Fig.5.3a shows XRD profiles demonstrating the effect of temperature on crystalline conversion of as-anodized

samples. The characteristic peaks of titanium anatase (near 25º) and rutile (near 27.5º) are evident. The presence of these phases was confirmed with TEM analysis (Fig.5.5). The XRD patterns for as-anodized and heat treated samples at 300C and 325C showed no crystalline peaks. Whereas the samples heated for 5 minutes at 350C, 400C, 450C and 500C showed conversion to the anatase rich structure near 25º with a small amount of rutile near 27.5º. Anatase is the first nanocrystalline phase detected at 350C. These results indicate that the isothermal transformation from amorphous to nanocrystalline anatase in air occurred near 350C. It is therefore evident that a heat treatment of 350C in air for 5 minutes is sufficient to induce anatase in TiNT surfaces prepared in an NH_4F-EG-DI water electrolyte anodized at 30V. The increasingly strong anatase peaks represents an anatase rich phase in the TiNTs. The increasing rutile peak also represents an increase in rutile weight fraction indicating the initialization of anatase to rutile transformation. In previously reported studies on powdered dry titania gels at temperatures above 350C, anatase transforms to brookite and/ or rutile, and then brookite transforms to rutile [12]. Our XRD results on nanotubes shows no brookite peaks in samples annealed at 350C for 5 minutes.

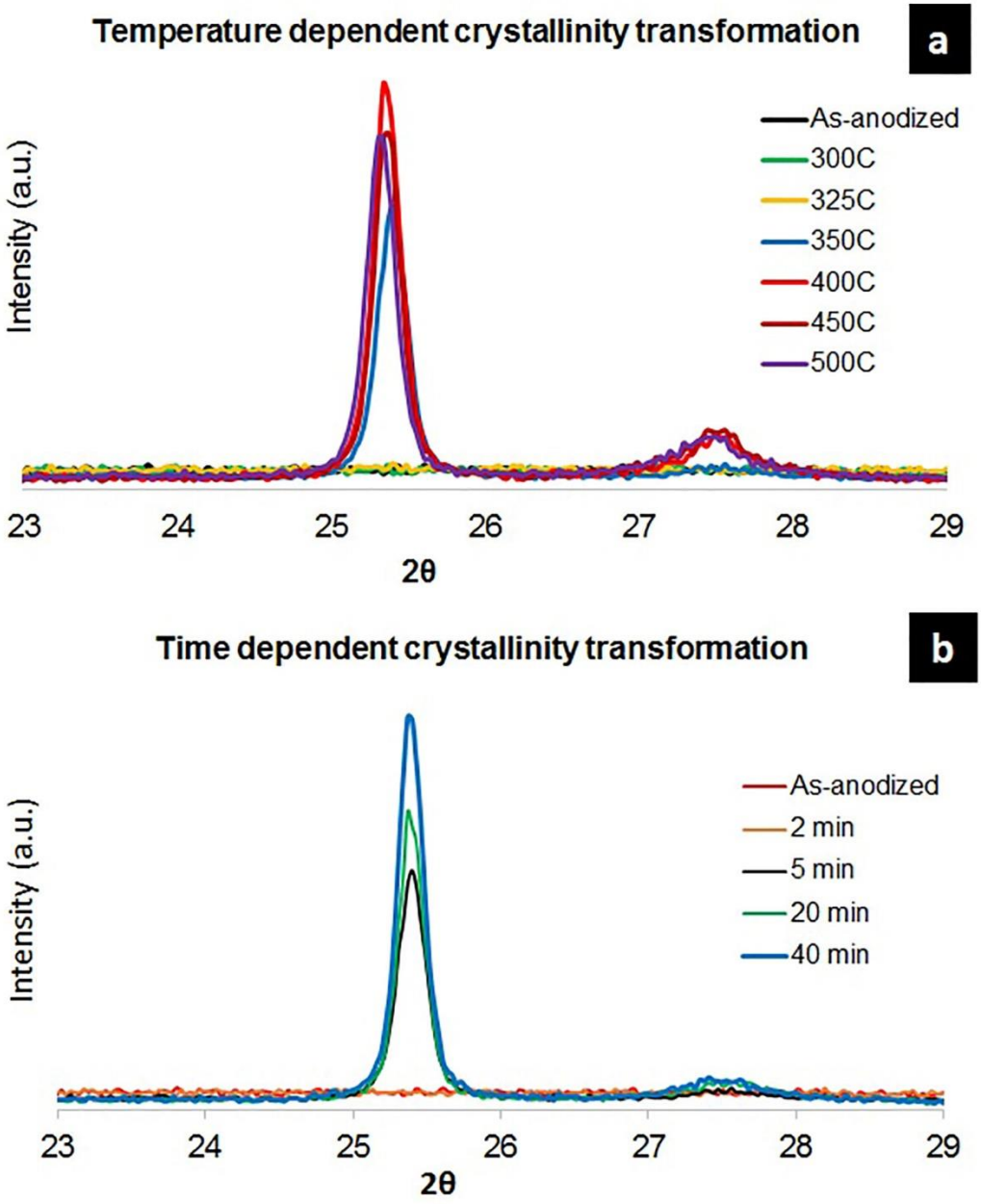

Figure 5.3 XRD patterns of (a) isochronal and (b) isothermal experiments, showing anatase and rutile peaks.

5.3.2 Isothermal experiments - Time dependent crystallinity transformation

To study the effect of heating time on the amorphous to anatase conversion of titania nanotubes, the samples were heated in air at 350C for 2, 5, 20 and 40 minutes. It is evident from Fig.5.3b that, the as-anodized samples and the samples heated for 2 minutes do not show crystallization whereas the 5 minutes and longer heating duration resulted in crystallization represented by the anatase peaks. Thus, knowing that the minimum temperature of 350C is required, the heating time as short as 5 minutes is sufficient for nearly complete amorphous to anatase conversion compared to 1h and longer.

5.3.3 Nanotube crystallization

The XRD data comes from a depth into the sample greater than the length of the nanotubes, which were approximately 1 μm long. Therefore, to ensure that the nanotubes alone had undergone anatase conversion, nanotubes were scratched off the substrate and examined by TEM. Fig.5.4 shows the TEM images of as-anodized TiNTs. The SAED diffraction pattern (Fig.5.4a) confirmed that the as-anodized TiNTs were amorphous. The synthesized TiO_2 shows a tubular structure with a diameter around 100nm (Fig.5.4b).

Fig.5.5 shows the structure of the TiO_2 nanotubes after heating for 5 minutes at 350C. SAED patterns (Fig.5.5b,c) from the top-side and lateral-side of the nanotubes shows a small fraction of diffraction rings, indicating a multi-crystalline structure of the nanotubes. The SAED pattern confirmed the crystallization to anatase TiO_2 occurred during the heating. The lattice image of the TiO_2 (Fig.5.5d) shows the lattice spacing (3.5Å) of the anatase (101) plane in accordance with [13-15], which further confirmed the

nanotubes are anatase. The dominance of the TiO_2 (101) plane shown in the XRD results is also evident. From the enlarged images of crystallites, it appears that the crystals were formed in the nanotube walls with amorphous regions surrounding the crystallites. Different regions of the tube walls were analyzed and most of the crystallites were found to be anatase with a small amount of rutile in the nanotubes. It also appears that the crystallization occurred along the nanotube length rather than across the thickness of the nanotube walls. These results are in accordance with [16] demonstrating initial crystallization structure in nanotubes.

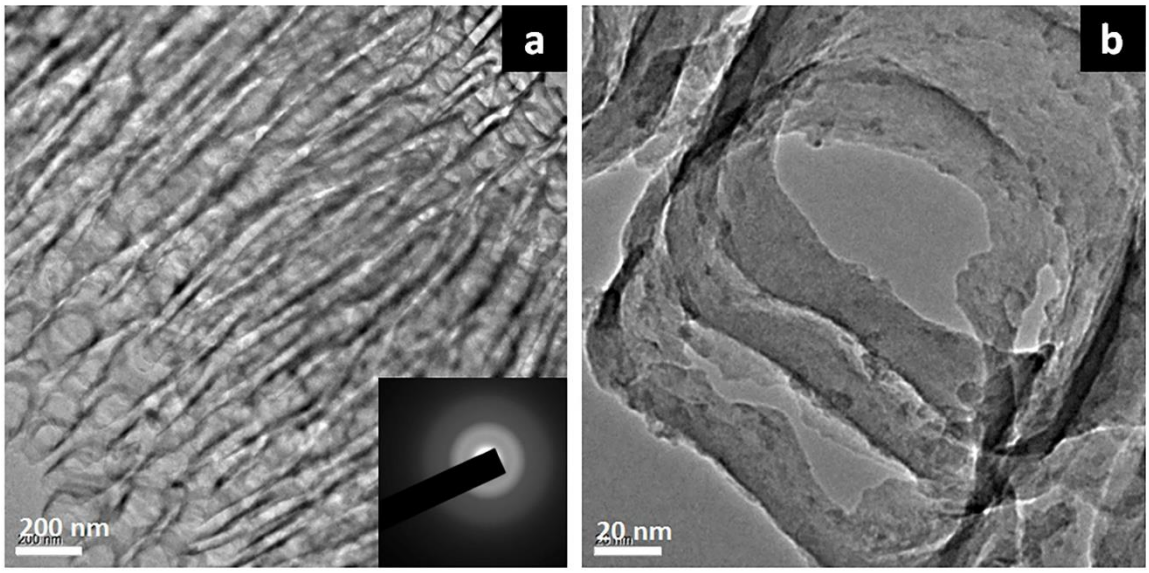

Figure 5.4 (a) TEM images of as-anodized TiNTs showing amorphous tube walls. The inset panel gives the corresponding SAED pattern. (b) High resolution TEM images of the nanotube walls.

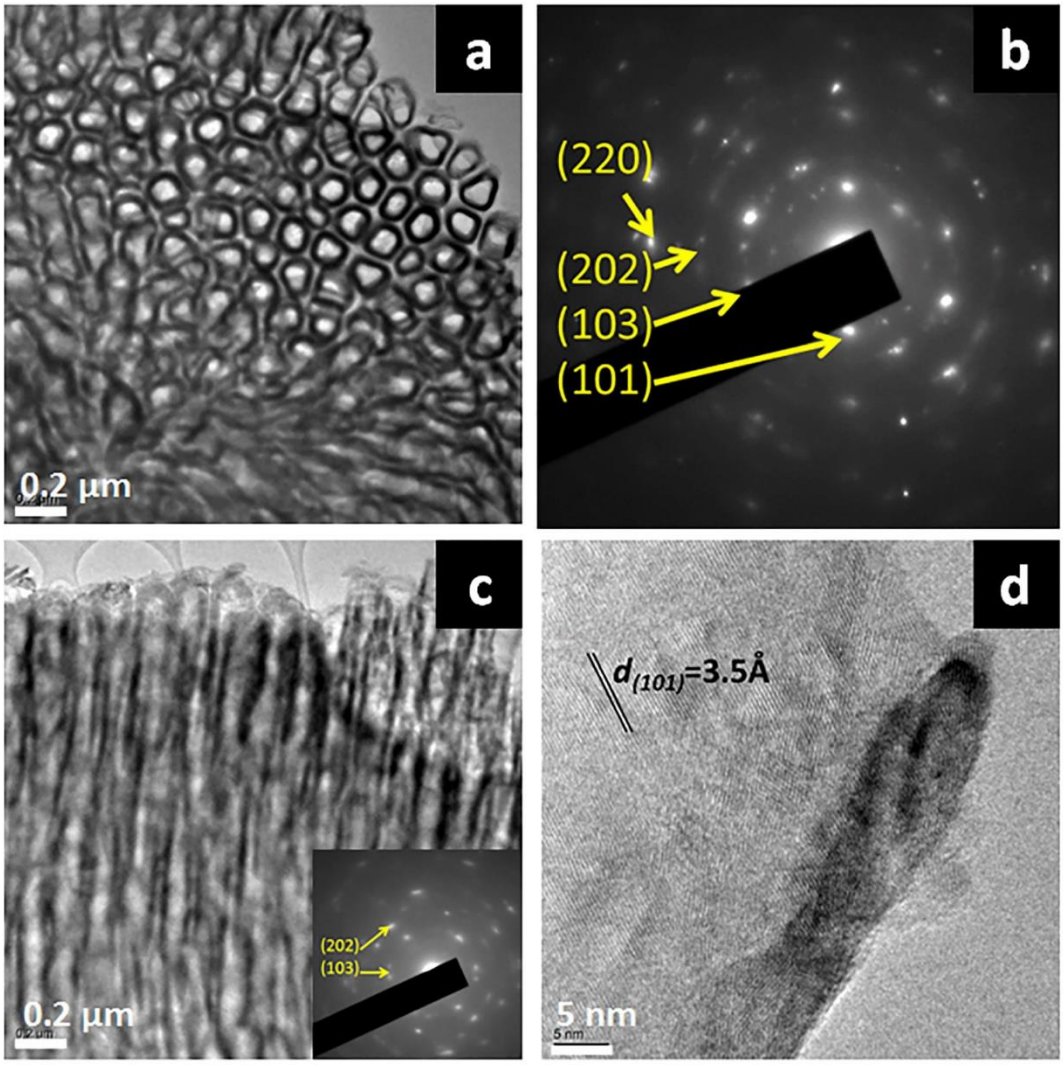

Figure 5.5 TEM images of TiNTs annealed at 350C for 5 minutes showing crystallites in tube walls. (a) The top view of the nanotubes and (b) its corresponding SAED pattern, (c) the lateral view of the nanotubes. The inset panel gives the corresponding SAED pattern pointing to (202) and (103) planes. (d) The lattice image of the nanotubes obtained from the lateral side showing (101) spacing of 3.5Å.

5.3.4 Crystallite size

Using the Sherrer equation, the average crystallite size (d) of anatase and rutile were calculated from the XRD (101) and (110) peak data, respectively.

$$d = K\lambda \,/\, \beta \cos\theta$$

where λ is the X-ray wavelength (1.540562 nm), K is shape factor (0.9), θ is the Bragg angle, and β is the line broadening at full-width half-maximum (FWHM) in radians. Fig.5.6 shows that, the average crystallite size does not show large variations with changing annealing time at 350C. The crystallite size of anatase (43 to 49 nm) is larger than rutile over the range of annealing times from 5-180 minutes. This indicates that for these anodized nanotubes, the heat of transformation needed for crystallization apparently depends more on heating temperature than heating time. As-anodized control nanotube samples without any heating showed no indication of any transformation.

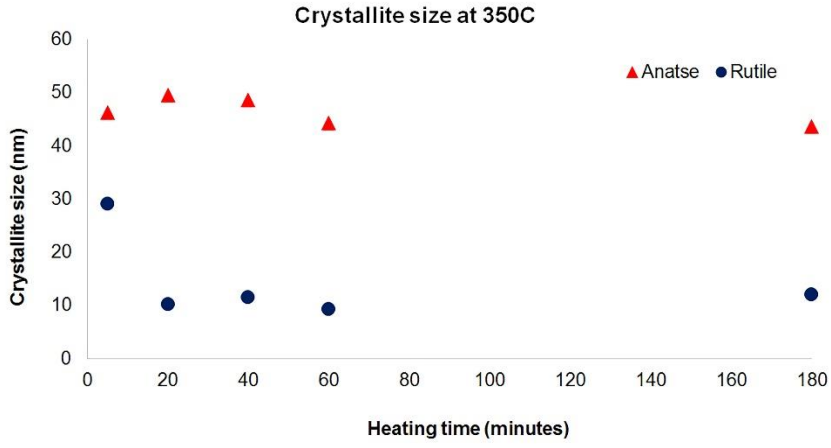

Figure 5.6 Crystallite size of TiNT samples heated at 350C calculated using Scherrer's equation.

5.3.5 Quantification of polymorphic transformation

To quantify the amorphous to anatase polymorphic transformation and determine the transformation rate coefficients, an additional set of experiments was conducted by heating the TiNT samples at 350C, 400C, and 450C for 5, 20 and 40 min each and crystallinity analysis was then done using XRD profiles for each sample. In the case of heat treated TiNT samples, due to the periodic 3D space arrangement of atoms in crystals, the X-rays get scattered only in certain directions when they hit the lattice planes formed by atoms. This causes emergence of high intensity crystalline peaks in the XRD profile. On the other hand, amorphous TiNTs lacking this periodicity with atoms randomly distributed in 3D space, causes X-rays to be scattered in many directions leading to a large bump distributed in a wide range (2θ) instead of peaks. Fig.5.7a shows a large bump distributed over 18 to 48 degrees in the case of as-anodized unannealed TiNT samples representing the amorphous phase. A few elemental titanium peaks can also be seen. Upon heat treating the TiNT samples, the crystalline peaks emerged from the amorphous region, indicating the amorphous to crystalline transformation. The elemental titanium peaks remain present in the as-anodized (amorphous) and heat treated (crystalline) TiNT samples. Additionally, the amorphous bump is much less pronounced in the heat-treated sample owing to anatase formation.

The crystallinity calculation was performed based on the presumption that the broad peak comes from the amorphous phase and sharp peaks come from crystalline phases. These peaks on an XRD of as-anodized and heat treated samples can be seen from Fig.5.7b.

The area under the XRD profile represents three types of data, the amorphous region, crystalline peaks, and the elemental titanium peaks. To measure the relative amounts of amorphous and crystalline phases present in the heat-treated TiNT samples, the area under each peak was calculated using crystallinity analysis capabilities of XRD software. The elemental titanium peaks, which are present in both heated and as-anodized TiNT samples are excluded in the area calculations. Thus, by calculating the total area under the XRD profile, and excluding the area under the elemental titanium peaks, yields a common area composed of amorphous and crystalline phases. To measure the crystalline fraction, the area under the crystalline peaks was calculated. In Fig.5.7b, the area shown in green below the crystalline peaks represents the untransformed amorphous fraction. In the case of grouped peaks (at 38°), sharing elemental and crystalline peaks, the ratio of areas under the individual peaks was calculated from the relative peak intensity ratios. The background subtraction and profile fitting of raw XRD profile was done to get the relative peak intensities.

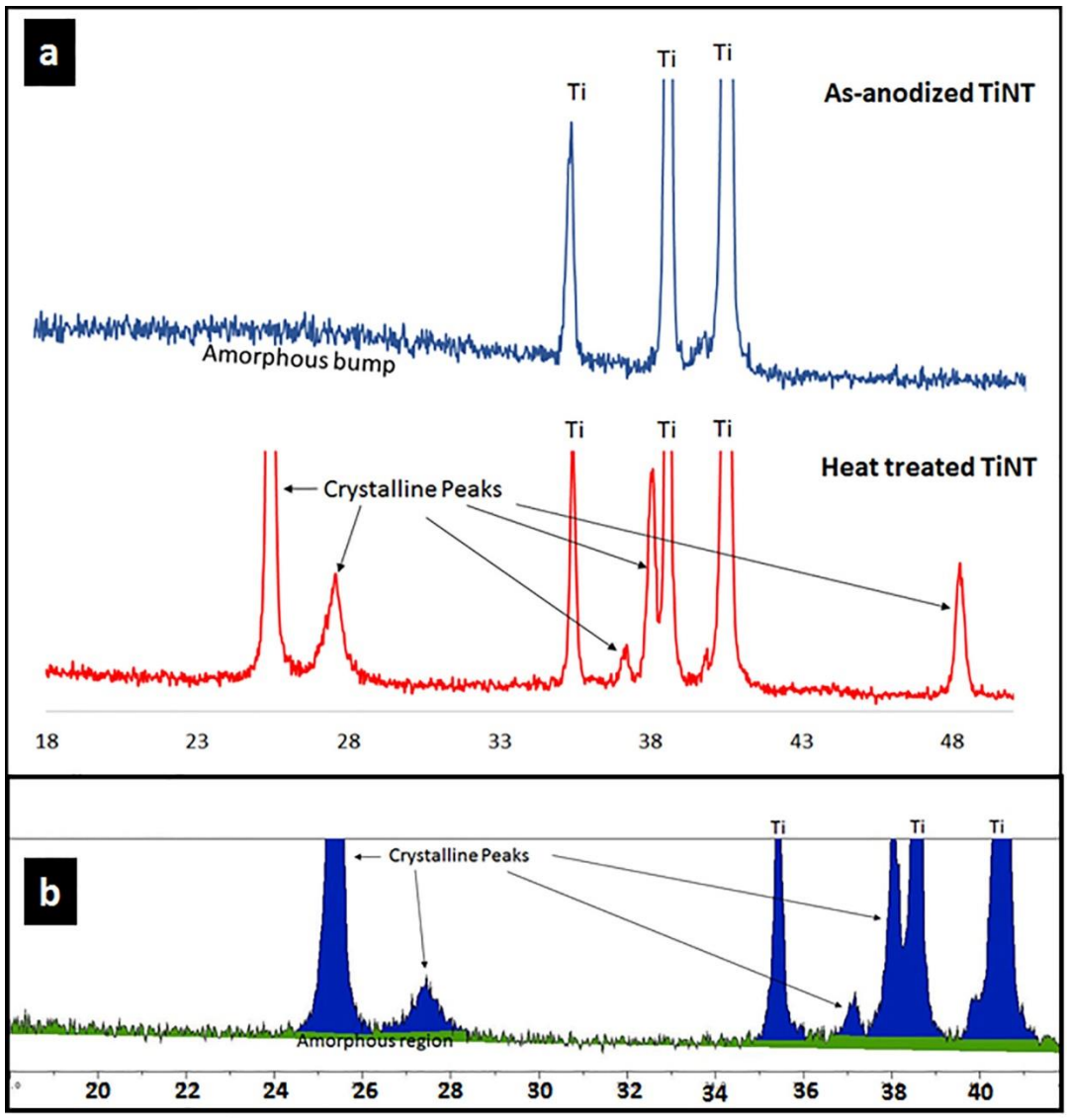

Figure 5.7 (a) Amorphous and crystalline regions and (b) measurement of crystalline fractions.

5.3.6 Activation energy

As anatase crystallization is a surface dominated nucleation process, to quantitatively describe the transformation of TiO_2 nanotubes, a kinetic model for amorphous TiO_2-to-anatase transformation proposed by Madras and McCoy [17] was adapted. This model represents coalescence by classical Smoluchowski theory and transformation by an overall first-order reaction, $\chi = k_p t$, where, χ is the time dependent crystalline weight fraction, k_p is the first order rate coefficient for transformation from amorphous to anatase, and t is the annealing time. Fig.5.8 shows the experimental data of annealing time dependence for amorphous to crystalline transformation at 350C (623K), 400C (673K) and 450C (723K). The points represent the data from the prior XRD calculations described in section 5.3.5.

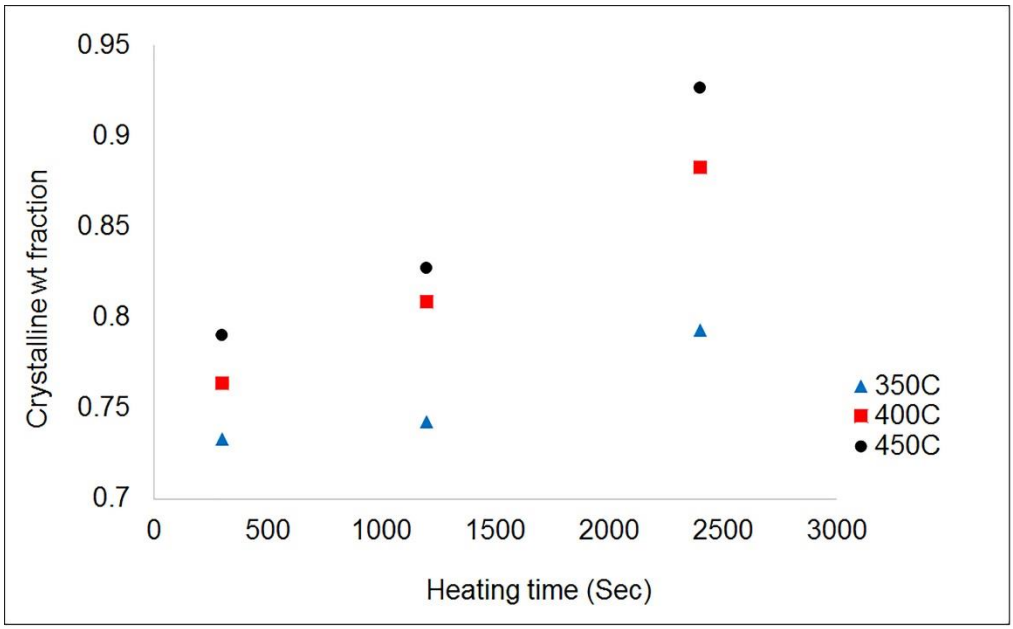

Figure 5.8 Amorphous to crystalline transformation at different temperatures.

The reaction rate depends on temperature, so the transformation rate coefficient (k_p) will be different for different temperatures. To determine the crystalline weight fraction (χ) at 350C, the known anatase content after 5 minutes heating was calculated to be 71.90%. Considering this as a starting point, or zero datum, to calculate the fraction of amorphous which got converted upon further heating, experimental data shows that further heating for 20 minutes total yields 74.24% anatase.

$$\chi = \frac{(anatase\ \%\ at\ 20\ min - anatase\ \%\ at\ 5\ min)}{anatase\ \%\ at\ 5\ min}$$

$$\chi = \frac{(74.24-71.90)}{71.90} = 0.03255.$$

Further heating for 40 minutes total at 350C yields 79.29% anatase,

$$\chi = \frac{(anatase\ \%\ at\ 40\ min - anatase\ \%\ at\ 5\ min)}{anatase\ \%\ at\ 5\ min}$$

$$\chi = \frac{(79.29-71.90)}{71.90} = 0.10278.$$

This indicates that heating for 20 minutes transformed an additional 3.26% to anatase from 5 minutes heating. Heating for 40 minutes, transformed an additional 10.28%. Similarly, using experimental data of anatase % achieved at temperatures of 400C and 450C at different times, the variable χ for amorphous to anatase transformation was calculated (Table 5.1) and the time dependence of the variable χ for amorphous to anatase transformation is plotted (Fig.5.9a).

Table 5.1 Variable χ for amorphous to anatase transformation

Time (Min)	Time (Sec)	χ for 350C	χ for 400C	χ for 450C
5	300	0	0	0
20	1200	0.03255	0.05907	0.04657
40	2400	0.10278	0.155992	0.172488

The values of the transformation rate coefficient K_p were obtained by regressing the experimental data of the transformation. It is evident from Fig.5.9a that the crystalline weight fraction is linear with heating time with a slope of k_p i.e. $\chi = k_p t$. The points in Fig.5.9a represent the calculated variable χ (Table 5.1) from the experimental data (Fig.5.8) and the slope of the trend lines represent the transformation rate coefficient k_p. Table 5.2 shows the values of 1000/T and ln(k_p), plotted in Arrhenius plot (Fig.5.9b).

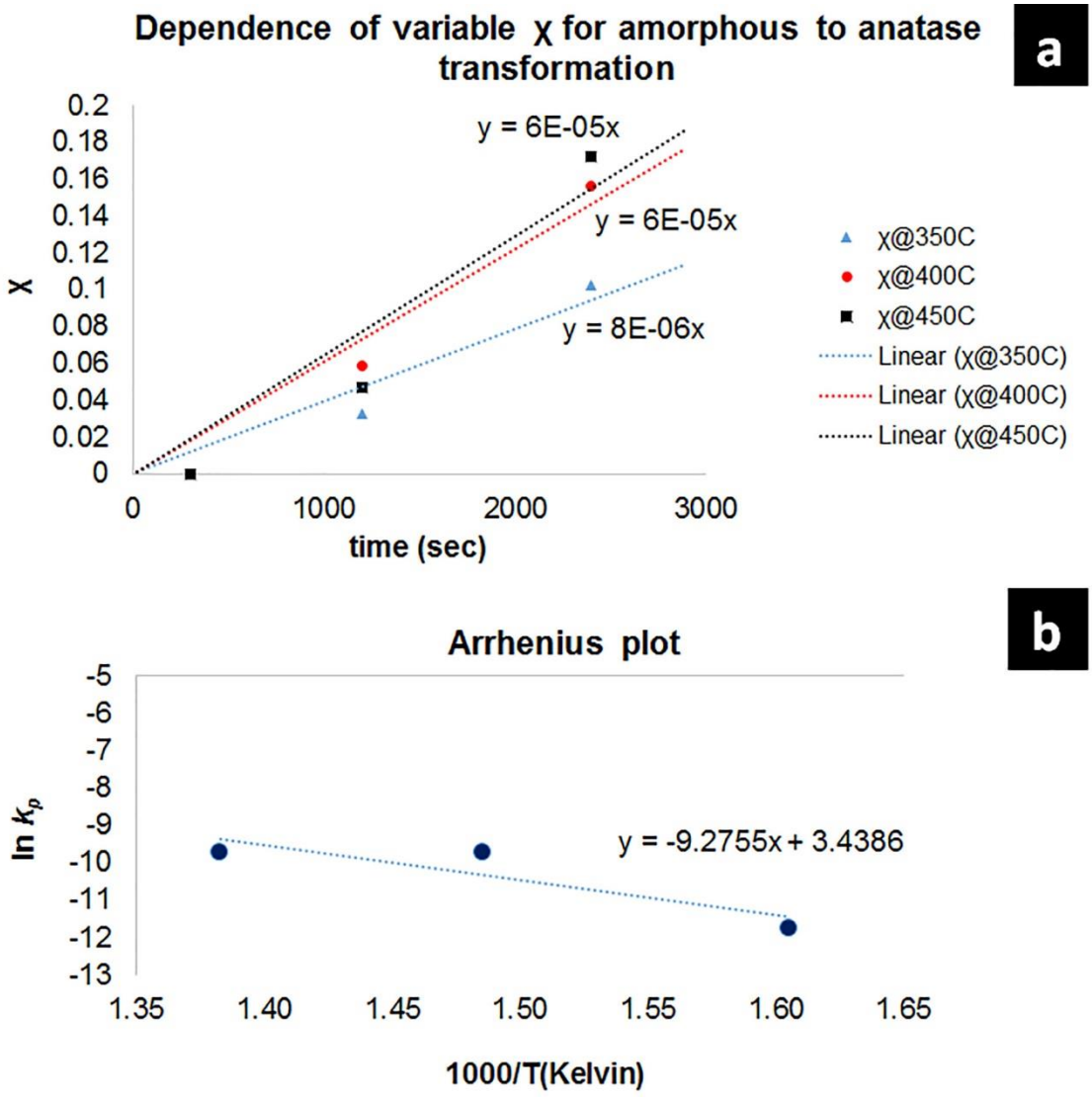

Figure 5.9 (a) The time dependence of variable χ for amorphous to anatase transformation. The points represent experimental data (Table 1), and lines are based on model used ($\chi = k_p t$). (b) Arrhenius plot of transformation rate coefficient (k_p).

Table 5.2 Vales of 1000/T and ln(k_p) calculated.

Temp (ºC)	Temperature (Kelvin)	1000/Temperature in Kelvin	k_p	ln(k_p)
350C	623	1.61	0.0000080	-11.736
400C	673.15	1.49	0.0000600	-9.721
450C	723.15	1.38	0.0000600	-9.721

In chemical kinetics, a reaction rate coefficient (k_p), quantifies the rate of a chemical reaction. The Arrhenius equation gives the dependence of the rate coefficient of a chemical reaction on absolute temperature. It has been reported that, the amorphous to anatase transformation is an independent solid-state transformation involving the transformation of each TiO_2 particle (and associated water molecules) with simultaneous dehydration and therefore has a latent heat [17]. The relationship between activation energy and the reaction rate can be represented by the Arrhenius equation ($k_p = A\ e^{-Ea/RT}$)[18], where k_p is the reaction rate coefficient, T is temperature in Kelvin, A is a constant, E_a is activation energy and R is the universal gas constant. Thus, for a reaction having a rate coefficient which follows the Arrhenius equation, a plot of ln(k_p) versus (1/T) gives a straight line, whose slope can be used to determine the activation energy (E_a). The slope of the line multiplied by the universal gas constant yields a value of E_a. Fig.5.9b shows the Arrhenius plot of the natural logarithm of the transformation rate coefficient (ln k_p) with (1000/T). The natural logarithm of the Arrhenius equation yields:

$$\ln(kp) = -\frac{\mathrm{Ea}}{\mathrm{R}}\left(\frac{1}{T}\right) + \ln(A)$$

which is in the form of a straight-line y = mx + c where, x is reciprocal of T. Rearranging gives,

$$\ln(kp) = -\frac{\mathrm{Ea}}{1000\mathrm{R}}\left(\frac{1000}{T}\right) + \ln(A)$$

Where the slope of the Arrhenius plot is, $m = \frac{-\mathrm{Ea}}{1000R}$.

Therefore, $-E_a = m * 1000R$ = -0.92755 (Kelvin) * 1000 * 8.3144 (J/mol.Kelvin) = 77.12 kJ/mol. This analysis will form the basis for the design of a production heat treating process that is briefly described in Chapter 8.

5.3.7 Morphological analysis

The electrochemical anodization gives increased true surface area with the same lateral area due to height and open volume between the nanotubes. The morphology and structure of TiNTs do not depend only on the anodization parameters, as the heat-treating conditions may affect the morphology. It has been reported that, the changes in crystalline structure that occur during heating lead to expansion of titania grains [16] and consequently the nanotube walls can coalesce, which may result in the collapse of the nanostructure to small diameter pores [19]. It is further reported that rutile crystallites grow in size with increasing temperature and finally, leads to the destruction of the nanotube structure if heated above 680C [16]. Fig.5.10 shows SEM images of as-anodized and heat treated samples. It is confirmed that the present range of annealing temperatures (300C to 500C) and heating times (5 to 40 minutes, and 180 minutes for controls) has no effect on the morphology of the nanotubes. The heat treatment did not change the nanotube

morphologies. Both images are at the same magnification, although not the same exact location. However, there were no obvious differences in the size and shape of the nanotubes for any of the samples.

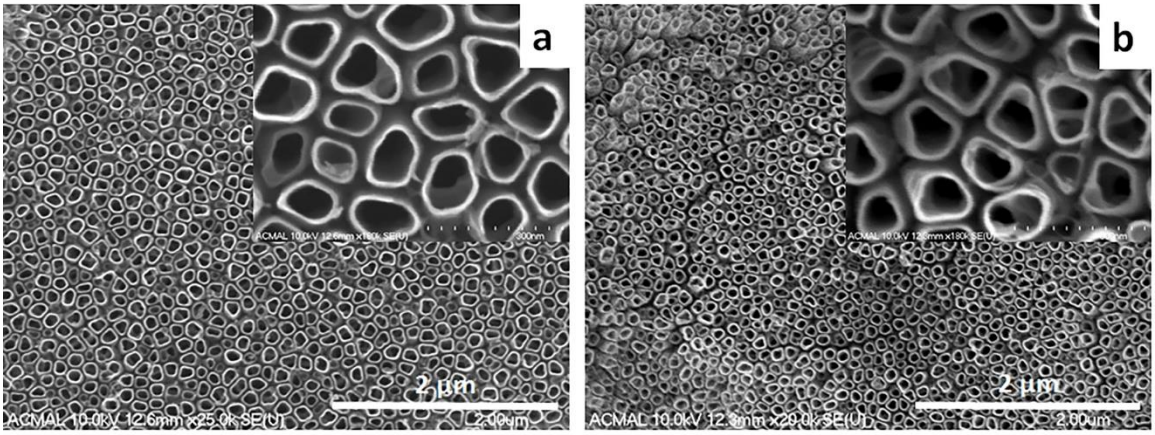

Figure 5.10 SEM images of (a) as-anodized and (b) 5 minutes annealed at 350C TiNT samples.

A comparison among EDS of the as-anodized TiNTs and those heated for 5 minutes at 350C, and the relative wt% of oxygen with respect to titanium upon heat treating, indicates the sample chemistry and the release of fluorine from the TiNTs without affecting morphology (Table 5.3). Residual fluorine in the as-anodized samples is normal due to the fluorine content in the electrolyte and the fact that it is fluorine that is chemically responsible for the nanotube formation [20]. The decreased wt% of fluorine indicates reduced residual fluorine from the electrolyte which may be beneficial from a regulatory standpoint [21, 22].

Table 5.3 EDS relative wt% analysis of as-anodized and 350C-5min heat treated sample.

Elements	Ti	Al	V	O	F	C	N
As-anodized Sample	57.51	4.92	0.93	28.55	3.53	0.26	4.30
Heat treated at 350C for 5 minutes	58.10	4.96	0.62	28.7	0.36	0.68	4.45

5.3.8 Temperature profile as function of depth

Because of the short time with which anatase formed in the approximately 1 micrometer long nanotubes, and that the foil samples were 0.5mm thick, it is important to investigate the time-dependent transient heat transfer into the nanotube surface layer and the underlying bulk titanium in a larger implant such as a hip stem. To estimate the heat penetration during heating at 350C for 5 minutes in a larger sample, the case of a Ti6Al4V hip stem with 25.4mm diameter and 250mm length was considered. The material properties of Ti6Al4V are density (ρ) = 4.43g/cc, thermal conductivity (λ) = 4.8W/mK, and specific heat (c_p) = 683J/kgK. It is assumed that the heat treatment on an industrial scale would be in a flow-through convection oven operating at or above 350C, therefore a surface boundary condition of 350C is assumed. Using a simplified one dimensional transient heat conduction equation in cylindrical coordinates, a Matlab code was used to study the radial temperature distribution below the surface as a function of depth (r) with respect to time.

$$\frac{\partial^2 T}{\partial r^2} = \left[\alpha\left(\frac{\partial^2 T}{\partial r^2} + \frac{1}{r}\frac{\partial T}{\partial r}\right)\right]$$

Where α is the thermal diffusivity,

$$\alpha = \frac{k}{\rho\, Cp}$$

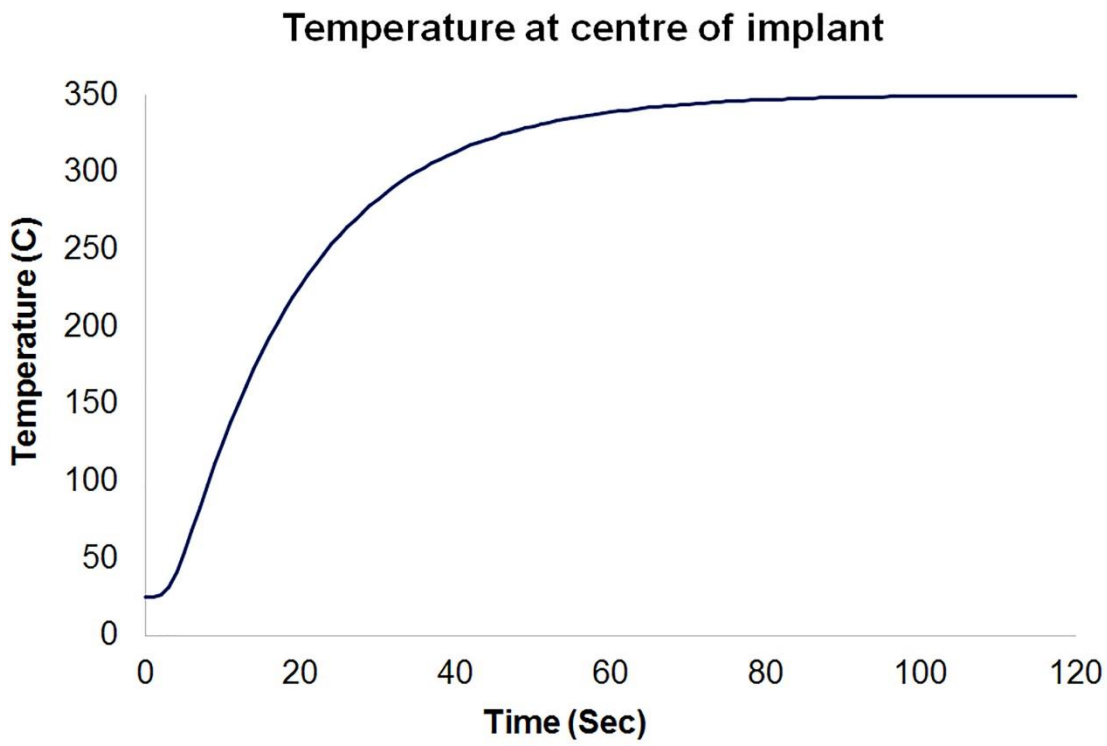

Figure 5.11 Radial temperature distribution profile below the surface with respect to time.

It can be seen from Fig.5.11 that after 90 seconds the temperature of the implant core becomes 350C and equalizes throughout the cross-section. The analysis also showed that the outermost 10 μm of the simulated hip stem reached 350C in much less than one minute, ensuring that anatase conversion will take place within the nanotube layer.

5.4 Conclusions

The transformation kinetics of amorphous to anatase titania nanotubes fabricated by electrochemical anodization using a safe electrolyte based on ammonium fluoride, ethylene glycol, and water shows that anatase transformation takes place at a temperature as low as 350C and time as short as 5 minutes. The conversion in the nanotubes has been confirmed by XRD and TEM diffraction images. It has been shown that the rapid heating will liberate residual fluorine in the anodized surface without affecting the morphology of the nanotubes. This quick, simple and economical technique is promising in industrial-scale manufacturing for the synthesis of anatase TiO_2 nanotube orthopedic implant surfaces favorable for improved bio-functional properties.

References

[1] Das K, Bose S, Bandyopadhyay A. TiO_2 nanotubes on Ti: Influence of nanoscale morphology on bone cell-materials interaction. J Biomed Mater Res A. 2009;90:225-37.

[2] Cai Q, Paulose M, Varghese OK, Grimes CA. The effect of electrolyte composition on the fabrication of self-organized titanium oxide nanotube arrays by anodic oxidation. Journal of Materials Research. 2011;20:230-6.

[3] Regonini D, Clemens FJ. Anodized TiO_2 nanotubes: Effect of anodizing time on film length, morphology and photoelectrochemical properties. Materials Letters. 2015;142:97-101.

[4] Shankar K, Mor GK, Prakasam HE, Yoriya S, Paulose M, Varghese OK, et al. Highly-ordered TiO_2 nanotube arrays up to 220 μm in length: Use in water photoelectrolysis and dye-sensitized solar cells. Nanotechnology. 2007;18:065707.

[5] Sun L, Zhang S, Sun XW, He X. Effect of electric field strength on the length of anodized titania nanotube arrays. Journal of Electroanalytical Chemistry. 2009;637:6-12.

[6] Mazare A, Dilea M, Ionita D, Titorencu I, Trusca V, Vasile E. Changing bioperformance of TiO_2 amorphous nanotubes as an effect of inducing crystallinity. Bioelectrochemistry. 2012;87:124-31.

[7] Regonini D, Bowen CR, Jaroenworaluck A, Stevens R. A review of growth mechanism, structure and crystallinity of anodized TiO_2 nanotubes. Materials Science and Engineering: R: Reports. 2013;74:377-406.

[8] Du GD, Wan B, Guo ZP, Shen JN, Li Y, Liu HK. Effect of annealing on electrochemical performance of anodized TiO_2 nanotubes for lithium ion batteries. Adv Sci Lett. 2011;4:469-73.

[9] Kondo. JN, Domen. K. Crystallization of mesoporous metal oxides. Chem Mater. 2008;20:835–47.

[10] He J, Zhou W, Zhou X, Zhong X, Zhang X, Wan P, et al. The anatase phase of nanotopography titania plays an important role on osteoblast cell morphology and proliferation. J Mater Sci Mater Med. 2008;19:3465-72.

[11] Giordano C, Saino E, Rimondini L, Pedeferri MP, Visai L, Cigada A, et al. Electrochemically induced anatase inhibits bacterial colonization on Titanium Grade 2 and Ti6Al4V alloy for dental and orthopedic devices. Colloids Surf B Biointerfaces. 2011;88:648-55.

[12] Banfield HZJ. Understanding polymorphic phase transformation behavious during growth of nanocrystalline aggregates: Insights from TiO_2. Journal of Physical Chemistry B. 2000;104:3481-7.

[13] Macak JM, Aldabergerova S, Ghicov A, Schmuki P. Smooth anodic TiO_2 nanotubes: annealing and structure. Physica Status Solidi (a). 2006;203:R67-R9.

[14] Ghafar Ali SHY, Jong Min Kum, Hamid Saeed Raza, Deliang Chen, Sung Oh Cho. Formation of hierarchical TiO_2 nanoporous structure from free-standing TiO_2 nanotubes layers. Journal of Nanoparticle Research. 2012;14.

[15] Albu SP, Ghicov A, Aldabergenova S, Drechsel P, LeClere D, Thompson GE, et al. Formation of double-walled TiO_2 nanotubes and robust anatase membranes. Advanced Materials. 2008;20:4135–9.

[16] Varghese OK, Gong D, Paulose M, Grimes CA, Dickey EC. Crystallization and high-temperature structural stability of titanium oxide nanotube arrays. Journal of Materials Research. 2011;18:156-65.

[17] Madras G, McCoy B. Kinetic model for transformation from nanosized amorphous TiO_2 to anatase. Crystal Growth and Design. 2007;7:250-3.

[18] Laidler KJ. The development of the arrhenius equation. J Chem Educ. 1984;61:494-8.

[19] Jarosz M, Syrek K, Kapusta-Kolodziej J, Mech J, Malek K, Hnida K, et al. Heat treatment effect on crystalline structure and photoelectrochemical properties of anodic TiO_2 nanotube arrays formed in ethylene glycol and glycerol based electrolytes. J Phys Chem C. 2015;119:24182-91.

[20] Zwilling V, Darque-Ceretti E, Boutry-Forveille A, David D, Y. PM, M. A. Structure and physicochemistry of anodic oxide films on titanium and TA6V alloy. Surface and Interface Analysis. 1999;27:629-37.

[21] Regonini D, Jaroenworaluck A, Stevens R, Bowen CR. Effect of heat treatment on the properties and structure of TiO_2 nanotubes: Phase composition and chemical composition. Surface and Interface Analysis. 2010;42:139-44.

[22] Bhosle S, Friedrich C. Effects of aging and thermal treatment on nanotextured titanium surfaces. Poster presented at ORS Annual Meeting. 2016 March 5-8;Orlando, FL.

Chapter 6

Fluorine in nanotube surfaces and anodization electrolyte*

Abstract

Fluorine, being electronegative and relatively small (van der Waals radius 1.47Å) has the potential to influence protein interactions with implant surfaces in the biological environment. Incorporation of a controlled amount of fluorine on implant surfaces can improve osseointegration. An appropriate amount of fluorine concentration in the electrolyte is essential for the formation of nanotube surfaces by electrochemical anodization, which decreases upon reuse of the electrolyte. This study accounts for the fluorine depletion in the electrolyte during anodization. The fluorine consumed by the formation of the titanium nanotube layer during electrochemical anodization of Ti6Al4V alloy foils was analyzed by scanning electron microscopy and energy dispersive X-ray spectroscopy.

6.1 Introduction

Recent developments in orthopedic implant surface modification calls for better knowledge and understanding of early stages of bone formation and dynamic process of osseointegration. The osteoblast growth on implant surface depends on surface topography

---

* *The material contained in this chapter is in preparation for submission to a journal. As the first author of this publication, I have done the fabrication of nanotube surfaces, SEM and EDS characterization, samples preparation for ICP-OES analysis, literature review, results analysis and writing the manuscript.*

and chemistry. Bone-like topography on the surface, and controlled chemical composition at the nanometer scale, can help the spreading and attachment of osteoblasts on the implant surface [1]. An experimental study on dogs reported that during healing of implants with different surface roughness, the degree and rate of osseointegration varies [2]. The surface modifications of implants, however, are not only limited to change in surface roughness. The moderately roughened (average $R_a = 0.91 \pm 0.14\mu m$) and fluoride modified (titanium fluoride 0.5 to 3 atomic%) surfaces support and promote cell proliferation and differentiation better than non-fluoride modified surfaces [3]. Another study reported that 1.21 wt% (1.88 atomic %) of fluorine in an implant surface enhances bone fixation [4]. Data presented on an experimental study on the mandibles of dogs suggests that the fluoride-containing implant surface promotes bone formation and osseointegration [5]. *In vivo* studies in rabbit tibia with fluoride modified titanium implants demonstrated better bone anchorage [6]. Enhanced osteoblastic differentiation was demonstrated *in vitro* and increased bone formation *in vivo* was demonstrated on fluoride ion modified TiO_2 grit blasted Cp titanium implants [7]. These studies reported that the modified biochemistry of implant surfaces may facilitate osseointegration and fluoride presence may be beneficial. The fate of the implant after implantation is largely affected by protein adsorption from the surrounding biological environment. It is generally understood that the proteins can act as a mediator to attract the negatively charged osteoblasts toward a negatively charged implant surface. Thus, a titanium nanotubular surface can provide binding affinity due to a higher magnitude of negative surface charge density [8].

Titanium nanotube (TiNT) surfaces are formed in fluoride-containing electrolyte by electrochemical anodization. The reproducibility of nanotubular structure depends on several process parameters, most notably the fluorine ion concentration in the electrolyte. Our previous study [9], revealed that reuse of the electrolyte causes depletion of fluorine concentration in the electrolyte resulting in morphological variations from fully developed nanotubes to a porous, less developed nanotube surface. This study further revealed that reuse of the electrolyte for anodizing multiple samples resulted in electrolyte contamination due to the etched metals released into the electrolyte. From a manufacturing control perspective, understanding and accounting for the decreased fluorine concentration in the electrolyte can provide better process control.

Electrochemical anodization of Ti6Al4V foils in 1L of electrolyte containing 98% ethylene glycol, 0.66 wt% NH_4F and 2% deionized water (LWHF electrolyte) was carried out at 60V for 40 minutes. The fluoride concentration in the electrolyte decreased in a log-linear fashion, from an initial value of approximately 3033ppm to approximately 333ppm, as measured by an ion sensitive electrode, after etching 345cm^2. Based on experimental data from this prior study [9], the objective of the present work was to identify and analyze the potential sources of fluorine consumption from the bulk electrolyte.

6.2 Materials and Methods

6.2.1 Substrate preparation

Alloy foils (0.5mm thick by 10mm wide) of ASTM B 265-11 grade 5 (TIMET, USA), were mechanically polished using #150 grit fine crocus cloth and #800 grit ultra-fine sanding cloth. After cleaning in DI water followed by acetone, the samples were dried in air at room temperature. The anodized portion of each sample was 10mm x 75mm.

6.2.2 Formation of nanotube surface

The nanotube layer was formed on the Ti6Al4V foils by electrochemical anodization using a DC power source (Protek 3006B), with 0-60VDC, 1.5A output. Electrolyte containing 98% ethylene glycol, 2% DI water and 0.66 wt% of NH_4F was used for etching. The foils were anodized at 60VDC for 40 minutes with a graphite rod cathode and the foil as the anode, at room temperature. After anodization, TiNT samples were air dried for 24h and ultrasonically cleaned in DI water for 5 minutes to remove possible surface aggregation formed over TiNT layer during anodization.

6.2.3 Surface characterization

Characterization of the as-anodized and sonicated TiNT surfaces was performed by field emission scanning electron microscopy (FESEM, Hitachi S-4700). The relative wt% chemical analysis was performed by EDS at 10 kV.

6.2.4 Statistical analysis

The EDS spectra were collected at four different locations on each sample for compositional characterization using standardless quantitative analysis and the data are reported as an average and range of those readings.

6.3 Results

6.3.1 SEM morphology

The change in morphology of the anodized layer was limited to only the surface aggregate formed on the top of the TiNT surface by depleting the fluoride concentration upon extended use of the electrolyte [9]. Ultrasonic cleaning of the surfaces revealed the tubular morphology obtained underneath the surface aggregation (Fig.6.1a). The variation in TiNT layer thickness was observed with the as-anodized and ultrasonically cleaned surfaces. The TiNT layer thickness (nanotube length) obtained with the as-anodized condition was approximately 4.5µm (Fig.6.1b) and with sonication the TiNT layer was approximately 3.5 µm (Fig.6.1c) after removal of surface aggregation.

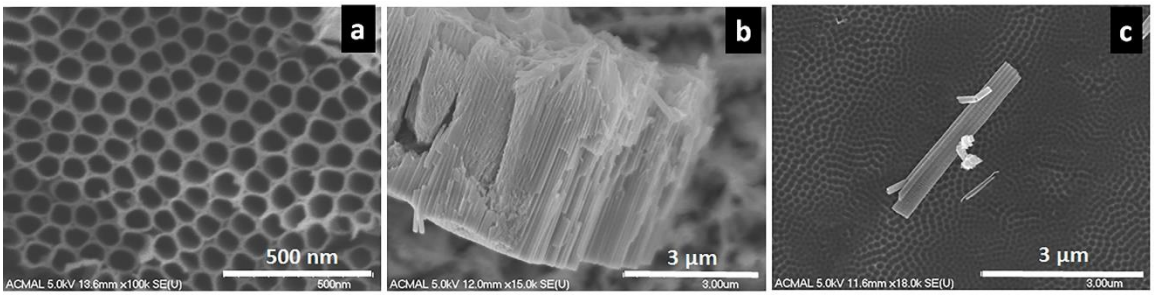

Fig.6.1 SEM micrographs of TiNT layer (a) top view of sonicated surface; (b) nanotube length in as-anodized surface; (c) nanotube length in ultrasonically cleaned surface.

6.3.2 Composition analysis of TiNT layer

To investigate the sources of fluorine consumption from the electrolyte during anodization, the first and obvious source was the TiNT layer. Table 6.1 summarizes the average element wt% from EDS analysis. The structures were characterized to compare

the effect of the fresh and reused electrolyte. EDS results revealed that, there was a decrease in the residual fluorine in the TiNT layer obtained from reused electrolyte. The wt% of fluorine in the TiNT layer decreased from 11.99 wt% with fresh electrolyte to 9.46 wt% with well-used electrolyte. It was hypothesized that upon extended reuse of the electrolyte, the decreased F^- ion concentration lowered the ionic migration, resulting in decreased fluoride complexes and variation in the chemical composition of nanotube layers. The measurements also tend to indicate that with fresh electrolyte the TiNTs are more heavily oxidized as seen by the oxygen drop from 34.29 to 27.98 wt%.

Table 6.1 Summary of average relative wt% of elements from EDS analysis.

Type of surface	Average relative wt% of elements				
	Ti	Al	V	F	O
Control (not anodized)	88.68	7.27	3.90	0	0.15
TiNT obtained with fresh electrolyte	47.51	3.64	2.57	11.99	34.29
TiNT obtained with well-used electrolyte	56.30	3.51	2.76	9.46	27.98

6.3.3 Investigation of nanotube bottoms and substrate

Titania nanotubes can fail by compression characterizing inelastic deformation behavior under compressive loads [10]. The nanotube arrays formed on alloy and Cp titanium in LWHF electrolyte (at 60V for 40min) were pulled-out from the substrate by axial tensile loading and characterized using SEM and EDS. The failure behavior of TiO_2 nanotube arrays under axial tensile loads were investigated and the chemical nature of the nanotube bottoms and underlying substrate were also quantified. The nanotube arrays failed along the weak 'failure interface' between the substrate and the outer bottom of the nanotubes under axial tensile loads. Fig.6.2 shows the pulled-out TiO_2 nanotubes surface

on Cp TiNT, nanotube bottoms, and left-behind substrate, representing a failure interface between the substrate and bottom of the nanotubes. It was observed that the nanotubes did not fail along the length, but failed from the bottom at the bulk material interface. It was observed that a texture comprising shallow depressions was created on the substrate due to pull-out of the tubes. Localized patterns in the underlying texture were observed at relatively higher magnification (not shown here) due to the biphasic nature of the Ti6Al4V alloy along the different grain boundaries of α – β phases. Due to the very difficult nature of measuring the axial tensile load at failure, data is not presented. However, the design of a shear strength test to be performed is presented in Chapter 8.

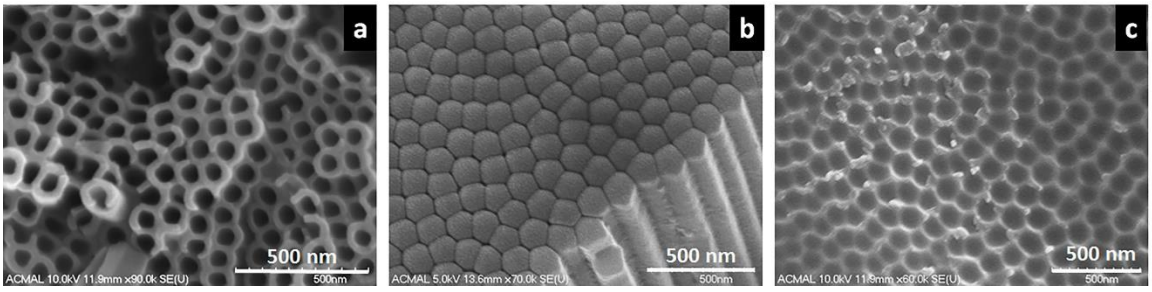

Figure 6.2 SEM image of the TiNTs (a) top view of nanotube surface (b) inverted bottoms of pulled-out nanotubes (c) left-behind substrate.

To quantify the chemical nature of the failure interface, energy dispersive spectroscopy (EDS) analysis was performed on the inverted nanotube bottoms and the substrate. The chemical composition shows a large increase in the amount of oxide formation at the nanotube bottoms that indicated the weakened failure interface. Table 6.2 summarizes the elemental composition determined from EDS results. The nanotube

chemical reaction equations from section 2.3.3 shows the formation and presence of TiO_2. Therefore, the oxygen-rich interface appears to be in the form of brittle TiO_2.

Table 6.2 Summary of average relative wt% of elements from EDS analysis of pulled-out TiNT arrays

Type of surface		Average relative wt% of elements				
		Ti	Al	V	F	O
Cp Titanium	Nanotube bottoms	54.51	--	--	7.54	37.94
	Substrate	99.18	--	--	--	1.01
Ti6Al4V	Nanotube bottoms	46.08	4.22	1.47	9.81	37.97
	Substrate	90.78	8.24	0.96	0	0

6.3.4 Fluorine leach out from TiNTs

To investigate the possibility of fluorine leaching out from the TiNT surface after implantation in a biological environment, TiNTs etched on Ti6Al4V surfaces were immersed in phosphate buffer solution (PBS) of pH 7.4, simulating body fluid. After immersion in a sealed container for 140 days, the TiNT surfaces were taken out from the buffer solution, rinsed in DI water and ambient dried. No morphological change was observed. Table 6.3 summarizes the average relative wt% of elements from EDS. Components of the PBS are included to show relative wt% contributions. The salts and gaseous elements observed on the surface indicated presence of dried PBS on the TiNT. The ratio of F : Ti before and after PBS immersion 0.25 and 0.11, indicated that the fluorine came out of nanotubes. This was also observed with ratio of F : Ti+Al+V before and after PBS immersion which was 0.22 and 0.1. This can be further quantified by estimating the mass of fluorine remaining in nanotubes after PBS immersion.

Table 6.3. Summary of average relative wt% of elements from EDS analysis of PBS immersed TiNTs

Type of surface	Average relative wt% of elements										
	Ti	Al	V	F	O	C	N	Na	P	Cl	K
PBS immersed TiNT	42.55	3.56	0.98	4.83	34.49	4.33	4.35	2.71	1.49	0.05	0.57

6.3.5 Estimation of mass of fluorine in TiNT layer

The volume of the Ti-alloy removed during anodization was calculated from the area fraction and nanotube length measurements using ImageJ analysis of the FESEM images. By knowing the volume of material removed during the nanotube layer formation, and the density of TiO_2 (4.23g/cc), the approximate mass of the remaining nanotube layer was calculated (Table 6.4). The heavily oxidized nanotube layer is closely approximated by using the density of TiO_2. Based on the mass composition of the Ti6Al4V alloy, the mass fraction of titanium present in the bulk alloy substrate was 90% and was used as the basis for the EDS relative mass percentages of the other elements. This approach is based on that in the original alloy, the relative mass of titanium to aluminum is 15 and titanium to vanadium is 22.5. In the TiNTs using the fresh electrolyte, these ratios from Table 6.1 are 13.1 and 18.5. Because Ti6Al4V is an alpha-beta phase alloy, some areas are aluminum-rich, while other areas are vanadium-rich compared to the overall average. The TiNTs from the reused electrolyte have the ratios of 16.0 and 20.4 which are reasonable given the nature of the overall measurements. By knowing the mass of Ti present per anodized area of the nanotube structure, and using the EDS wt% ratio of Ti:F, the

estimation of the mass of fluorine per area (μg/cm^2) present in TiNTs was calculated. Table 6.4 shows the calculations for estimating the mass of residual fluorine in TiNTs formed in fresh and used electrolyte. The amount of fluorine remaining in the TiNT surface depends on the fluorine concentration in the electrolyte. A higher fluorine concentration in the electrolyte led to a higher residual fluorine per area in the TiNT surfaces. It has been reported that during anodization, the growth of nanotubes leads to the formation of the hexafluorotitanate complex, TiF_6^{2-}, due to fluorine diffusion from the electrolyte [11]. The presence of fluorine in the anodized surfaces is indicative of TiF_6^{2-} formed during etching. The decreased fluorine wt% observed in the surfaces with used electrolyte can be attributed to fewer TiF_6^{2-} complexes formed and shallower nanotubes. The fresh electrolyte yielded 124.9 μg/cm^2 of residual fluorine in the as-anodized TiNTs and 97.14 μg/cm^2 in ultrasonically cleaned TiNTs. This indicates that the aggregation layer above the well-formed nanotubes (sometimes called 'nanograss' in some literature) removed by sonication was also rich in fluorine as was expected. The used electrolyte (with F^- concentration of 333ppm) yielded 83.07 μg/cm^2 of residual fluorine in the as-anodized TiNTs and 64.61 μg/cm^2 of residual fluorine in ultrasonically cleaned TiNTs again showing a fluorine-rich aggregation layer.

Table 6.4 Estimation of the mass of residual fluorine in TiNTs formed with the fresh and well-used electrolyte.

Sample description	% of surface removed upon etching (from ImageJ)	Nanotube length (μm)	Volume of unetched oxide layer (cm^3/cm^2)	Mass of unetched TiNT layer ($\mu g/cm^2$)	Mass of TiNT layer ($\mu g/cm^2$)	Mass of titanium in TiNT layer ($\mu g/cm^2$)	EDS wt% of Ti	EDS wt% of Fluorine	Ratio of EDS wt% of F/Ti	Mass of TiNT x ratio of EDS wt% = Mass of Fluorine ($\mu g/cm^2$)
As-anodized TiNT in fresh electrolyte	74	4.5	4.5	1904	495	445.4	47.5	11.99	0.25	124.9
As-anodized TiNT in used electrolyte	74	4.5	4.5	1904	495	445.4	56.3	9.45	0.16	83.07
Sonicated TiNT in fresh electrolyte	74	3.5	4.5	1481	385	346.4	47.5	11.99	0.25	97.14
Sonicated TiNT in used electrolyte	74	3.5	3.5	1481	385	346.4	56.3	9.45	0.16	64.61
TiNT on TPS hip stem implant	54	1.2	1.2	510	230	210.1	63.18	6.54	0.10	24.17
PBS immersed as-anodized TiNT in fresh electrolyte	74	4.5	4.5	1904	495	445.4	42.55	4.83	0.11	56.18

*To calculate mass, used density of TiO_2 = 4.23 g/cm^3
**The % of titanium by weight in metal = 90%

6.3.6 Composition analysis of cathode

The graphite cathode, directly involved in the anodization, was investigated as a potential source of fluorine consumption. Table 6.5 summarizes the average relative wt% composition of the cathode from EDS analysis. It was confirmed that there was no fluorine or metals present on the cathode. Hence, the cathode was not considered in the electrolyte fluorine consumption analysis.

Table 6.5. Summary of average relative wt% of cathode surface.

Element	Ti	Al	V	F	O	N	Si	C
Cathode	0	0	0	0	3.87	1.83	0.07	94.20

6.3.7 Composition analysis of metal particles dissolved in electrolyte

From the experimental fluorine depletion data [9], the metals released into the electrolyte during anodization were identified as the next candidates for fluorine consumption during anodization. To extract the released metal particles from the electrolyte, a 10ml sample from the used bulk electrolyte was dried to a powder at 250C in Teflon evaporating dishes. EDS analysis was performed on these particulates. Fig.6.3 shows SEM images of various sizes of particulates extracted from the heat dried electrolyte. The smallest metal particle observed was approximately 500nm.

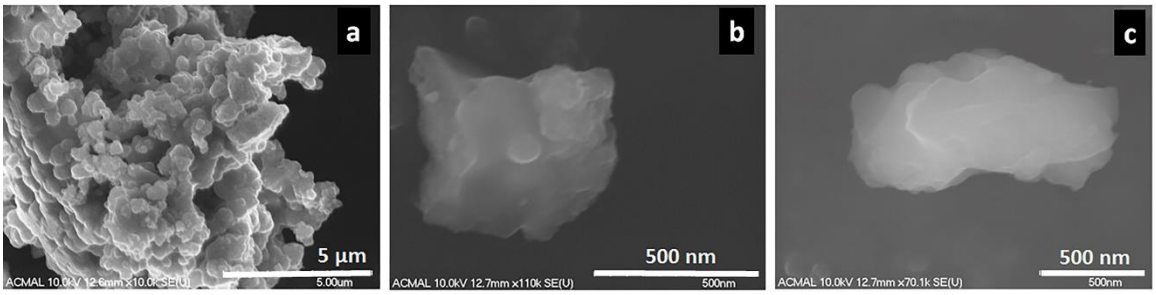

Figure 6.3 Metals particulates extracted from heat dried electrolyte. (a) large metals residue constituted of small particles; (b) smallest particle observed; (c) small particle.

As a second method to verify the chemical composition of the metals released into the electrolyte, a 10ml sample from the used electrolyte was centrifuged at 4500rpm for 1h. The centrifuging in a Thermo Fisher Sorvall™ ST 8 centrifuge with TX-150 swinging bucket rotor number 75005701 (giving 3260 g) resulted in white sedimentation of particles in the electrolyte. After pipetting out the electrolyte from the centrifuge tubes, the white sediment was left behind. This sediment was dissolved in DI water and heat dried at 250C in Teflon evaporating dishes for EDS chemical composition analysis. Fig.6.4 shows the SEM images of the centrifuged sediments.

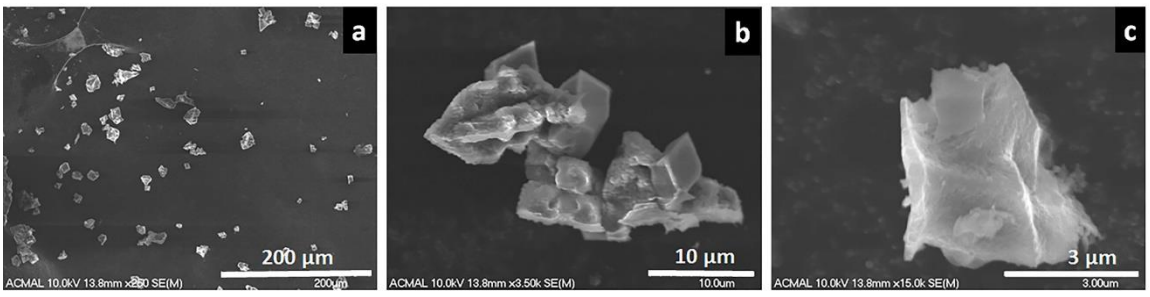

Figure 6.4 Particulates sediment extracted from centrifuged electrolyte. (a) particles on carbon tape at relatively low magnification; (b) residue of aggregated small particles; (c) smallest particle observed from centrifuged electrolyte.

Table 6.6 Summary of average relative wt% of elements from EDS analysis of particles.

	EDS average relative wt%							
Metal particles extracted from electrolyte	C	N	Ti	Al	V	F	O	K
Extracted from heat-dried electrolyte	6.7	3.28	56.26	0.81	1.89	13.6	16.18	1.15
Sediment from centrifuged electrolyte	11.73	--	26.03	8.38	0.46	35.54	17.83	--

Table 6.6 summarizes the average element wt% composition of different metal particles from EDS analysis. In this analysis, additional elements were interrogated to see if there was possible contamination from the particle separation processes. Because of the small particle size, the carbon presence is most likely due to the carbon tape holding the particles for SEM imaging and the nitrogen and potassium are considered background from the ammonium fluoride used in the electrolyte and possible glassware presence in the anodization. Metal particles extracted by centrifuging and heat-drying both showed a strong presence of fluorine. Due to the small size of the particles, a large variation in chemical composition was observed. It was confirmed though that the released metal particles into the electrolyte were another significant source of fluorine consumption from the electrolyte.

6.4 Discussions

From a manufacturing control perspective, the fluorine available in the electrolyte for repeatable electrochemical anodization of TiNT structures decreased from an initial value of approximately 3.421 g/L (3033ppm) to approximately 0.376 g/L (333ppm) after etching a cumulative area of 345 cm^2 over 23 samples. The sources for fluorine

consumption were the TiNT surface, sonicated aggregated surface layer, and the metal particles dissolved in the electrolyte. The as-anodized TiNTs using fresh electrolyte resulted in 124.9 μg/cm^2 and reused electrolyte resulted in 83.07 μg/cm^2 of residual fluorine. This is about 15.97 at% and 13.89 at% of fluorine on the TiNTs, respectively. Such surfaces can be heat treated to achieve anatase conversion and the target concentration of 1.88 at% fluorine on the TiNTs which may facilitate enhanced osseointegration [4] requiring further *in vivo* investigations. These results are useful for monitoring the amount of residual fluorine in the TiNTs during anodization. This further suggests that an average of 104μg/cm^2 fluorine was retained in the TiNT structures, which gives a total of 35.8mg/L of fluorine removed by fluoride complexes associated with 90% titanium. Thus, a total of 39.38 mg/L of fluorine will be consumed by the TiNT structure after anodizing 345cm^2. To put this into perspective, a large orthopedic hip stem implant (Fig.6.5) will consume 24.17 μg/cm^2 of fluorine while anodized in HWLF electrolyte, and with a total surface area of 367 cm^2, leads to total of 8.87 mg/L of fluorine consumption. With this information, the fluorine depletion from the electrolyte can be estimated in a production environment by knowing the surface areas of the variety of implants processed, and the total volume of electrolyte used.

Figure 6.5 Image of thermal plasma sprayed (TPS) hip stem implant and smaller acetabular cup.

The EDS analysis showed strong evidence of fluorine retained by metal particles dissolved in the electrolyte from the formation of the nanotubes. Thus, by knowing the mass of fluorine retained in the implant surface and the mass in the electrolyte, an electrolyte filtration and fluorine replenishment strategy can be used to maintain the required fluorine concentration in the electrolyte to obtain the desired anodized nanotube structures. The size of the metal particles detected was from 500 nm to a few microns. The particulate particles from heat dried electrolyte showed higher residual fluorine even after heating. This indicates the possibility of highly fluoride-rich metal particles dissolved in the electrolyte. It was difficult to account for the mass of fluorine present in the dissolved metals particles. Thus, a series-filtration strategy could be helpful. As fluorine is the critical element for the nanotube formation process, its total concentration must be controlled. To

replenish the fluorine periodically depends on the total or incremental area of implants anodized in a given volume of electrolyte.

Additionally, during PBS immersion of TiNTs for 140 days, the mass of residual fluorine in the TiNTs decreased from 124.9 $\mu g/cm^2$ to 56.18 $\mu g/cm^2$. This indicates that about 45% of the fluorine from the TiNTs leached out into the PBS in 140 days. Although not measured, it is expected that the rate of diffusion into the PBS was higher during the earlier part of the immersion. The mass of residual fluorine contained in the as-anodized titanium nanotube surface of a TPS implant (surface area 367 cm^2) was estimated to be 8.87 mg, which after 140 days of implantation may leach out a total 4mg (45%) into body fluid. This indicates an average 0.028 mg of fluorine leaching per day into the body after implantation, probably higher directly after implantation. The minimum fluorine dose that causes acute toxicity is 0.1 to 0.8 mg of fluorine per kg of body weight [12]. The dose of fluorine which induces nausea is 0.12 mg/kg (i.e. 7.2 mg of fluorine/60 kg of body weight) [13]. The minimal dose causing chronic fluoride toxicity was reported to be 6 mg/day for 10 yr or more. A daily minimum dose as low as 6.2 to 6.6 mg/day, can cause skeletal fluorosis. Arthritis has been reported at water fluorine levels of just 1.7 ppm which may be associated with a daily dose of 5 to 6 mg/day [14-16]. Comparing the minimal dose of harmful fluorine reported in the literature and the fluorine that leached out into the PBS, the estimated levels of possible fluorine leaching into body fluid upon implantation should be very low. Thus, the levels of residual fluorine observed with titanium nanotube surfaces are very low compared to the minimal doses reported to affect the human body.

References

[1] Le Guehennec L, Soueidan A, Layrolle P, Amouriq Y. Surface treatments of titanium dental implants for rapid osseointegration. Dent Mater. 2007;23:844-54.

[2] Abrahamsson I, Berglundh T, Linder E, Lang NP, Lindhe J. Early bone formation adjacent to rough and turned endosseous implant surfaces. An experimental study in the dog. Clin Oral Implants Res. 2004;15:381-92.

[3] Isa Z, Schneider G, Zaharias R, Seabold D, Stanford C. Effects of fluoride-modified titanium surfaces on osteoblast proliferation and gene expression. Int J Oral Maxillofac Implants. 2006;21:203-11.

[4] Li Y, Zou S, Wang D, Feng G, Bao C, Hu J. The effect of hydrofluoric acid treatment on titanium implant osseointegration in ovariectomized rats. Biomaterials. 2010;31:3266-73.

[5] Abrahamsson I, Albouy JP, Berglundh T. Healing at fluoride-modified implants placed in wide marginal defects: an experimental study in dogs. Clin Oral Implants Res. 2008;19:153-9.

[6] Ellingsen JE, Johansson C, Wennerberg A, Holmen A. Improved retention and bone-to-implant contact with fluoride-modified titanium implants. International Journal of Oral & Maxillofacial Implants. 2004;19:659-66.

[7] Cooper LF, Zhou Y, Takebe J, Guo J, Abron A, Holmen A, et al. Fluoride modification effects on osteoblast behavior and bone formation at TiO_2 grit-blasted c.p. titanium endosseous implants. Biomaterials. 2006;27:926-36.

[8] Gongadze E, Kabaso D, Bauer S, Park J, Schmuki P, Iglic A. Adhesion of osteoblasts to a vertically aligned TiO_2 nanotube surface. Mini-Reviews in Medicinal Chemistry. 2013;13:194-200.

[9] Bhosle SM, Tewari R, Friedrich CR. Dependence of nanotextured titanium orthopedic surfaces on electrolyte condition. Journal of Surface Engineered Materials and Advanced Technology. 2016;06:164-75.

[10] Shokuhfar T, Arumugam GK, Heiden PA, Yassar RS, Friedrich C. Direct compressive measurements of individual titanium dioxide nanotubes. ACS Nano. 2009;3:3098-102.

[11] Macak JM, Tsuchiya H, Ghicov A, Yasuda K, Hahn R, Bauer S, et al. TiO_2 nanotubes: Self-organized electrochemical formation, properties and applications. Current Opinion in Solid State and Materials Science. 2007;11:3-18.

[12] The minimum dose that produces acute fluoride toxicity. Fluoride Action Network. 2016.

[13] Kenji A. Re-examination of acute toxicity of fluorine. Fluoride Research 1997;30:89-104.

[14] Ge; X, Jiang; Y, Tang; G, Zhang; M, Zhao Y. Investigations on the occurrence of osteoarthritis in middle-aged and elderly persons in fluorosis-afflicted regions of gaomi city with high fluoride concentration in drinking water. Preventive Medicine Tribune. 2006;12:57-8.

[15] Cook H. The lancet: Fluoride studies in a patient with arthritis. Fluoride Action Network 2016.

[16] Jay DS, Linda MW. Acute fluoride toxicity from ingesting home-use dental products in children, birth to 6 years of age. Journal of Public Health Dentistry. 1997;57.

Chapter 7

Facile synthesis of nanosilver-incorporated titanium nanotube antibacterial surfaces*

Sachin M. Bhosle[1,2], Craig R. Friedrich[1]

[1] *Department of Mechanical Engineering, Multi-Scale Technologies Institute, Michigan Technological University. USA*

[2] *Vidya Pratishthan's Kamalnayan Bajaj Institute of Engineering and Technology, Baramati, India*

Abstract

The battle against post-operative infection in orthopedic surgery calls for the development of surfaces with antibacterial activity on the implant side of the bacterial biofilm. Incorporation of nanosilver into titanium nanotube surfaces offers a potential solution. This study presents a novel single-step anodization approach for incorporating nanosilver particles within and among anodized titanium nanotube surfaces using a new hybrid electrolyte. The amount of nanosilver deposited on titanium nanotubes was analyzed by varying the silver concentration in the hybrid electrolyte. Successful

* *The material contained in this chapter is in preparation for submission to a journal. As the first author of this publication, I have done the fabrication of nanotube surfaces, SEM and EDS characterization, literature review, results analysis and writing the manuscript.*

fabrication of titanium nanotubes by anodization of foils, rods and thermal plasma sprayed surfaces of Ti6Al4V, and simultaneous nanosilver deposition was quantified by field emission scanning electron microscopy and X-ray energy dispersive spectroscopy. Upon post-anodization heat treatment, the amorphous to anatase conversion of these structures was confirmed using X-ray diffraction analysis. This study presents a simple single-step fabrication of antibacterial titanium nanotube surfaces allowing controlled nanosilver deposition needed to avoid unintended cytotoxicity.

7.1 Introduction

Lack of osseointegration and infection are among the major reasons for implant revision surgery. Despite sterilization protocols, chronic infection remains among the most serious post-arthroplasty problems. With diverse methods of antibacterial surface treatments such as germ-free surgical procedures and rigorous sterilization, bacterial infection still occurs post-surgery [1]. This may lead to complicated and expensive revision surgery requiring implant removal, increasing costs and trauma to the patient. Therefore, a clear understanding of infection pathogenesis involving microbiological interactions with the host defense system is essential [2]. Post-operative periprosthetic infections are reported to be higher than 25% [3]. There is early acute infection developed within the first 1-3 months post-surgery, and chronic infection within 3 to 24 months [4]. The reduced immunity at the tissue-implant contact, and the formation of a biofilm at the implant surface makes the implant prone to infection [5]. While understanding the resistance mechanism of the biofilm to bactericidal agents, it is important to note that the penetration of a

bactericidal agent cannot be opposed only by the barrier layer offered by the exopolysaccharide matrix, but there exist other mechanisms which help biofilm survival. These mechanisms of the biofilm's antibacterial resistance are due to several factors such as cell protection against antibacterial action by slow growth rate, increased cell density and late exponential growth owing to nutrient limitation, physiological changes associated with stress response, heterogeneity and location of cells within the biofilm, and phenotype induction [6]. To alleviate the biofilm formation, the bacterial adhesion and colonization need to be understood. Once the biofilm is formed by bacteria adhesion, it develops resistance to antibacterial treatment and host immunity response further becoming hard to remove, and is the primary cause of high rates of infection [6, 7]. Bacteria needs strong early attachment with the implant surface to initiate the biofilm-associated phenotype (protection from antibiotics) and produce micro-colonies. The pathogenic matrix takes advantage of weak body immune defense at the tissue-biomaterial interface. If the osteoblast cell wins the adhesion competition on the biomaterial substrate before the bacteria, then it reduces the chances of bacteria initiating the biofilm. Within this time-window opportunity, an antibacterial strategy can be utilized to discourage bacterial adhesion so that host cells can compete with bacteria for attachment [8]. Thus, a preventive approach on and below the implant surface level could be a winning strategy to target initial bacterial inhibition and increasing local immune response of the implant surface. Developing biofilm-resistant implants seems reasonable. Staphylococcal species are the most frequent and responsible bacteria with strong antibiotic resistance, contributing about

78% of implant-related infections [9]. While designing bactericidal surfaces for implants, the biocompatibility and long-term antibacterial ability is important [8].

In the context of nanoscale biological interactions, nanotexturing of implant surfaces could be a promising multifunctional approach giving enhanced osseointegration, anti-infective and bactericidal drug eluting capabilities. The nanotexturing of long-established implant metals such as CoCrMo and titanium alloys has demonstrated enhanced osteoblast functions [10, 11] owing to similar chemical properties as that of the bulk material and the biomimetic nature of the surface with increased surface area due to nanometer scale roughness. Specifically, anodized titanium dioxide nanotube surfaces are reported to foster osseointegration with enhanced biocompatibility compared to plain titanium surfaces [12]. The TiNTs possess a Young's modulus of 36-43GPa [13] which is closer to trabecular (10.4-14.8GPa) and cortical (18.6-20.7GPa) bone [14] representing closer mechanical properties to that of natural bone. TiNTs are demonstrated to induce growth of hydroxyapatite in simulated body fluid [15]. Improved biocompatibility of TiNTs has been reported with higher extracellular matrix formation, cell attachment due to anchoring, spreading, early differentiation and increased osteoblast proliferation [16] and increased *in vivo* bone formation [17]. While the nanotubes alone have been reported to show some antibacterial properties [18-21], the morphological (open volume) nature of TiNTs can be advantageous for storage, transport and delivery of drugs [22, 23] and antimicrobial agents. Thus, TiNTs attract attention as encouraging bioactive surface modification for strong and speedy bone regeneration. The needed long-term antibacterial ability of biomaterials can be served with vertically-aligned open-porous TiNT surfaces.

Silver (Ag) is a well-established biocidal agent which is effective against a wide range of species. Recently, the effect of silver nanoparticles are reported to induce antibacterial [24] and enhanced photocatalytic [25] ability on titanium dioxide with increased surface area. *In vitro* studies with silver-integrated coatings have shown long-term antibacterial effect against *Staphylococcus aureus* and *Pseudomonas aeruginosa* on fibre reinforced composite implant surfaces [26]. The *in vitro* non-cytotoxicity of nano-Ag integrated surfaces makes them a reliable antibacterial option for implants [27]. The carefully controlled loadings of silver nanoparticles (about 0.4μg/cm^2) can kill 99.99% antibiotic resistant bacteria and also help mammalian cell function [28]. The coatings of Ag incorporated TiO_2 can kill bacteria (*staphylococcus aureus*) completely within 24h along with improved surface hydrophilicity [29]. Silver coated human implants possess high coating stability with low release of active Ag^+ ions (highest 56.4ppb) in blood over 15-month post-surgery with no toxic side effects observed [1] whereas, silver levels of 200 ppb (<2μg/L) in human serum are normal [30]. This builds a strong basis of belief and potential for development of nanotube implant surfaces with a controlled amount of Ag in the TiNTs to achieve improved antibacterial activity without cytotoxicity. These surfaces, capable of silver-ion release can give long-term antibacterial ability and help grow mammalian cells. In the work reported here, the integration of a controlled amount of silver into TiNTs on a variety of Ti6Al4V substrates is reported. To achieve a target amount of Ag incorporation in the TiNTs (0.4μg/cm^2 in this work), a single-step electrochemical anodization process using a newly developed hybrid electrolyte that controls the silver content while ensuring desired nanotube morphology is described.

7.2 Materials and Methods

7.2.1 Substrate preparation

Three types of substrates; foils, rods and thermal plasma sprayed (TPS) alpha/beta titanium alloy (Ti6Al4V) were electrochemically anodized to fabricate nanotubes on the surface. Alloy foils (0.5mm thick) of ASTM B 265-11 grade 5 (TIMET, USA), were mechanically polished using #150 grit fine crocus cloth and #800 grit ultra-fine sanding cloth. After cleaning in deionized (DI) water followed by acetone, the samples were dried in air at room temperature. Coupons 10mm x 30mm x 0.5mm thick were cut from the foils. Alloy rods (3mm diameter and 30mm long) ASTM B348 grade 5 (TIMET, USA) and TPS alloy surfaces of commercial hip stem implants were cleaned as received with no further preparation.

7.2.2 Design of hybrid electrolyte

Ethylene glycol (EG) and DI water-based electrolytes containing NH_4F are well established recipes for fabricating nanotube morphologies on titanium substrates [31-34]. Our recent studies demonstrated the fabrication of nanotubes with inter-tubular spacing of 10-15nm on foil (at 30V in 4h) and on TPS (at 60V in 40min) titanium surfaces with 0.2 wt% of NH_4F [35]. This was designed to achieve well-separated nanotubular morphology favourable for osteoblast function and to keep fluorine content in the electrolyte as low as possible knowing that anodic nanotubular structures possess residual fluorine from

electrolyte species [32, 36]. A hybrid electrolyte, using a combination of NH_4F and AgF (US patent 9376759) [37] yielding a specific concentration of fluorine and Ag, was used to prepare three different concentrations of silver in the electrolyte while maintaining a constant total fluoride concentration that ensures a consistent nanotube surface. This electrolyte composition design was based on the mass percent of NH_4F and AgF which results in a fluorine concentration of 103mg/100mL of total electrolyte from the earlier work. Because fluorine is the critical element for the nanotube formation process, its total concentration must be controlled. To provide the total fluorine mass concentration required in the electrolyte from AgF alone would result in excessive silver in the anodized surface which would be detrimental to mammal cells. Therefore, the electrolyte design first establishes a desired silver concentration, thereby setting the fluorine amount due to AgF alone. The required additional fluorine to bring the total fluorine to 103mg/100mL is provided by the additional NH_4F. Three combinations of AgF and NH_4F in 60 vol% of EG and 40 vol% of DI water are summarized in Table 1. Based on the amount of Ag, the electrolyte recipes are hereafter abbreviated as low-Ag, medium-Ag and high-Ag electrolytes.

Table 7.1 Design of hybrid electrolyte

	Constituents added in 60% EG and 40% DI water (v/v)		Respective mass of element from each constituent			Resulting concentration of elements	
Electrolyte	AgF	NH_4F	Fluorine from AgF	Fluorine from NH_4F	Ag from AgF	Total F	Total Ag
	(g/100mL)				(mg/100mL)		
Low-Ag	0.02	0.195	2.99	100.027	1.60	103	1.60
Medium-Ag	0.04	0.19	5.99	97.462	3.21	103	3.21
High-Ag	0.2	0.142	29.95	73.097	16.05	103	16.05

7.2.3 Formation of nanotube surface

The nanotubes were formed by electrochemical anodization of Ti6Al4V substrates using a DC power source (Protek 3006B), with output 0-60VDC, 1.5A. The foil and rod surfaces were electrochemically anodized at 30VDC for 4h, whereas the TPS samples were electrochemically anodized at 60VDC for 40 minutes, both with a graphite rod as the cathode and the Ti6Al4V as the anode, at room temperature. These times and voltages were established from the prior studies. After anodization, TiNT samples were ultrasonically cleaned in DI water for 5 minutes and air dried for 24h to remove possible surface aggregation and Ag-flakes formed over the TiNTs for the higher silver concentrations during anodization. Each Ti6Al4V alloy substrate (foils, rods and TPS), was anodized with the above described three types of electrolytes (low-Ag, medium-Ag and high-Ag). The specific anodization conditions used for different substrate type and resulting morphological parameters (diameter and length) are summarized later in Table 7.2.

7.2.4 Surface characterization

Characterization of the as-anodized and sonicated Ag-TiNT surfaces was performed by field emission scanning electron microscopy (FESEM, Hitachi S-4700). The relative wt% chemical analysis was performed by energy dispersive spectroscopy (EDS) on the FESEM at 10 kV. X-ray diffraction (XRD - Scintag XDS 2000 Powder) patterns of annealed samples were taken to identify phase structures using an X-ray diffractometer having a CuKα characteristic radiation source. Diffraction patterns were collected in the range of 23-29º with a scan rate of 0.0015º/min with a step size of 0.03º and X-ray radiation of Cu-Kα (λ-1.540562 A) at 45kV and 35mA.

7.2.5 Statistical analysis

The EDS spectra were collected at four different locations on each TiNT surface for compositional characterization using standardless quantitative analysis on FESEM and the data are reported as an average and range of those readings.

7.3 Results

The silver in nanoscale form, even at very low concentrations (mg/L) exhibits strong antibacterial effect, chemical reactivity and solubility [8, 38-40]. Anodization produced an Ag-incorporated TiNT layer on the surfaces. There were observable changes during anodization which were different than anodization in the regular electrolyte containing only NH_4F. It is hypothesized that, during anodization, the electronic charge transfer caused adsorption of Ag^+ in the electrolyte along with hydrogen bubbles evolved (as generally observed in regular NH_4F containing electrolyte) on the graphite cathode. Whereas F^- ions while moving towards the anode may have carried some Ag towards the anode. This caused a simultaneous development of nanotubes and Ag incorporation. Fig.7.1 shows a schematic representation of the Ag-incorporated TiNT (Ag-TiNT) formation mechanism. There is a possibility that during anodization the Ag incorporated in the TiNTs was transformed to AgO due to electrochemical oxidation in acidic environment and oxidation susceptibility of high surface energy Ag nanoparticles [34].

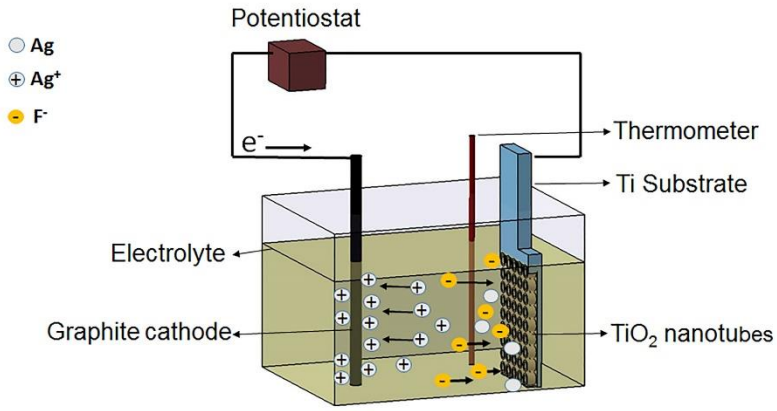

Figure 7.1 Schematic representation of Ag incorporated TiNT formation.

7.3.1 Morphological and chemical analysis

Fig.7.2a shows the FESEM images of as-anodized Ag-TiNTs showing presence of large Ag-nanoparticles sitting on the top of the nanotubes. The silver incorporation over TiNTs is observed in two forms. There are small silver nanoparticles inside the tubes and adhering to the outside of the tube walls (medium-Ag rods in Fig.7.2a). Secondly, large silver flakes (1-3 μm) are sitting on the top of nanotube arrays (Low-Ag foil in Fig.7.2a). These loosely adhering Ag nanoparticles were removed upon ultrasonic cleaning for 5 minutes in DI water, leaving behind tightly adhering spherical Ag-nanoparticles (10-20 nm) sticking to the tube walls (high-Ag rods and TPS). This can be seen in Fig.7.2b which shows SEM images of morphologies representing ultrasonically cleaned TiNT surfaces. The ultrasonic cleaning removed adsorbed Ag reducing the possibility of excessive Ag^{+} release in early stages after implantation. The anodization conditions and morphological parameters of TiNTs are summarized in Table 7.2. The nanoparticles sticking to the inner and outer walls of the nanotubes even after sonication indicates firmly attached nanoparticles. The potency of silver even at very little concentrations and comparatively large volume availability makes Ag-TiNTs structures a potential candidate possessing long-term antibacterial abilities. This can further be improved by tailoring the amount of Ag incorporated.

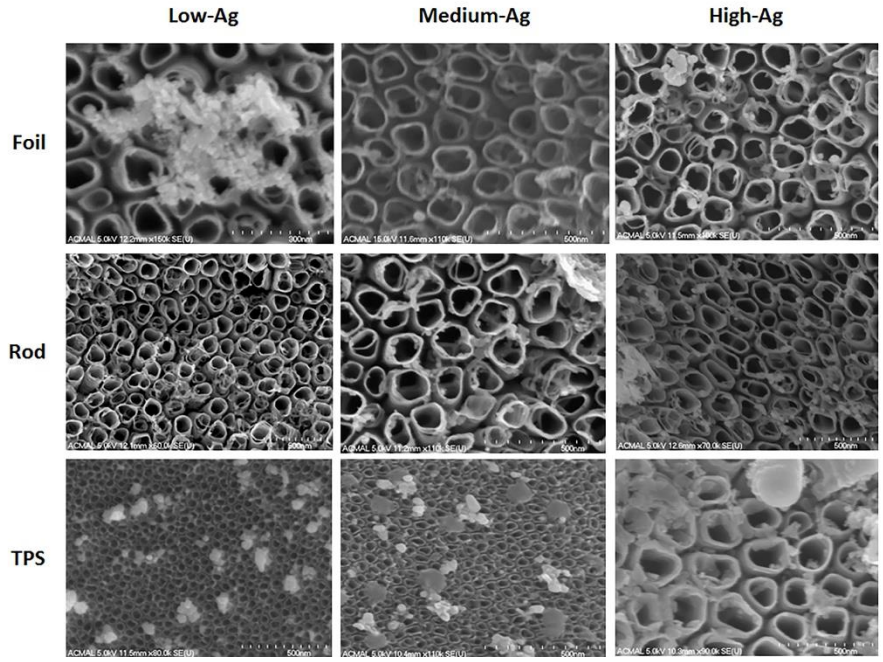

Figure 7.2a SEM images of as-anodized Ag-TiNT

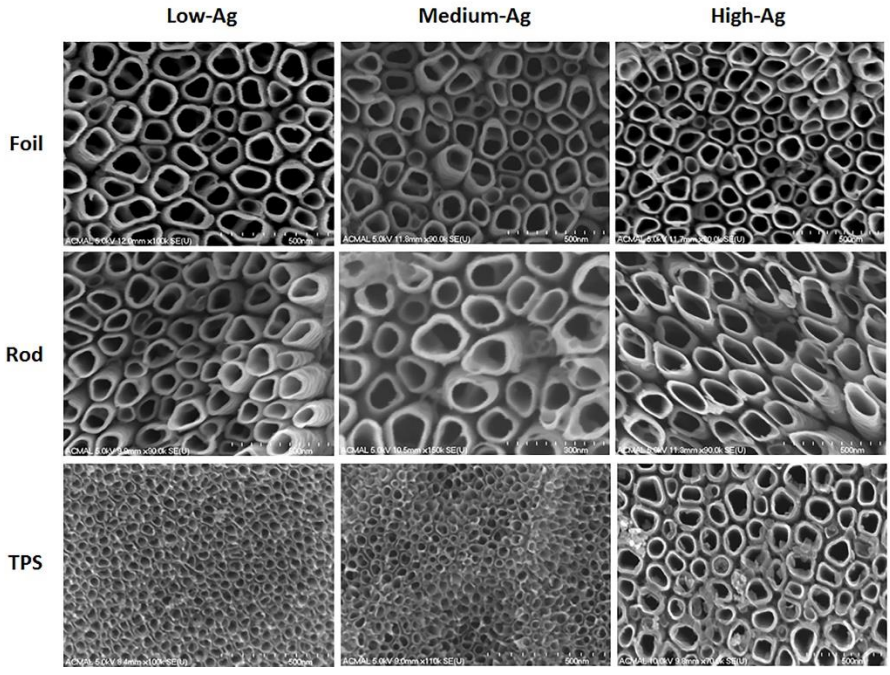

Figure 7.2b SEM images of ultrasonically cleaned Ag-TiNT

Table 7.2 Morphological parameters of TiNTs

Ti6Al4V Substrate	Anidization conditions	Ag-concentration in Electrolyte	Average Tube diameter (nm)	Average Tube length (nm)
Foil	30V-4h	Low	120	1150
		Medium	120	1150
		High	130	1150
Rod	30V-4h	Low	115	1050
		Medium	125	1400
		High	135	1100
TPS	60V-40min	Low	35	500
		Medium	40	500
		High	65	500

The removal of loosely adherent silver accumulation from the TiNTs by sonication was reflected in the EDS analysis. Fig.7.3 shows a representative EDS spectrum of as-anodized and ultrasonically cleaned Ag-TiNTs. The change in the respective intensities of Ag peaks at 3 keV was observed. The Ag-TiNTs developed in the high-Ag electrolytes at the higher anodization voltage (60V) on a relatively harder TPS substrate showed a higher amount of Ag deposition over the TiNT surfaces. The amount of Ag on and in the TiNTs showed dependence on AgF concentration in the electrolyte (low, medium and high), the type of alloy substrate (foil, rod and TPS), anodization voltage and time, and the condition of the TiNT surface (as-anodized or ultrasonically cleaned after anodizing). This was reflected in the quantitative EDS analysis. The relative wt% variations in composition are summarized in Table 7.3.

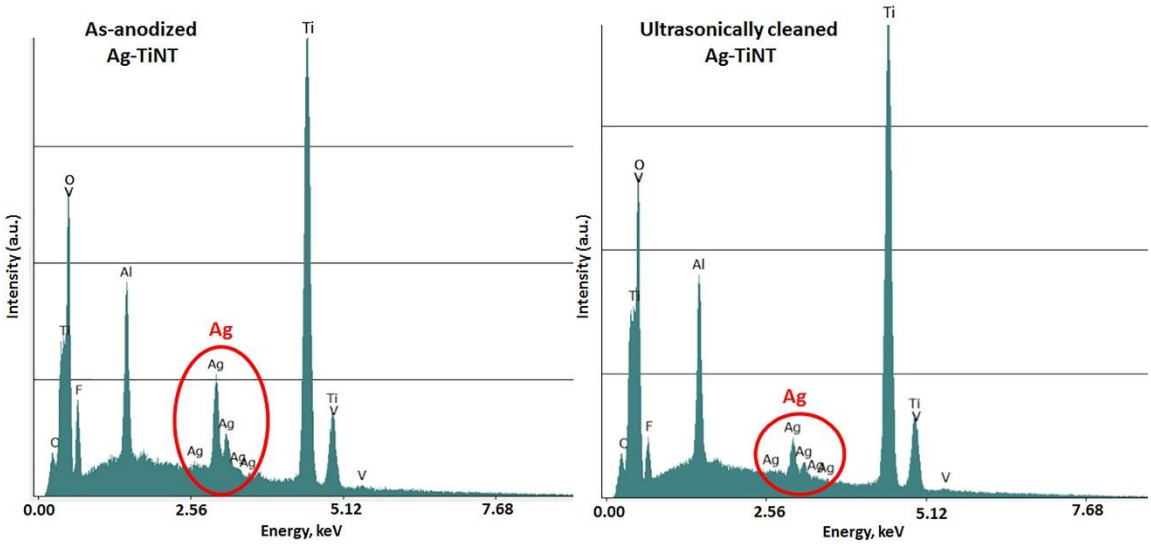

Figure 7.3 Representative EDS spectra of as-anodized and ultrasonically cleaned Ag-TiNT on TPS surface.

Table 7.3 Average EDS Ag wt% in TiNT

	Average Ag wt% in TiNT (As-anodized)			Average Ag wt% in TiNT (Ultrasonically cleaned)		
	Foil	Rod	TPS	Foil	Rod	TPS
Low-Ag	0.125	0.337	0.370	0.010	0.080	0.358
Medium-Ag	0.772	0.543	1.365	0.217	0.117	0.545
High-Ag	1.077	1.057	5.205	0.290	0.740	2.040

7.3.2 Estimation of amount of silver in nanotube surfaces

The volume of material removed during anodization was calculated from the area fraction and nanotube length measurements using ImageJ analysis of the FESEM images. By knowing the volume of alloy removed during the nanotube formation, and the density of TiO_2 (4.23g/cc), the mass of the remaining nanotube layer was calculated. Based on the

mass composition of Ti6Al4V alloy, the mass fraction of titanium present in the bulk alloy substrate was 90% and was used as the relative basis for the EDS relative mass percentages of the other elements. This gave the mass of titanium present in the anodized nanotubular layer. By knowing the mass of Ti present per anodized area of the nanotube structure and using the EDS wt% ratio of Ti:Ag, the estimation of the mass of silver per area ($\mu g/cm^2$) present in Ag-TiNTs was calculated.

Fig.7.4 shows the relationship between the Ag mass per area of the anodized TiNTs and the Ag concentration in the electrolyte. It can be clearly seen that the amount of Ag in the TiNT surface as a result of anodization depends on the Ag-concentration in the electrolyte. The higher Ag concentration in the electrolyte led to a higher deposition of Ag per area over the TiNT surfaces. The data generally shows a logarithmic relationship. To achieve the target concentration of $0.4\mu g/cm^2$ Ag on the TiNTs, these results are useful for designing the electrolyte. The results show that a wide range of Ag-deposition in the TiNTs on a variety of substrates is possible. For foils, the low-Ag recipe yielded $0.46\mu g/cm^2$ of Ag on the as-anodized TiNT. Rods anodized in the low-Ag recipe, and upon sonication, yielded $0.31\mu g/cm^2$ of Ag. TPS substrates had higher Ag in the TiNTs compared to foils and rods. The low-Ag recipe with TPS upon sonication led to $0.57\mu g/cm^2$ of Ag. This may be attributed to the higher anodization voltage (60 VDC) used for TPS surfaces which created nanotubes in comparatively less time (40 minutes) than on foils and rods (4h), even though the nanotubes fabricated at 60VDC were both smaller diameter and shorter than on the foils and rods. The smaller diameter nanotubes have more total surface area inside and outside the nanotubes, per lateral area, than the larger diameter nanotubes on foils and rods.

This indicates that the electrolyte concentration and anodization conditions can be used to control Ag surface concentration. Such surfaces may provide resistance against infection requiring further *in vivo* investigations on silver ion release rate. The Ag nanoparticle embedded titanium surfaces release Ag^{+} ions, and creates a proton depleted region between the bacterial membrane and the implant surface [8, 41]. The process reported provides a quick and simple method for integrating nanosilver at the implant surface level.

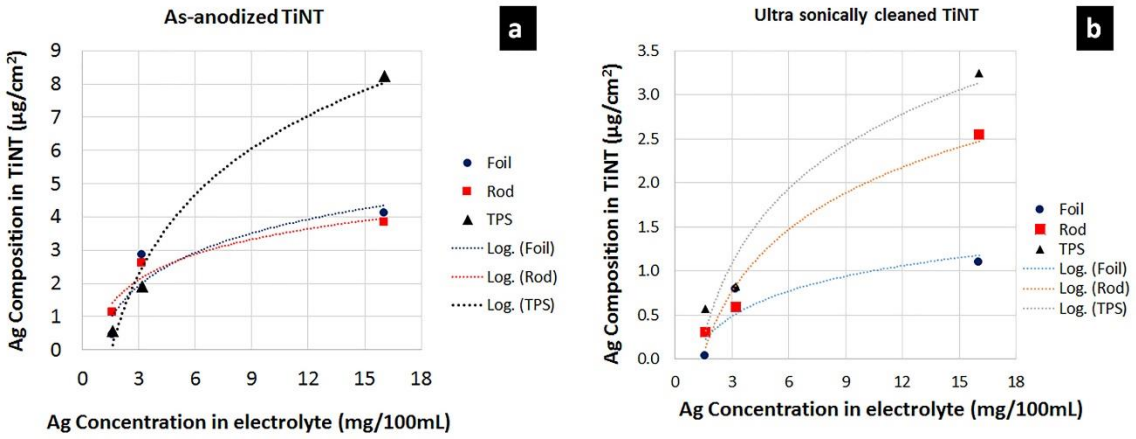

Figure 7.4 Ag-composition in as-anodized and sonicated Ag-TiNT surfaces with respect to Ag-concentration in electrolyte.

The surface properties of biomaterials can influence cell function in the biological environment hence along with morphology and chemistry, the crystallinity of the nanotube surface is another reported factor that can affect osteoblast function [42]. Heat treated TiO_2 nanotubes of Ti and Ti6Al7Nb, with a specific anatase to rutile ratio, shows increased hydrophilicity, enhanced bone adhesion due to high surface reactivity, increased osteoblast differentiation, gene expression and improved electrochemical stability [42]. Enhanced

osteoblast adhesion and proliferation on anatase titania occurs compared to rutile and amorphous films [43]. Anatase Ag-integrated TiNTs have shown antibacterial efficacy against periodontal pathogens *in vitro* [44]. Figure 7.5 shows XRD spectra of TiNT and Ag-TiNT foils annealed at 350ºC for 40 minutes. Peaks corresponding to anatase and rutile were observed on both samples. This confirmed that the presence of Ag on TiNT surface did not influence crystallinity transformation of the structure.

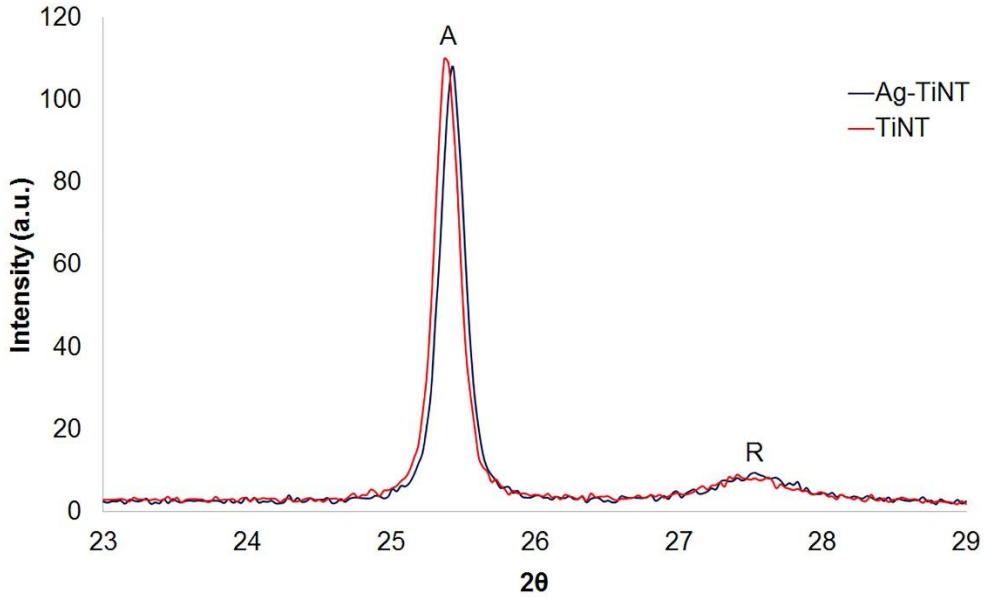

Figure 7.5 XRD pattern of TiNT and Ag-TiNT annealed at 350ºC for 40 min.

7.4 Discussion

To add antibacterial efficacy to TiNTs, different methods have been reported by researchers for the modification of TiNTs in recent years, utilizing high surface area and drug reserving capabilities of nanotubes. A recent study on the modification of implant

surfaces reports zirconium-incorporated TiNTs showed increased *in vitro* bioactivity and corrosion resistance [31]. Gold nanoparticle integrated TiNTs formed by post-anodization magnetron sputtering leads to a heterogeneous structure [45]. Recently zinc [46] and copper [47] incorporated TiNTs have been reported as alternative bactericidal agents. It is anticipated that the bacterial resistance to zinc might develop over time [48], which suggests the need of a combined approach of using multiple bactericidal agents together to address wider defense. A TiNT surface, modified by loading Ag nanoparticles via decomposition of $AgNO_3$ by annealing (500ºC-3h) followed by coating quaternary ammonium salt, showed dual action of long term antibacterial ability and *in vitro* biocompatibility [49]. A similar process of Ag-TiNT formation by post-anodization immersion into $AgNO_3$ and drying in air, followed by annealing at 450ºC for 3h and UV exposure, is another multi-step process [50]. Another process for silver deposition by post-anodization electroplating requires rinsing in acetone, isopropanol and DI water each for 5 minutes [34]. On the contrary, the method discussed in this study is much simpler and a promising approach allowing control over the amount of Ag incorporated and the tube dimensions. This process integrates nanosilver in the same single process that forms the nanotubes and the concentration of nanosilver in the surface can be controlled by the proper design of the new hybrid electrolyte.

7.5 Conclusions

The synthesis, characterization and evaluation of Ag-TiNTs, as a potential antibacterial surface is described. A low cost, environmentally friendly and simple yet

reliable process which can give reproducible results in implant manufacturing was demonstrated. In this work a simple single step anodization method was demonstrated for integration of a controlled amount of nanoscale Ag over TiNT surfaces. This method offers opportunities in developing antibacterial titanium orthopedic surfaces for potentially preventing periprosthetic infection. Appropriate selection of electrolyte recipe and anodization conditions, allows controlled Ag deposition on nanotubular titanium orthopedic implant surfaces to mitigate cytotoxicity. Our results exploited the drug serving capacity of TiNT, which is valuable in future research in this direction. Issues related to biomechanical properties and biological interactions of such materials needs further investigations in clinical settings.

Acknowledgements

This work performed under the M-TRAC program was supported by Grant Case-48161 of the 21st Century Jobs Trust Fund received through the Michigan Strategic Fund from the State of Michigan. The M-TRAC program is funded by the Michigan Strategic Fund with program oversight by the Michigan Economic Development Corporation. The work was also supported by the Multi-Scale Technologies Institute at Michigan Technological University.

References

[1] Hardes J, Ahrens H, Gebert C, Streitbuerger A, Buerger H, Erren M, et al. Lack of toxicological side-effects in silver-coated megaprostheses in humans. Biomaterials. 2007;28:2869-75.

[2] Song Z, Borgwardt L, Hoiby N, Wu H, Sorensen TS, Borgwardt A. Prosthesis infections after orthopedic joint replacement: the possible role of bacterial biofilms. Orthop Rev. 2013;5:65-71.

[3] Kapadia BH, Berg RA, Daley JA, Fritz J, Bhave A, Mont MA. Periprosthetic joint infection. Lancet. 2016;387:386-94.

[4] Zimmerli W, Trampuz A, Ochsner PE. Prosthetic-joint infections. N Engl J Med. 2004;351:1645-54.

[5] Zhao L, Chu PK, Zhang Y, Wu Z. Antibacterial coatings on titanium implants. J Biomed Mater Res B Appl Biomater. 2009;91:470-80.

[6] Mah TFC, O'Toole GA. Mechanisms of biofilm resistance to antimicrobial agents. Trends Microbiol. 2001;9:34-9.

[7] Monteiro DR, Gorup LF, Takamiya AS, Ruvollo-Filho AC, de Camargo ER, Barbosa DB. The growing importance of materials that prevent microbial adhesion: antimicrobial effect of medical devices containing silver. Int J Antimicrob Agents. 2009;34:103-10.

[8] Gallo J, Holinka M, Moucha CS. Antibacterial surface treatment for orthopaedic implants. Int J Mol Sci. 2014;15:13849-80.

[9] Campoccia D, Montanaro L, Arciola CR. The significance of infection related to orthopedic devices and issues of antibiotic resistance. Biomaterials. 2006;27:2331-9.

[10] Webster TJ, Ejiofor JU. Increased osteoblast adhesion on nanophase metals: Ti, Ti6Al4V, and CoCrMo. Biomaterials. 2004;25:4731-9.

[11] Mendonca G, Mendonca DB, Aragao FJ, Cooper LF. Advancing dental implant surface technology from micron to nanotopography. Biomaterials. 2008;29:3822-35.

[12] Oh S, Daraio C, Chen LH, Pisanic TR, Finones RR, Jin S. Significantly accelerated osteoblast cell growth on aligned TiO_2 nanotubes. J Biomed Mater Res A. 2006;78:97-103.

[13] Crawford GA, Chawla N, Das K, Bose S, Bandyopadhyay A. Microstructure and deformation behavior of biocompatible TiO_2 nanotubes on titanium substrate. Acta Biomater. 2007;3:359-67.

[14] Rho JY, Ashman RB, Turner CH. Youngs modulus of trabecular and cortical bone material - Ultrasonic and microtensile measurements. J Biomech. 1993;26:111-9.

[15] Oh SH, Finones RR, Daraio C, Chen LH, Jin S. Growth of nano-scale hydroxyapatite using chemically treated titanium oxide nanotubes. Biomaterials. 2005;26:4938-43.

[16] Das K, Bose S, Bandyopadhyay A. TiO_2 nanotubes on Ti: Influence of nanoscale morphology on bone cell-materials interaction. J Biomed Mater Res A. 2009;90:225-37.

[17] Vara A, Baker EA, Salisbury M, Fleischer M, Bhosle SM, Friedrich C, et al. Enhancing osseointegration of orthopaedic implants with titania nanotube surfaces. Foot & Ankle Orthopaedics. 2016;1:1.

[18] Ercan B, Taylor E, Alpaslan E, Webster TJ. Diameter of titanium nanotubes influences anti-bacterial efficacy. Nanotechnology. 2011;22:295102-12.

[19] Perez-Jorge C, Conde A, Arenas MA, Perez-Tanoira R, Matykina E, de Damborenea JJ, et al. In vitro assessment of staphylococcus epidermidis and staphylococcus aureus

adhesion on TiO_2 nanotubes on Ti-6Al-4V alloy. J Biomed Mater Res A. 2012;100:1696-705.

[20] Peng Z, Ni J, Zheng K, Shen Y, Wang X, He G, et al. Dual effects and mechanism of TiO_2 nanotube arrays in reducing bacterial colonization and enhancing C3H10T1/2 cell adhesion. Int J Nanomed. 2013;8:3093-105.

[21] Golda-Cepa M, Syrek K, Brzychczy-Wloch M, Sulka GD, Kotarba A. Primary role of electron work function for evaluation of nanostructured titania implant surface against bacterial infection. Mater Sci Eng C Mater Biol Appl. 2016;66:100-5.

[22] Torres CC, Campos CH, Diaz C, Jimenez VA, Vidal F, Guzman L, et al. PAMAM-grafted TiO_2 nanotubes as novel versatile materials for drug delivery applications. Mater Sci Eng C Mater Biol Appl. 2016;65:164-71.

[23] Wang Q, Huang JY, Li HQ, Chen Z, Zhao AZ, Wang Y, et al. TiO_2 nanotube platforms for smart drug delivery: A review. Int J Nanomed. 2016;11:4819-34.

[24] Abdel-Fatah WI, Gobara MM, Mustafa SFM, Ali GW, Guirguis OW. Role of silver nanoparticles in imparting antimicrobial activity of titanium dioxide. Mater Lett. 2016;179:190-3.

[25] Sobana N, Muruganadham M, Swaminathan M. Nano-Ag particles doped TiO_2 for efficient photodegradation of direct azo dyes. J Mol Catal A-Chem. 2006;258:124-32.

[26] Nganga S, Travan A, Marsich E, Donati I, Soderling E, Moritz N, et al. In vitro antimicrobial properties of silver-polysaccharide coatings on porous fiber-reinforced composites for bone implants. J Mater Sci Mater Med. 2013;24:2775-85.

[27] Alt V, Bechert T, Steinrucke P, Wagener M, Seidel P, Dingeldein E, et al. An in vitro assessment of the antibacterial properties and cytotoxicity of nanoparticulate silver bone cement. Biomaterials. 2004;25:4383-91.

[28] Agarwal A, Weis TL, Schurr MJ, Faith NG, Czuprynski CJ, McAnulty JF, et al. Surfaces modified with nanometer-thick silver-impregnated polymeric films that kill bacteria but support growth of mammalian cells. Biomaterials. 2010;31:680-90.

[29] Necula BS, Fratila-Apachitei LE, Zaat SA, Apachitei I, Duszczyk J. In vitro antibacterial activity of porous TiO_2-Ag composite layers against methicillin-resistant staphylococcus aureus. Acta Biomater. 2009;5:3573-80.

[30] Abraham T. Wan, Robert A. J. Conyers, Chris J. Coombs, Masterton JP. Determination of silver in blood urine and tissues of volunteers and burn patients. Clin Chem. 1991;37:1683-7.

[31] Indira K, KamachiMudali U, Rajendran N. In vitro bioactivity and corrosion resistance of Zr incorporated TiO_2 nanotube arrays for orthopaedic applications. Appl Surf Sci. 2014;316:264-75.

[32] Bhosle SM, Tewari R, Friedrich CR. Dependence of nanotextured titanium orthopedic surfaces on electrolyte condition. Journal of Surface Engineered Materials and Advanced Technology. 2016;06:164-75.

[33] Raja KS, Gandhi T, Misra M. Effect of water content of ethylene glycol as electrolyte for synthesis of ordered titania nanotubes. Electrochemistry Communications. 2007;9:1069-76.

[34] Zhao Y, Xing Q, Janjanam J, He K, Long F, Low KB, et al. Facile electrochemical synthesis of antimicrobial TiO_2 nanotube arrays. Int J Nanomedicine. 2014;9:5177-87.

[35] Sachin M. Bhosle, Craig R. Friedrich. Effects of aging and thermal treatment on nanotextured titanium surfaces. ORS Annual Meeting, Orlando, FL, USA. 2016;March 5-8.

[36] Regonini D, Jaroenworaluck A, Stevens R, Bowen CR. Effect of heat treatment on the properties and structure of TiO_2 nanotubes: Phase composition and chemical composition. Surface and Interface Analysis. 2010;42:139-44.

[37] Friedrich CR, Shokuhfar T. Compositions, methods and devices for generating nanotubes on a surface. Google Patents; 2013.

[38] Bondarenko O, Ivask A, Kakinen A, Kurvet I, Kahru A. Particle-cell contact enhances antibacterial activity of silver nanoparticles. PLoS One. 2013;8:e64060.

[39] Panacek A, Kolar M, Vecerova R, Prucek R, Soukupova J, Krystof V, et al. Antifungal activity of silver nanoparticles against candida spp. Biomaterials. 2009;30:6333-40.

[40] Ales Panacek LK, Robert Prucek, Milan Kolar, Renata Vecerova, Nadezda Pizu rova, Virender K. Sharma, Tatjana Nevecna, and Radek Zboril. Silver colloid nanoparticles: Synthesis, characterization and their antibacterial activity. J Phys Chem B. 2006;110:16248-53.

[41] Rizzello L, Pompa PP. Nanosilver-based antibacterial drugs and devices: mechanisms, methodological drawbacks, and guidelines. Chem Soc Rev. 2014;43:1501-18.

[42] Mazare A, Dilea M, Ionita D, Titorencu I, Trusca V, Vasile E. Changing bioperformance of TiO_2 amorphous nanotubes as an effect of inducing crystallinity. Bioelectrochemistry. 2012;87:124-31.

[43] He J, Zhou W, Zhou X, Zhong X, Zhang X, Wan P, et al. The anatase phase of nanotopography titania plays an important role on osteoblast cell morphology and proliferation. J Mater Sci Mater Med. 2008;19:3465-72.

[44] Yeniyol S, He Z, Yuksel B, Boylan RJ, Urgen M, Ozdemir T, et al. Antibacterial activity of as-annealed TiO_2 nanotubes doped with Ag nanoparticles against periodontal pathogens. Bioinorg Chem Appl. 2014;2014:829496.

[45] Li J, Zhou H, Qian S, Liu Z, Feng J, Jin P, et al. Plasmonic gold nanoparticles modified titania nanotubes for antibacterial application. Applied Physics Letters. 2014;104:261110.

[46] Hu H, Zhang W, Qiao Y, Jiang X, Liu X, Ding C. Antibacterial activity and increased bone marrow stem cell functions of Zn-incorporated TiO_2 coatings on titanium. Acta Biomater. 2012;8:904-15.

[47] Hang R, Gao A, Huang X, Wang X, Zhang X, Qin L, et al. Antibacterial activity and cytocompatibility of Cu-Ti-O nanotubes. J Biomed Mater Res A. 2014;102:1850-8.

[48] Raphel J, Holodniy M, Goodman SB, Heilshorn SC. Multifunctional coatings to simultaneously promote osseointegration and prevent infection of orthopaedic implants. Biomaterials. 2016;84:301-14.

[49] Chen X, Cai K, Fang J, Lai M, Li J, Hou Y, et al. Dual action antibacterial TiO_2 nanotubes incorporated with silver nanoparticles and coated with a quaternary ammonium salt (QAS). Surface and Coatings Technology. 2013;216:158-65.

[50] Zhao L, Wang H, Huo K, Cui L, Zhang W, Ni H, et al. Antibacterial nano-structured titania coating incorporated with silver nanoparticles. Biomaterials. 2011;32:5706-16.

Chapter 8

Future Work

Based on the work outlined in previous chapters, and a new understanding of the manufacturing processes for developing nanotube surfaces on orthopedic implants, several future directions for the continued analysis and evaluation of industrial process improvement and surface modifications are suggested in this chapter. These future research directions are aimed at overcoming the manufacturing challenges and further clinical and laboratory investigations of nanotextured titanium implant surfaces. These directions include (i) biological evaluations, (ii) filtration of metals contamination from reused electrolyte and fluorine replenishment, (iii) further determining nanotube strength, (iv) design of an annealing process, and (v) process investigations using newly developed hybrid electrolyte.

8.1 Biological evaluations of Ag-TiNT surfaces

Periprosthetic infections are related to procedural and host factors and may occur immediately following or up to several years after surgery. I have showed that antibacterial properties can be added to nanotube surfaces by incorporation of a controlled amount of nano silver. Following the technology described for the synthesis of silver integrated antibacterial nanotube surfaces, the clinical applications of this technology will require *in vitro* and *in vivo* analysis of biofilm inhibition and evaluation of antibacterial ability of

these surfaces. However, to envision clinical applications of this technology, further investigations related to the effect on the osteogenic environment are needed. The underlying mechanism of osteoblast adhesion on Ag-TiNT surfaces remains unknown and its potential application to other tissue engineering materials has not been explored.

To evaluate the inhibition of biofilm formation and bactericidal activity, *in vitro* studies can be conducted to demonstrate the ability of TiNT surfaces to both kill bacteria and inhibit their adhesion. Clinical isolates of Methicillin-resistant Staphylococcus aureus (MRSA) can be obtained from a joint aspiration of an orthopedic patient with an infected total joint replacement, and snap frozen until use. To assess the effect of various implant surfaces on inhibition of biofilm formation by MRSA, coupons of each material group can be prepared. Two control groups can be tested, including: (1) as-received Ti6Al4V and (2) thermal plasma sprayed Ti6Al4V. Four different TiNT surfaces can be included, with nanotube diameters of 60nm, 80nm, 110nm, and 150nm, as well as a group consisting of Ag-TiNT.

To compare the antibacterial and osseointegrative properties of titantia nanotube-modified, plasma-sprayed titanium, and unmodified titanium surfaces in a clinically-relevant *in vivo* model, animal work can be proposed and performed in accordance with an IACUC-approved protocol. The groups can include: (control group 1) unmodified Ti6Al4V surface, (control group 2) plasma sprayed, (group 3) TiNT surfaces and (group 4) silver incorporated TiNT surface. Following implantation, a human clinical isolate of MRSA suspended in culture media can be introduced to the implant. Osseointegration can

be assessed with high-resolution microcomputed tomography (μCT) at the study endpoint. In each group, the implants can be retrieved and sonicated in culture media. Liquid from the sonication can then be used to quantify the number of viable bacteria attached to the implant surface. As of this writing, the *in vitro* work is beginning with collaborators at another location.

8.2 Filtration of metals contamination from reused electrolyte and fluorine replenishment

I showed that the consistent dissolution of metals occurs into the electrolyte during anodization (Fig.8.1). Reuse of the electrolyte for multiple anodizations or larger implants will cause contamination of the electrolyte which further affects anodization conditions and eventual changes in resulting morphologies of the anodized surfaces. Reuse of the electrolyte helps to make the process economical in an industrial scale, but it must be controlled.

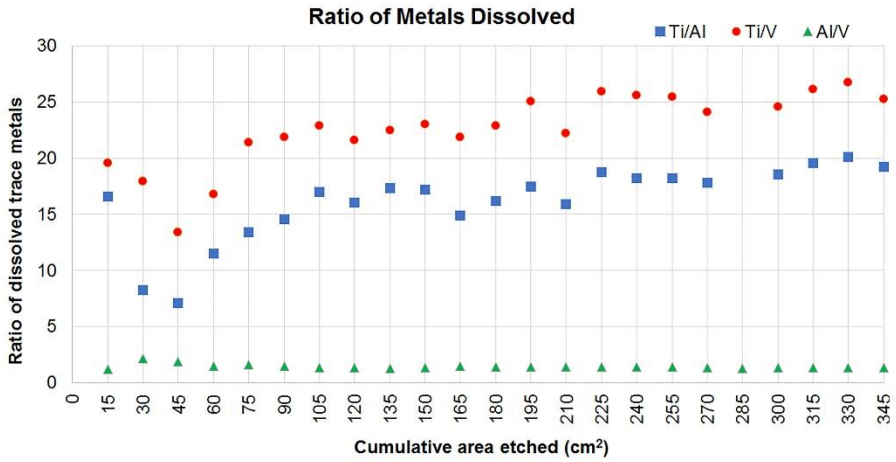

Fig.8.1 Ratios of metals dissolved over cumulative area anodized.

Figure 8.1 shows that the ratios of the etched alloying metals in the electrolyte are very close to those ratios in the original surface. A filtration process that captures the particulate contamination should maintain a relative constant electrolyte chemistry, where no alloying elements remain. In this direction, syringe filtration using 0.2 μm pore-size filters was attempted to determine the filtration efficiency of reused electrolyte. A set of three electrolyte samples (10 ml each) were filtered using 0.2 μm filters and the filtered electrolyte samples were heat-dried at 250C in Teflon evaporating dishes. The heat dried residual particulates were dissolved in 2% nitric solution and ICP-OES analysis was performed to determine the presence of dissolved metals particles in the filtered electrolyte. The results of ICP-OES tests are summarized in Table 8.1.

Table 8.1 Trace metal analysis of syringe filtered electrolyte.

	Trace metal analysis before syringe filtration (mg/L)			Trace metal analysis after syringe filtration (mg/L)		
Sample #	Ti	Al	V	Ti	Al	V
1	132.2	7.2	4.9	121.9	3.8	4.8
2	136.0	7.0	4.6	130.2	4.0	4.8
3	142.1	6.7	4.9	116.8	3.9	4.3
Total metals contamination (mg/L)						
Sample #	Before			After		
1	144.27			130.56		
2	147.59			138.99		
3	153.64			124.98		

The trace metals blank analysis showed that, 8% to 15% particles which were larger than 0.2 micron were filtered and about 85% of the particles were smaller than 0.2 microns which may be filtered with smaller pore filters. This further suggests that a series of filters

ranging from 500nm to 100nm could be used in series (from larger to smaller) to overcome a problem of clogging large particles into smaller pore filters. Another approach could be to use stirred cell filtration which works on pressure based sample concentration. Pressure-driven filtration coupled with magnetic stirred cells (Amicon) commercially available can handle up to 400ml of liquid and use PTFE membranes ranging from 100 nm to 0.45 µm. Used in conjunction with an external compressed gas source and a magnetic stirrer, the stirred cells provide high concentration factors and high sample recovery for liquids. The smallest size filters capable of handling 10ml sample size use 15 - 75 psi maximum pressure, and can be used for laboratory experimental purpose. A comparative analysis of stirred-cell filtration and series filtration can be useful to explore the appropriate filtration strategy applicable for industrial use. A comparative analysis of stirred-cell filtration and series filtration of reused electrolyte to remove the dissolved metals during anodization will help in the more efficient utilization of reused electrolyte and could reduce the costs in industrial manufacturing.

The experimental results also showed that reusing the electrolyte, rather than disposing after each use, led to fluorine removal from the electrolyte. It is important to replenish depleted fluorine in the electrolyte to achieve consistent results from a manufacturing and regulatory perspective. Thus, a fluorine replenishment strategy can be designed for industrial applications. From the experimental results, it is relatively easy to predict the remaining fluorine in the electrolyte as a function of total area etched, knowing the initial concentration and electrolyte volume. This strategy would help to periodically replenish fluorine depending on the total or incremental area of implants anodized. Thus

knowing a *priori* the total area of different implants to be etched, the fluorine content in the electrolyte could be controlled.

The fluorine depletion and electrolyte contamination due to dissolved metals presented in Chapter 3 are based on titania nanotube surfaces etched on coupons cut from flat foils (total area 345cm^2) and anodized in LWHF electrolyte (0.66wt% NH_4F). However, it has been observed that the thermal plasma sprayed commercial implants can be etched in HWLF electrolyte (0.2wt% NH_4F) recipe, which has much lower initial fluorine concentration compared with the LWHF recipe. The fluorine depletion and metals contamination study of TPS commercial implants anodized using HWLF recipe can give more relevant data useful for industrial process control.

8.3 Determining shear strength of nanotubes

In previous chapters of this dissertation, the morphological, chemical and wetting properties of TiNTs have been discussed. A biocompatible TiO_2 nanotube layer on a titanium implant increases the contact area with bone upon implantation. Although it appears, the TiNT layer has a low chance of delamination compared to other cemented surfaces, the nanotube strength must be evaluated for survivability of nanotubes against surgical loads. Fig.8.2 shows a schematic representation of a proposed experimental setup which can be used for evaluation of nanotube strength against shear forces. A combination of variable normal and shear loads can be used for shear loading of the nanotube layer and can be subjected to sliding between two pieces of bone simulant material. The survivability and deformation behavior of nanotubes at different loads can be analyzed with scanning

electron microscopy before and after loading at each step. This experimental procedure is currently being assembled.

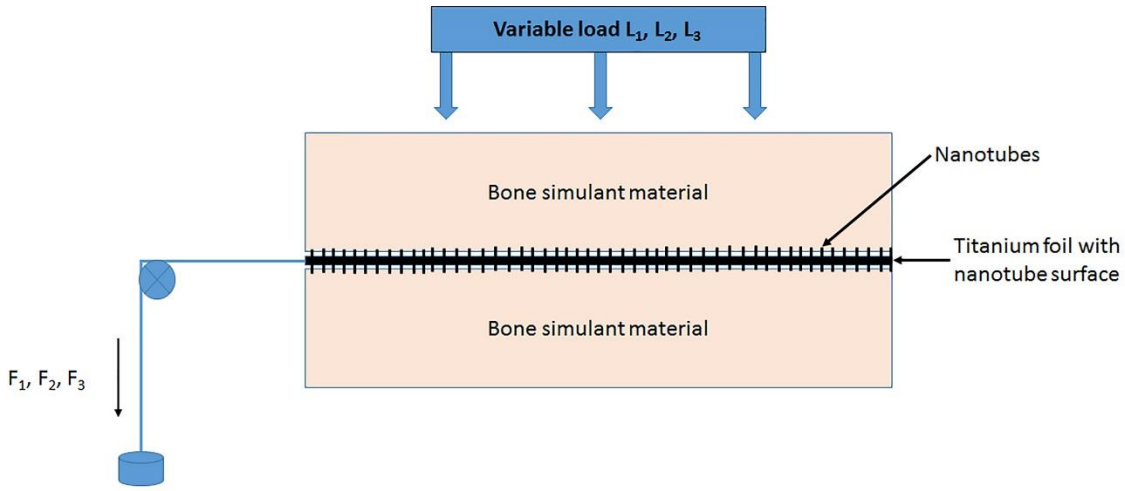

Figure 8.2 Schematic experimental setup for shear strength and survivability analysis of nanotubes.

8.4 Designing a flow-through furnace

In Chapter 5, it was determined that 77.12 kJ/mol of activation energy is required to convert amorphous titania nanotubes into crystalline anatase. The experimental analysis also demonstrated that only 5 minutes of heating at 350C can result in the amorphous-crystalline conversion. This can be used to estimate the heat absorbed by the nanotube layer for an implant based on surface area, and the required thermal power delivery for a continuous annealing process for a specified implant throughput rate. The atomic mass of titanium is 47.86 and that of oxygen is 16, which yields 79.86 g/mol for TiO_2. The mass of the TiNT layer on a TPS surface is 233µg/cm^2 and a large hip stem has a surface area of 367 cm^2, giving a total surface mass of 1.071 millimole. Therefore, the energy required for

conversion of the TiNT surface layer on a hip stem is 82.6 J over a duration of 5 minutes, or 0.28 W.

The analysis above considers only the nanotube layer but over 5 minutes the bulk of the implant will be heated. Therefore, based on a large hip stem, the volume is 127cm^3 with a mass of 0.56 kg. Therefore, the total energy absorbed by this hip stem to reach 350C is 104 kJ. Finally, the power required for the 5-minute duration is 347 W. Therefore, using this data, the preliminary design of a flow-through furnace for specific industrial applications can be estimated.

8.5 Process investigations using newly developed hybrid electrolyte

The various investigations performed using the NH_4F-based electrolytes can be repeated for processes utilizing hybrid electrolytes using a combination of NH_4F and AgF. While using the hybrid electrolyte, silver ions will also actively participate in the anodization and has effects on current densities and charge transfer. Therefore, a detailed investigation of the most influential factors affecting nanotube morphology using a hybrid electrolyte will be important for the development of antibacterial surfaces. Investigations completed on the depletion of fluorine and metals contamination with NH_4F electrolyte can be repeated using a hybrid electrolyte because silver replenishment, along with fluorine replenishment, would be required for process control. The removal of only substrate metals (Ti,Al,V) contamination while retaining silver in the electrolyte could be challenging and worth investigating.

Appendix

Appendix 1: Copyright for the Manuscript Published in Journal of Surface Engineered Materials and Advanced Technology

Sachin M. Bhosle, Radheshyam Tewari, Craig R. Friedrich. Dependence of Nanotextured Titanium Orthopedic Surfaces on Electrolyte Condition, *Journal of Surface Engineered Materials and Advanced Technology*, 2016, 6, 164-175.

Michigan Tech

Sachin Bhosle <smbhosle@mtu.edu>

Your paper is published on JSEMAT: Vol.6 No.4 2016! [ID: 1180338]

jsemat@scirp.org <jsemat@scirp.org> Wed, Jan 25, 2017 at 10:41 PM
To: smbhosle <smbhosle@mtu.edu>

Dear Sachin Bhosle,

You can use the article, but please indicate the resource of it in your dissertation.

Best regards
Martina MA
JSEMAT Editorial Office
Paper Submission Entrance
Facebook: https://www.facebook.com/tingting.ma.315213
Twitter: https://twitter.com/Martina81989884

If you have any complaints or suggestions, please contact feedback@scirp.org.

2/15/2017 Michigan Technological University Mail - Your paper is published on JSEMAT: Vol.6 No.4 2016! [ID: 1180338]

Michigan Tech

Sachin Bhosle <smbhosle@mtu.edu>

Your paper is published on JSEMAT: Vol.6 No.4 2016! [ID: 1180338]

Sachin Bhosle <smbhosle@mtu.edu> Wed, Jan 25, 2017 at 12:11 PM
To: jsemat <jsemat@scirp.org>

Hello Dr. Chunlan Ye,

I am the first author of this paper. This paper is part of my PhD work and I need to add it to my dissertation.

Can you please send me the permission to put it into my thesis as this might be under journal's copyright?

Thanking you.

Sincerely,
Sachin Bhosle